LIGHT SCATTERING STUDIES
ON THE COIL-GLOBULE PHASE TRANSITION
OF SINGLE POLYMERS IN SOLUTION

by

GERALD ADAMS SWISLOW

B.S., University of Michigan
(Ann Arbor 1977)

SUBMITTED IN PARTIAL FULFILLMENT OF THE

REQUIREMENTS FOR THE DEGREE OF

DOCTOR OF PHILOSOPHY

at the

MASSACHUSETTS INSTITUTE OF TECHNOLOGY

AUGUST, 1984

Signature of Author: _____
Department of Physics
August 17, 1984

Certified by: _____
Professor Toyoichi Tanaka
Thesis Supervisor

Accepted by: _____
Professor George F. Koster
Chairman, Departmental Committee

LIGHT SCATTERING STUDIES

ON THE COIL-GLOBULE PHASE TRANSITION

OF SINGLE POLYMERS IN SOLUTION

by

Gerald Adams Swislow

Submitted to the Department of Physics on August 20, 1984,
in partial fulfillment of the requirements
for the degree of Doctor of Philosophy.

ABSTRACT

The coil-globule phase transition is the reversible, conformational change of a single linear polymer molecule from an extended coil in the high temperature (or good solvent) phase to a tightly packed globule in the low temperature (or poor solvent) phase. Since the mid-1960's, many theories have been proposed to describe the transition between coil and globule. However, no experimental confirmation of the collapsed, globular phase existed before the work described in this dissertation. The globular phase is present in solution only at low concentrations of polymer. Measurement of the size of single polymers in such dilute solutions had been beyond the reach of conventional techniques. The light scattering experiments described within this dissertation represent the first measurements of the complete coil-globule phase transition.

These experiments investigated two polymer-solvent systems. For solutions of polyacrylamide (M_W=5-6×10^6) in acetone-water mixtures, at concentrations of polymer less than 10μg/ml and at a temperature of 25°C, a sharp decrease in the radius of gyration (R_G) and hydrodynamic radius (R_H) occurred at an acetone concentration of 39%. Measurements of the R_H continued to 80% acetone concentration, well into the globular phase.

In polystyrene (M_W=2.6×10^7) and cyclohexane solutions, with polymer concentrations as low as 0.01μg/ml, varying the temperature induced the transition. The coexistence curve, which shows the temperatures and concentrations at which the solution separates into polymer-rich and polymer-poor phases, was determined in this low

concentration regime. The measurements of the polymer size were obtained above the phase separation temperature. Between 35°C and 30°C, R_H decreased sharply from ~1300 to ~700Å while R_G dropped from ~1800 to ~500Å. In the limit of the collapsed globular state the ratio of R_G to R_H was 0.74±0.04, close to the value for a solid isotropic sphere. The exponents for the reduced-temperature dependence of the expansion factor in the collapsed region, -0.34±0.04 for R_G and -0.36±0.04 for R_H, agree with the mean-field theory prediction of -1/3.

Evidence of a sharp increase in amplitude and a sharp decrease in the rate of intramolecular density fluctuations within the individual polymer molecules was also observed near the transition. Such behavior of density fluctuations is characteristic of critical phenomenon associated with phase transitions.

An extension of Flory's mean-field theory for a single polymer qualitatively describes the collapse in radius. In addition, the first theoretical considerations of critical density-fluctuations within a single polymer molecule are presented. The predicted temperature dependence of the amplitude and rate of the fluctuations also qualitatively agrees with the observations.

This dissertation also includes a description of the light scattering instrument built to make the sensitive measurements at low levels of scattering.

Thesis Supervisor: Toyoichi Tanaka

Title: Professor of Physics

TABLE OF CONTENTS

LIST OF FIGURES

LIST OF TABLES

CHAPTER 1

INTRODUCTION

The distinctive feature of the polymer is its structure -- hundreds to hundreds of thousands of small molecules (often identical) are covalently linked together to form a flexible, randomly coiled chain. This picture of the polymer was first proposed by Staudinger in 1920 [1], and it marks the beginning of polymer science.

The flexibility of the chain comes from the ability of the bonds joining the polymer segments to rotate. When the number of segments is large, the number of possible configurations of the chain is tremendous. Because the configurations are so numerous, mechanistic calculations of chain dimensions and dynamics are impossible. For the same reason, however, the polymer chain is well-suited for treatment by statistical methods.

The simplest model of a polymer chain neglects any interaction among segments. The problem of describing the average distance, say, between the ends of the chain is equivalent to the statistical problem of a determining the distance between the end points of a 3-dimensional random walk. The solution to that problem is well known, and the result is that the average end-to-end distance of the polymer chain is proportional to the square root of the number of segments in the chain.

In a solution of real polymers, the interactions among the segments and solvent molecules affect the configuration of the chains. One interaction that is always present is the hard-core, or "excluded volume", repulsion between segments, which tends to expand the coil. The temperature-dependent energy of interaction between segments and between segments and solvent molecules can favor either segment-segment attraction or segment-segment repulsion. If the net interaction between segments is repulsive, corresponding to the "good solvent" environment and usually associated with high temperatures, the polymer chain is again expanded. If the net interaction is attractive, corresponding to a "poor solvent" and low temperatures, the polymers in the solution normally aggregate, producing phase separation of the polymer solution. At a particular temperature (Flory's "theta temperature"), the attractive and repulsive interactions are nearly balanced, favoring the random-walk configuration.

The first statistical mechanical treatments of this kind of phase separation in polymer solutions were given independently by Flory [2] and Huggins [3] in 1942. Although they realized a single chain would contract in a poor solvent, their theories rightly showed that the distance between individual chains needed to avoid interpolymer aggregation required solutions too dilute to detect single collapsed chains using any then known experimental technique. Thus, theories to describe the average extension of polymer chains in solution were only concerned with and valid in the good and theta solvent regimes. Flory's successful (mean-field) theory treating single

polymers under these conditions is contained his 1953 book [4].

There is a mention of single polymer contraction in a 1960 paper by Stockmeyer [5], but the first statistical treatment describing polymer dimensions over the range of expanded coil to compact "globule" came in 1965 from Ptitsyn and Eizner [6] who coined the phrase "coil-globule transition". They treated the polymer as a van der Walls gas confined by an elastic membrane, and predicted the segments would condense to a compact form as the temperature is lowered. In this picture the phase transition within the polymer is analogous to the phase separation of the polymer solution. Several similar treatments soon followed [7-9]. A much broader interest in the coil-globule transition developed during the 1970's [10]. Observations of the transition of DNA to a compact form in polymer solutions [11], more sensitive experiments to detect the onset of polymer contraction in dilute solutions [12-14], and development of renormalization group techniques for the study of phase transitions sparked the renewed theoretical interest in the phase transition of a single polymer [15-24].

There is no agreement, however, among the theorists on how the polymer changes from expanded random coil to collapsed globule. The mean-field theories generally predict that chains with a particular flexibility will undergo a discrete, first-order phase transition. Others suggest there will be a second order phase transition only in the limit of infinite molecular weight chains, while real polymers will undergo a smooth transition. Still others are concerned with

the structure of the globule, does it have a dense core with an expanded exterior? Until the results described in this dissertation, there were no measurements of the complete coil-globule transition to test any theory.

Another aspect to the problem of individual polymers in solution is the dynamics of the single chains. Interest in this problem arose in attempts to explain the anomalously large viscosities of polymer solutions [25-27]. Typically, the polymer chain is modeled as a sequence of beads and massless springs, with the beads also coupled by the hydrodynamic interaction mediated by the solvent. In the expanded coil state, where there is little segment-segment contact, the model has been successful. However, there has been no theory specifically concerned with the dynamics of density fluctuations within a single polymer near the coil-globule transition. Since fluctuations play an important role in critical phenomenon [28], a theory appropriate for the single polymer near the phase transition is presented in this dissertation. Because even a small increase in the amplitude of the internal density fluctuations of the polymer near the critical point can include the entire polymer, we model the fluctuations as breathing modes of an elastic sphere.

Application of light scattering to the study of polymer solutions was suggested by Debye [29] in 1944, and became widely used to characterize the size of polymers in solution [4]. Following the invention of the laser in the late 1960's, and subsequent development of the quasi-elastic light scattering technique, a sufficiently sen-

sitive method became available for not only following the change in size of single polymer chains down to the globule state, but also measuring intramolecular dynamics. Great care is required in such an experiment, because of the low level of signal. The first successful application of dynamic-light scattering techniques to measure the entire coil-globule transition are contained in this dissertation.

The remaining chapters are organized as follows. Chapter 2 presents a mean-field theory for the temperature dependence of the expansion factor of a single polymer chain in solution, using the method of Flory [4] extended to the poor solvent regime by Eizner [8]. The order of the collapse phase transition is shown to depend on the flexibility of the physical chain. A stiff chain will undergo a first-order phase transition, while a flexible chain will smoothly change from coil to globule as the temperature is lowered. Also included are new considerations of the elasticity of a single chain. At a critical value of the chain flexibility, the compressibility of the chain is shown to diverge.

Chapter 3 presents the theoretical basis for the light scattering measurements of the hydrodynamic radius and the radius of gyration of the single chains, and the measurement of the amplitude and relaxation time of the lowest order mode of internal density fluctuations within a single chain. The measurements of the radius of gyration are based on a new technique appropriate for the dilute solutions needed for existence of the globule state. The angular dissymmetry in the intensity of the light scattered by the polymer

molecules is obtained by determining the amplitude of the intensity fluctuations from the correlation function of the scattered light. A new approach for obtaining the elasticity of the polymer from light scattering measurements is also presented.

The light scattering experiments on polyacrylamide chains in acetone-water mixtures and polystyrene chains in cyclohexane are described, and the results shown in Chapter 4. A fit of the data for polystyrene in cyclohexane to the mean-field theory of Chapter 2 is consistent with a sharp, but still smooth transition for a flexible chain. The predictions for the compressibility of the chain at the transition qualitatively agree with the measurements, which show a significant "softening" of the chain near the transition temperature.

The apparatus built for these experiments is described in Chapter 5, and suggestions for further experiments are given in Chapter 6.

References

1. H. Staudinger, "Uber Polymerisation", Berichte d. D. Chem Gesellschaft **53** pp. 1073-1085 (1920).

2. P.J. Flory, "Thermodynamics of high polymer solutions", J. Chem. Phys. **10** pp. 51-61 (1942).

3. M.L. Huggins, "Thermodynamic properties of solutions of long-chain components", Ann. N.Y. Acad. Sci **43**(1) pp. 1-32 (1942).

4. P.J. Flory, Principles of Polymer Chemistry, Cornell University Press, Ithaca (1953).

5. W.H. Stockmayer, "Problems of statistical thermodynamics of dilute polymer solutions", Makro. Chemie. **35** pp. 54-74 (1960).

6. O.B. Ptitsyn and Y.Y. Eizner, "Theory of globule to coil transitions in macromolecules", Biofizika **10**(1) pp. 3-6 (1965).

7. O.B. Ptitsyn, A.K. Kron, and Y.Y. Eizner, "The models of denaturation of globular proteins. I. Theory of globula-coil transitions in macromolecules", J. Polymer Sci. C **16** pp. 3509-3517 (1968).

8. Y.Y. Fizner, "Globule-coil transitions in homogeneous macromolecules", Vysokomol. Soyed. **A11**(2) pp. 364-371 (1969).

9. I.M. Lifshitz, "Some problems of the statistical theory of biopolymers", Soviet Phys. JETP **28**(6) pp. 1280-1286 (1969).

10. C. Williams, F. Brochard, and H.L. Frisch, "Polymer collapse", Am. Rev. Phys. Chem. **32** pp. 433-451 (1981).

11. L.S. Lerman, "A transition to a compact form of DNA in polymer solution", Proc. Nat. Acad. Sci. USA **68**(8) pp. 1886-1890 (1971).

12. C. Cuniberti and U. Bianchi, "Dilute solution behavior of polymers near the phase separation temperature", Polymer **15** pp. 346-350 (1974).

13. E. Slagowski, B. Tsai, and D. McIntyre, "The dimensions of polystyrene near and below the theta temperature", Macromolecules **9** pp. 687-688 (1976).

14. M. Nierlich, J.P. Cotton, and B. Farnoux, "Observation of the collapse of a polymer chain in poor solvent by small angle neutron scattering", J. Chem. Phys. **69**(4) pp. 1379-1383 (1978).

15. C. Domb, "Phase transition in a polymer chain in dilute solution", Polymer **15** pp. 259-262 (1974).

16. P.G. deGennes, "Collapse of a polymer chain in poor solvents", J. Physique **36** pp. 1-3 (1975).

17. J. Mazur and D. McIntyre, "The determination of chain statistical parameters by light scattering measurements", Macromolecules **8**(4) pp. 464-476 (1975).

18. C. Domb and A.J. Barrett, "Universlity approach to the expansion factor of a polymer chain", Polymer **17** pp. 179-184 (1976).

19. P.G. deGennes, "Collapse of a flexible polymer chain II", J. Physique L **39**(17) pp. L299-301 (1978).

20. C.B. Post and B.H. Zimm, "Internal condensation of single DNA molecule", Biopolymers **18** pp. 1487-1501 (1979).

21. I.C. Sanchez, "Phase transition behavior of the isolated polymer chain", Macromolecules **12**(5) pp. 980-988 (1979).

22. A.Z. Akcasu and C.C. Han, "Molecular weight and temperature dependence of polymer dimensions in solution", Macromolecules **12**(2) pp. 276-280 (1979).

23. K. Kremer, A. Baumgartner, and K. Binder, "Collapse transition and crossover scaling for self-avoiding walks on the diamond lattice", J. Phys. A **15** pp. 2879-2897 (1981).

24. G. Allegra and F. Ganazzoli, "Coil-globule transition in polymer solutions", Macromolecules **16**(8) pp. 1311-1317 (1983).

25. J.G. Kirkwood and J. Riseman, "The intrinsic viscosities and diffusion constants of flexible macromolecules in solution", J. Chem. Phys. **16**(6) pp. 565-573 (1948).

26. P.E. Rouse, Jr., "A theory of the linear viscoelastic properties of dilute solutions of coiling polymers", J. Chem. Phys. **21**(7) pp. 1272-1280 (1953).

27. B.H. Zimm, "Dynamics of polymer molecules in dilute solution: Viscoelasticity, flow birefringence and dielectric loss", J. Chem. Phys. **24**(2) pp. 269-278 (1956).

28. H.E. Stanley, Introduction to Phase Transitions and Critical Phenomena, Oxford, New York (1971).

29. P. Debye, "Light scattering in solutions", J. Appl. Phys. **15**(3) pp. 338-342 (1944).

CHAPTER 2

THEORY FOR THE COIL-GLOBULE TRANSITION

2.1. Introduction

This chapter presents a mean-field theory for the equilibrium expansion-factor of a single polymer, based on the model developed by Flory [1]. The transition between coil and globule is interpreted as a phase transition that can be first order, second order, or smooth depending on the value of a parameter that characterizes the flexibility of the polymer backbone. An expression for the compressibility of the single coil is also derived. Finally, similar mean-field approaches to the problem are reviewed.

2.2. Some Definitions

Several parameters must be defined for the derivations that follow in this chapter. First, consider the ideal polymer chain. It has N segments, each of length a. There are no restrictions on the orientation of successive segments. Interaction among segments, including steric interference, is neglected. The possible orientations of such a chain are identical to the paths of an N-step 3-dimensional random walk of step-length a. Each path can be characterized by the end-to-end distance h,

$$h = \left| \sum_i \vec{r}_i \right| , \tag{2.1}$$

where $\vec{r}_i$ is a vector from the origin at the beginning of the first

step to the end of the ith step. For N large, the mean-square end-to-end distance $\langle h_0^2 \rangle$ over all possible paths is, as for a random walk,

$$\langle h_0^2 \rangle = Na^2 \ . \tag{2.2}$$

(The subscript 0 will henceforth refer to the ideal or random-walk polymer.) The probability that a particular path has end-to-end distance h is given by the normalized Gaussian distribution,

$$P(h) = \left[\frac{9}{\pi \langle h_0^2 \rangle}\right]^{3/2} e^{-\frac{9h^2}{\langle h_0^2 \rangle}} \ . \tag{2.3}$$

Laboratory measurements usually determine the radius of gyration rather than the end-to-end distance. The radius of gyration s (elsewhere in this dissertation denoted R_G) is the root-mean-square distance of the segments from the molecular center of mass at $\vec{R}_{CM}$,

$$\langle s^2 \rangle = \frac{1}{N} \sum_i |\vec{r}_i - \vec{R}_{CM}|^2 \ . \tag{2.4}$$

It is straightforward to show that for a Gaussian chain, s and h are simply related [1],

$$\langle s^2 \rangle = 6 \langle h^2 \rangle \ . \tag{2.5}$$

In real polymers, the chain configuration does not generally obey the random walk formulas owing to segment-segment interactions. However, under certain conditions the real chain will nearly obey random walk statistics with h (and s) proportional to the square root of polymer molecular weight, $M_W^{1/2}$. These conditions occur in the bulk (melt) polymer state and under specific solvent conditions for

polymer solutions. A scaling of the observed size of the polymer chains with $M_w^{1/2}$ defines the ideal chain environments. It is not necessary for N to correspond to the number of monomers in the chain. Instead, N and a are identified as an effective segment number and an effective segment length, where the effective segment will encompass several real monomers.

The extent to which the size of the chain deviates from the ideal is given by the expansion factor α, where

$$\alpha^2 = \frac{\langle h^2 \rangle}{\langle h_o^2 \rangle} = \frac{\langle s^2 \rangle}{\langle s_o^2 \rangle} . \tag{2.6}$$

The second equality is not generally valid, but does hold for Gaussian chains, assumed in the model presented in this discussion.

One more parameter will be needed to describe the real chain. It is related to the molecular volume of an effective segment, V_1. We will let b characterize the radius of an effective segment such that

$$V_1 = a\, b^2 . \tag{2.7}$$

We can then define a parameter w,

$$w = \frac{b}{a} \tag{2.8}$$

that characterizes the flexibility of the chain. A low value of w corresponds to a stiff chain where the shape of the effective segments is long and thin. As the length of the effective segment decreases, the flexibility increases. The flexibility will soon be shown to profoundly effect the transition from coil to globule.

Also needed in the following discussion is the molecular volume of the real chain, V_p. In terms of already introduced parameters, it satisfies the relation

$$N = \frac{V_P}{V_1} . \tag{2.9}$$

2.3. Free Energy of a Polymer Chain in Solution

This discussion will predict how the expansion factor of a real chain in solution will depend on the characteristics of the chain, with parameters N, a, and w, and on the solvent environment. First, the free energy of the chain in solution must be calculated. We need only consider the difference between the total free energy of the solution and the free energies of the pure polymer and pure solvent components. The net free energy will be called ΔF. It is composed of two parts, an enthalpic or heat of mixing component, ΔH, and an entropic contribution, ΔS,

$$\Delta F = \Delta H - T\Delta S , \tag{2.10}$$

where T is the solution temperature.

Only binary interactions will be considered in determining ΔH, thus

$$\Delta H = kT\chi n_1\phi . \tag{2.11}$$

Here, n_1 is the number of solvent molecules in the volume, and ϕ is the volume fraction of polymer. The product $n_1\phi$ is proportional to the probability of contact between a solvent molecule and a segment of the polymer. χ is a parameter that characterizes the free-energy

increase per contact divided by kT, and depends on temperature, the particular solvent-polymer combination, and possibly the solute concentration. The temperature dependence is usually adequately treated by defining an ideal or compensation temperature Θ, and writing

$$\chi = \frac{1}{2} - \psi\left(1 - \frac{\Theta}{T}\right) , \tag{2.12}$$

where ψ is an interaction parameter with a negligible temperature dependence. When $T = \Theta$, the effect of binary interactions vanishes. Any concentration dependence of χ will be neglected.

The entropic contribution can be considered to be composed of two parts. The first, ΔS_{mix}, is associated with the disorientation or mixing of the solvent and the polymer, calculated with no restriction on the configuration of the polymer. The second contribution to the net entropy, ΔS_{el}, accounts for the decrease in the number of configurations available to the chain as it is swells or shrinks relative to the ideal state. (Remember, in the pure (or bulk) polymer state the chain assumes a random walk configuration.) This contribution is called the rubber elasticity of the polymer chain.

The entropy of mixing is calculated using a simple lattice model for the polymer and solvent. The result will, however, contain no parameters of the lattice. The solvent molecules and effective segments are assumed to occupy identical lattice sites. The lattice coordination number is z. The first segment of the polymer is placed on an arbitrary site. There are $z - 1$ sites for the next segment to occupy. As successive segments are placed on the lattice, there is a possibility an adjacent site will already be occupied by a segment

placed earlier than the previous one. To account for these long-range interferences analytically is an intractable problem. Instead, a mean-field approximation is made whereby the probability a site is occupied is assumed proportional to the number of segments already placed on the lattice. That probability is $1 - i/n_0$ for the ith segment, where $n_0 = n_1 + N$ is the number of lattice sites. Thus the number of ways to distribute the polymer over the lattice is

$$\Omega_{mix} = \prod_{i=1}^{N} (z - 1)\left(1 - \frac{i}{n_0}\right) = \left(\frac{z - 1}{n_0}\right)^N \frac{n_0!}{(n_0 - N)!} = \left(\frac{z - 1}{n_1 + N}\right)^N \frac{(n_1 + N)!}{n_1!} . \tag{2.13}$$

After the polymer is placed on the lattice, there is only one way to add the remaining solvent molecules. The net entropy of mixing will be given by

$$\Delta S_{mix} = S(n_1, N) - S(n_1, 0) - S(0, N) . \tag{2.14}$$

Since $S = k \ln \Omega$, and by employing Stirling's approximation for the factorials, $x! = x \ln x - x$, the result,

$$\Delta S_{mix} = -k n_1 \ln(1 - \phi) , \tag{2.15}$$

is obtained, where $(1 - \phi) = \frac{n_1}{n_1 + N}$ is the volume fraction of the solvent, and z, the lattice coordination number, has disappeared.

To calculate ΔS_{el}, consider an ensemble of ν Gaussian chains. In the ideal state the probability ω_i of a chain end occurring in a spherical shell a distance r from the center of the polymer is

$$\omega_i = \left[\frac{3}{2\pi\langle r_o^2\rangle}\right]^{3/2} e^{-\frac{3r^2}{2\langle r_o^2\rangle}} 4\pi r^2 dr \ . \tag{2.16}$$

After an isotropic expansion (or contraction) by the factor α, the distribution is still Gaussian except that the mean is increased by a factor α. Looking at the expansion in another way, a chain ending between r and r + dr after expansion corresponds to a chain originally having an end in the spherical shell at $4\pi r^2 dr/\alpha^3$. The number of chains in the ensemble after such expansion (or contraction) with an end between r and r + dr is then

$$\nu_i = \nu\left[\frac{3}{2\pi\langle r_o^2\rangle}\right]^{3/2} e^{-\frac{3r^2}{2\langle r_o^2\rangle\alpha^2}} 4\pi\frac{r^2 dr}{\alpha^3} \ . \tag{2.17}$$

The number of distinguishable configurations Ω_{el} will be given by the product of ω_i for each configuration, $\prod_i \omega_i^{\nu_i}$, times the number of permutations of the chains over the various configurations, $\nu!\prod_i \frac{1}{\nu_i!}$.

Therefore,

$$\Omega_{el} = \nu!\prod_i \frac{\omega_i^{\nu_i}}{\nu_i!} \ , \tag{2.18}$$

and

$$\begin{aligned}\Delta S_{el} &= k \ln \Omega_{el} \\ &= k\sum_i \nu_i \ln\frac{\nu\omega_i}{\nu_i} \ ,\end{aligned} \tag{2.19}$$

again, obtained by using Stirling's approximation for the factorials. Substituting for ω_i and ν_i, converting the sum over i to an integral

over r, and setting $\nu = 1$, since we are considering only one chain, yields the final result,

$$\Delta S_{el} = k\left[\frac{3}{2}(1 - \alpha^2) + 3\ln\alpha\right] . \tag{2.20}$$

This expression has its maximum value at $\alpha = 1$.

We can now combine these results to write an expression for the net free energy of a polymer chain in solution,

$$\Delta F = \Delta H_{mix} - T\Delta S_{mix} - T\Delta S_{el} , \tag{2.21}$$

or

$$\frac{\Delta F}{kT} = n_1 \ln(1 - \phi) + \chi n_1 \phi + \frac{3}{2}\alpha^2 - 3\ln\alpha . \tag{2.22}$$

The segment concentration was assumed constant within the polymer chain in calculating the heat and entropy of mixing. However, under most solvent conditions the polymer has a loose coil configuration, with a greater segment density at the center. Equation 2.22 should then be written,

$$\frac{\Delta F}{kT} = \int_0^\infty [\ln[1 - \phi(r)] + \chi\phi(r)]dn_1(r) + \frac{3}{2}\alpha^2 - 3\ln\alpha , \tag{2.23}$$

where

$$dn_1(r) = \frac{[1 - \phi(r)]4\pi r^2 dr}{V_1} . \tag{2.24}$$

We assume that the segment density obeys a Gaussian distribution and write

$$\phi(r) = V_P\left[\frac{3}{2\pi\langle r_o^2\rangle\alpha^2}\right]^{3/2} e^{-\frac{3r^2}{2\langle r_o^2\rangle\alpha^2}} . \tag{2.25}$$

For ϕ small, the logarithm in the integral can be expanded. Keeping

terms to third order in ϕ, and performing the integration yields the result,

$$\frac{\Delta F}{kT} = N\left[(\chi - 1) + \frac{(\frac{1}{2} - \chi)\omega}{2^{3/2}\alpha^3} + \frac{\omega^2}{2\cdot 3^{5/2}\alpha^6}\right] + \frac{3}{2}\alpha^2 - 3\ln\alpha \ , \qquad (2.26)$$

where

$$\omega = V_P\left[\frac{3}{2\pi\langle r_o^2\rangle}\right]^{3/2} = (\frac{9}{\pi})^{3/2}N^{-1/2}w^2 \ . \qquad (2.27)$$

The third-order term in the expansion partially accounts for ternary interactions among segments.

In Figure 2.1 the free energy, $\frac{\Delta F}{kT}$, is plotted as a function of the expansion factor α for several values of χ and for three different values of the flexibility. The minimum in the curve for a particular value of χ determines the value of α corresponding to the equilibrium state. When there are two minima, the lower determines the equilibrium state.

There is a qualitative difference in the curves for different values of the flexibility. The difference is made clear in Figure 2.2, which is a plot of the equilibrium expansion-factor versus flexibility for successive values of χ, obtained by finding numerically the value of α that minimizes the free energy of mixing for particular values of χ and w. These curves resemble the isotherms of van der Walls gas. The figure should be interpreted by considering, for a fixed value of the flexibility, the corresponding value of the expansion factor while χ varies from right to left, which is equivalent to lowering the temperature. If w is large (a flexible

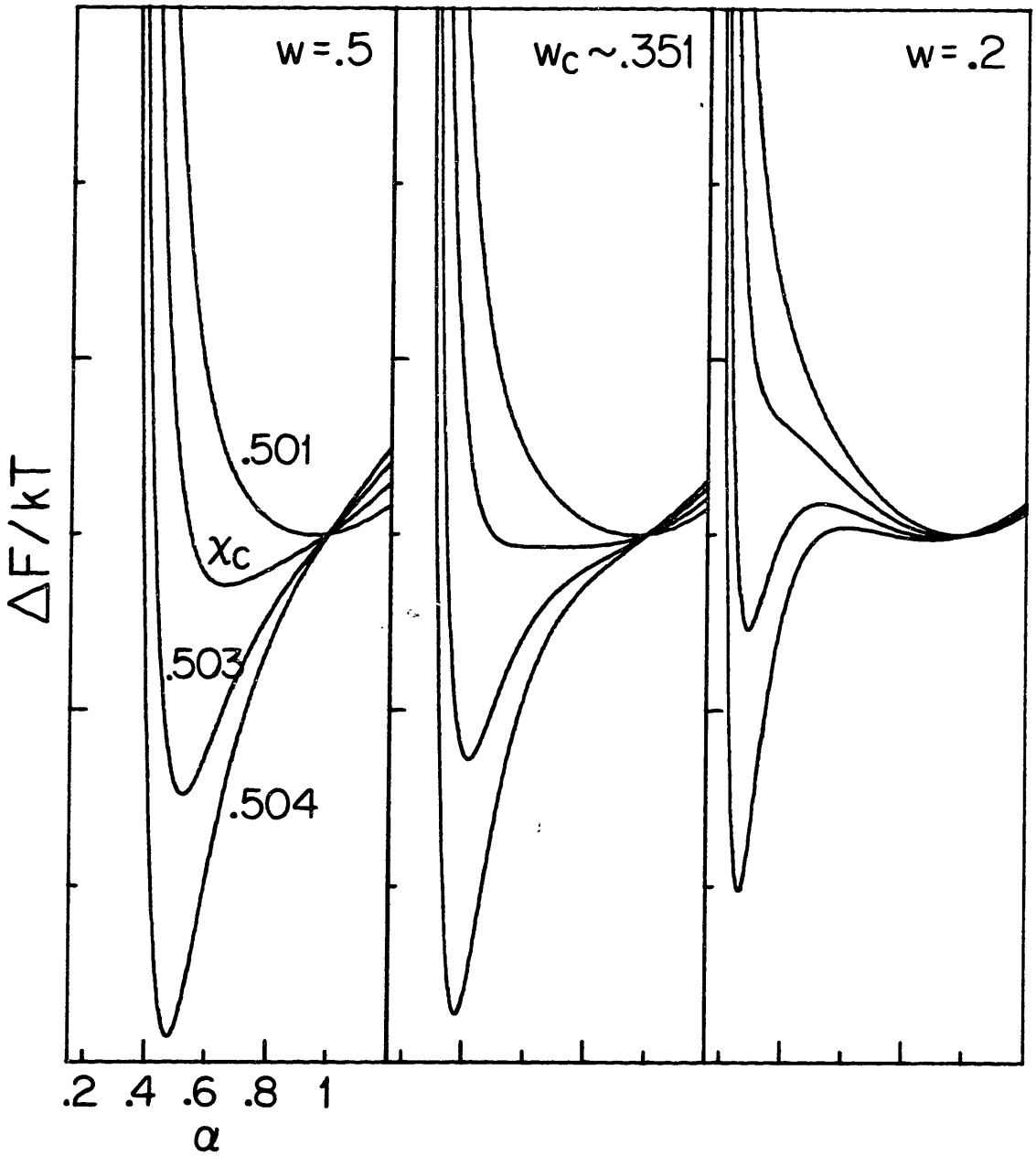

Figure 2.1 Free Energy Function for a Single Polymer. The equilibrium size of the polymer corresponds to the value of α at the free energy minimum. The curves are for successive values of χ corresponding to temperatures below Θ, with $\chi_c = 0.50256$. The parameter N is 200,000. The flexibility is above, at, and below the critical flexibility w_c in the left, center, and right figures. The free energy is offset to 0 at $\alpha = 1$ for each curve.

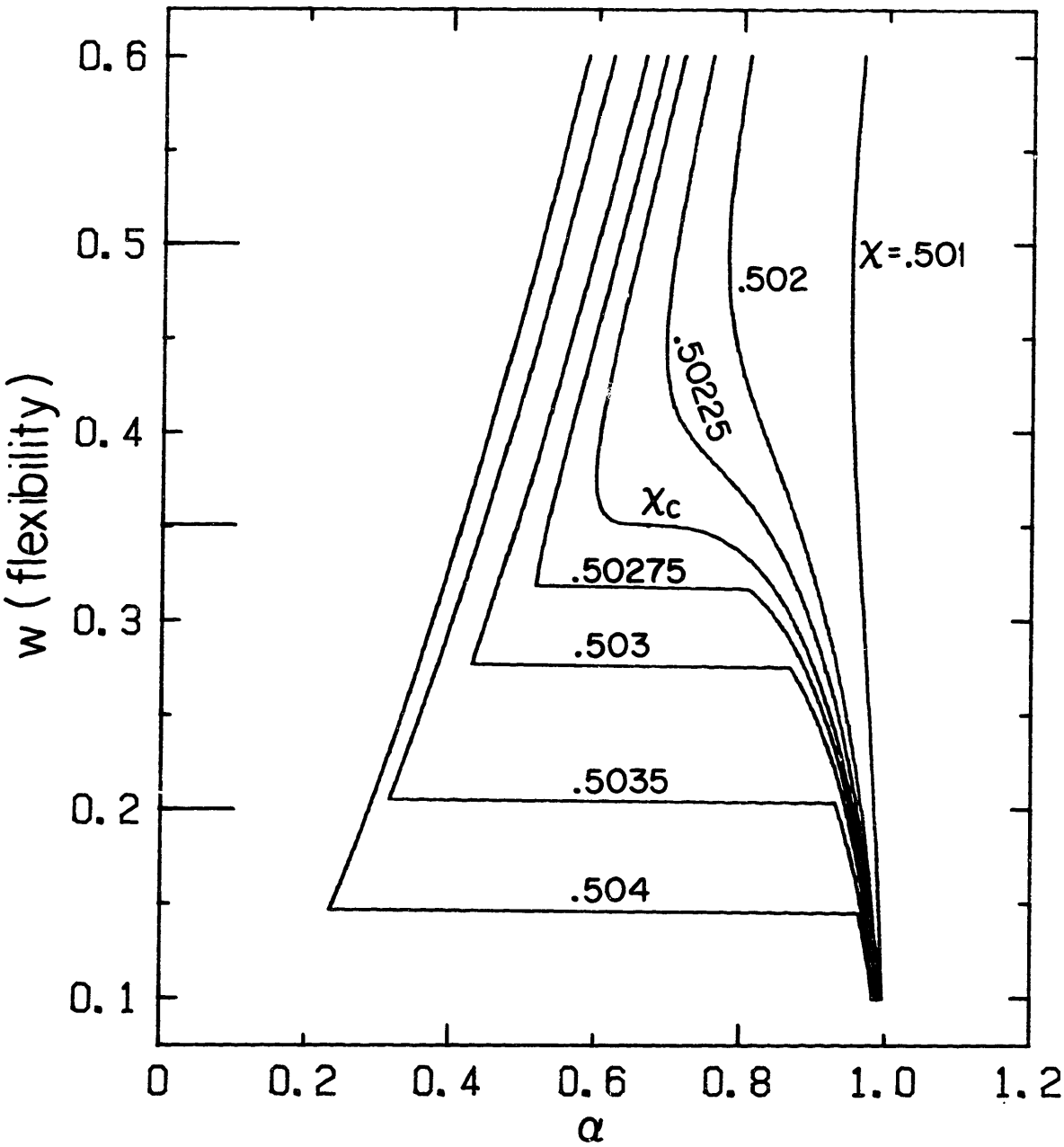

Figure 2.2 Effect of Chain Flexibility on Equilibrium Size. Each curve is for a fixed value of χ, with the same value of N as in Figure 2.1. Traveling from right to left for fixed w corresponds to decreasing the temperature -- α changes abruptly for w below w_c. The extended tick marks on the left correspond to the flexibilities plotted in Figure 2.1.

chain), the expansion factor decreases smoothly. If w is small (a stiff chain), the transition while χ is varied becomes discontinuous, and the equilibrium state of the polymer changes discretely from expanded coil to collapsed globule. The critical value w_c separates the smooth from the discontinuous transition.

An explicit equation for the expansion factor is obtained by differentiating the expression for the free energy (Equation 2.26) with respect to α, and requiring the result be equal to zero, since the equilibrium value for α corresponds to a minimum. The result is

$$\alpha^5 - \alpha^3 - \frac{y}{\alpha^3} = z \ , \tag{2.28}$$

where

$$y = \frac{3^{7/2}}{\pi^3} w^4 \ , \tag{2.29}$$

and

$$z = \left(\frac{9}{2\pi}\right)^{3/2} \left(\frac{1}{2} - \chi\right) N^{1/2} w^2 \ . \tag{2.30}$$

Equation 2.28 is a key result of this derivation. Several other theoretical approaches to the coil-globule transition, some of which are described below, lead to results of the same form.

Figure 2.3 is a plot of α as a function χ according to Equation 2.28 for w above, at, and below w_c for a narrow range of χ. When there are 2 real roots to the equation, the root corresponding to the lower value of the free energy expression, Equation 2.26, is used.

Several predictions can made from Equation 2.28. First, for polymer-solvent solutions of identical chemical composition, but with

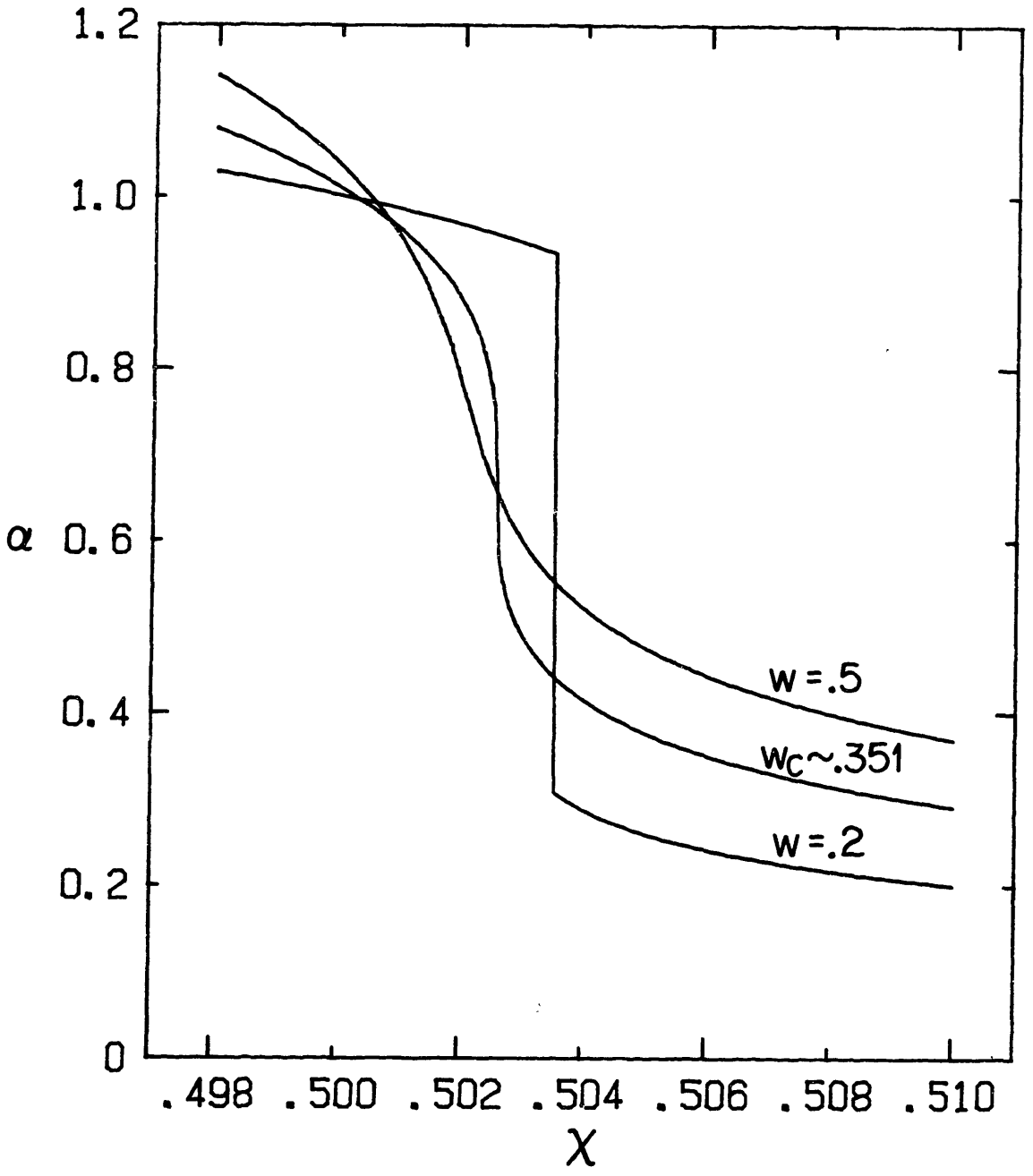

Figure 2.3 Expansion Factor vs. Interaction parameter. The same values of w and N are used as in Figure 2.1. Values of $\chi < 0.5$ correspond to temperature above θ. For a stiff chain, there is a discrete collapse.

polymers of different molecular weight, the expansion factor vs. temperature curves will be identical if the reduced temperature is scaled by the square root of the molecular weight. The asymptotic behavior of the expansion factor can be obtained from Equation 2.28. In the expanded coil state with $\alpha \gg 1$,

$$\begin{aligned} \alpha &\sim N^{1/10}\left(1 - \frac{\Theta}{T}\right)^{1/5} \\ r &\sim N^{3/5}\tau^{1/5} , \end{aligned} \qquad T \gg \Theta \qquad (2.31)$$

where $\tau = (1 - \Theta/T)$ is the reduced temperature, and r is a characteristic polymer dimension. In the globule state with $\alpha \ll 1$,

$$\begin{aligned} \alpha &\sim N^{-1/6}\left(1 - \frac{\Theta}{T}\right)^{-1/3} \\ r &\sim N^{1/3}\tau^{-1/3} \end{aligned} \qquad T \ll \Theta \qquad (2.32)$$

At the critical point, the function $y(\alpha) = \alpha^8 - \alpha^5 - z\alpha^3$ (nearly the function plotted in Figure 2.2) has an inflection point, and both the first and second derivatives vanish. Taking the derivatives and solving the resulting two equations yields,

$$\begin{aligned} \alpha_c &= \left(\frac{9}{20}\right)^{1/2} \sim 0.671 \\ y_c &= \frac{1}{4}\alpha_c^6 \sim 0.0228 \\ w_c &= \left(\frac{\pi^3 y_c}{3^{7/2}}\right)^{1/4} \sim 0.351 \\ \chi_c &= \frac{1}{2} + \frac{2^{9/2}}{5 \cdot 3^{5/4}} N^{-1/2} \sim 0.5 + 1.15 N^{-1/2} \end{aligned} \qquad (2.33)$$

In this model, whether the transition between coil and globule is first order (discontinuous), second order (continuous through the critical point), or smooth depends only on the flexibility of the

chain. The critical temperature,

$$T_c \sim \Theta\left[1 - \frac{1.15}{\psi N^{1/2}}\right]^{-1} , \tag{2.34}$$

approaches the ideal temperature Θ as $N \to \infty$.

2.4. Bulk Modulus and Compressibility

The isothermal bulk modulus K_T of a single polymer in solution can be defined just as for a gel [2],

$$K_T = \phi \left(\frac{\partial \pi}{\partial \phi}\right)_T , \tag{2.35}$$

where π is the osmotic pressure of the polymer coil. The osmotic pressure is,

$$\pi = -\frac{1}{V_1}\frac{\partial \Delta F}{\partial n_1} = -\frac{1}{V_1}\frac{\partial \Delta F}{\partial \phi}\frac{\partial \phi}{\partial n_1} \tag{2.36}$$

Since,

$$\frac{\partial \phi}{\partial n_1} = \frac{\partial}{\partial n_1}\left[\frac{V_P}{V_P + n_1 V_1}\right] = -\phi^2 \frac{V_1}{V_P} = -\frac{\phi^2}{N} , \tag{2.37}$$

the osmotic pressure becomes,

$$\pi = \frac{\phi^2}{V_1 N}\frac{\partial \Delta F}{\partial \phi} . \tag{2.38}$$

Using Equation 2.26 for the free energy of the single polymer yields,

$$\pi = \frac{kT N \phi_o}{V_P}\left[N\left[\frac{(\frac{1}{2} - \chi)\omega}{2^{3/2}\alpha^2} + \frac{\omega^2}{2 \cdot 3^{5/2}\alpha^3}\right] - \frac{1}{\alpha^{1/3}} + \frac{1}{\alpha}\right] , \tag{2.39}$$

where

$$\alpha^3 = \frac{\phi_o}{\phi} . \tag{2.40}$$

Since

$$\phi_o \sim \frac{V_P}{\langle r_o^2 \rangle^{3/2}} \, . \tag{2.41}$$

the bulk modulus is then given by,

$$K_T \sim \frac{kT}{\langle r_o^2 \rangle^{3/2}} \left[N \left[\frac{(\frac{1}{2} - \chi)\omega}{2^{1/2}\alpha^6} + \frac{\omega^2}{3^{3/2}\alpha^9} \right] - \frac{1}{3\alpha} + \frac{1}{\alpha^3} \right] \, . \tag{2.42}$$

The isothermal compressibility, κ_T, of the coil is the inverse of the bulk modulus and is plotted in Figure 2.4. At the critical flexibility, the compressibility diverges.

2.5. Similar Theories

Setting y = 0 in Equation 2.28 yields Flory's result for the expansion factor of a single polymer in a good solvent [1]. Strangely enough, however, Flory never considers the implications of his equations in the poor solvent regime, well below the Θ temperature. He seemed convinced that the onset of interpolymer aggregation would prevent the complete collapse of single molecules. Apparently the first to consider the regime with $\alpha < 1$ were Ptitsyn and Eizner in 1965 [3]. They obtained an equation with the same form as Equation 2.28 by modeling the polymer as a van der Walls gas of non-interacting segments, and adding the Flory rubber elasticity terms. Later, Eizner [4] presented a derivation in the same form as that presented in this chapter for the free energy of a Gaussian coil, and in addition, carried through the calculations for a homogeneous sphere, a model more appropriate for the globule state. For this latter model, the form obtained for Equation 2.28 is identical, but the numerical coefficients vary.

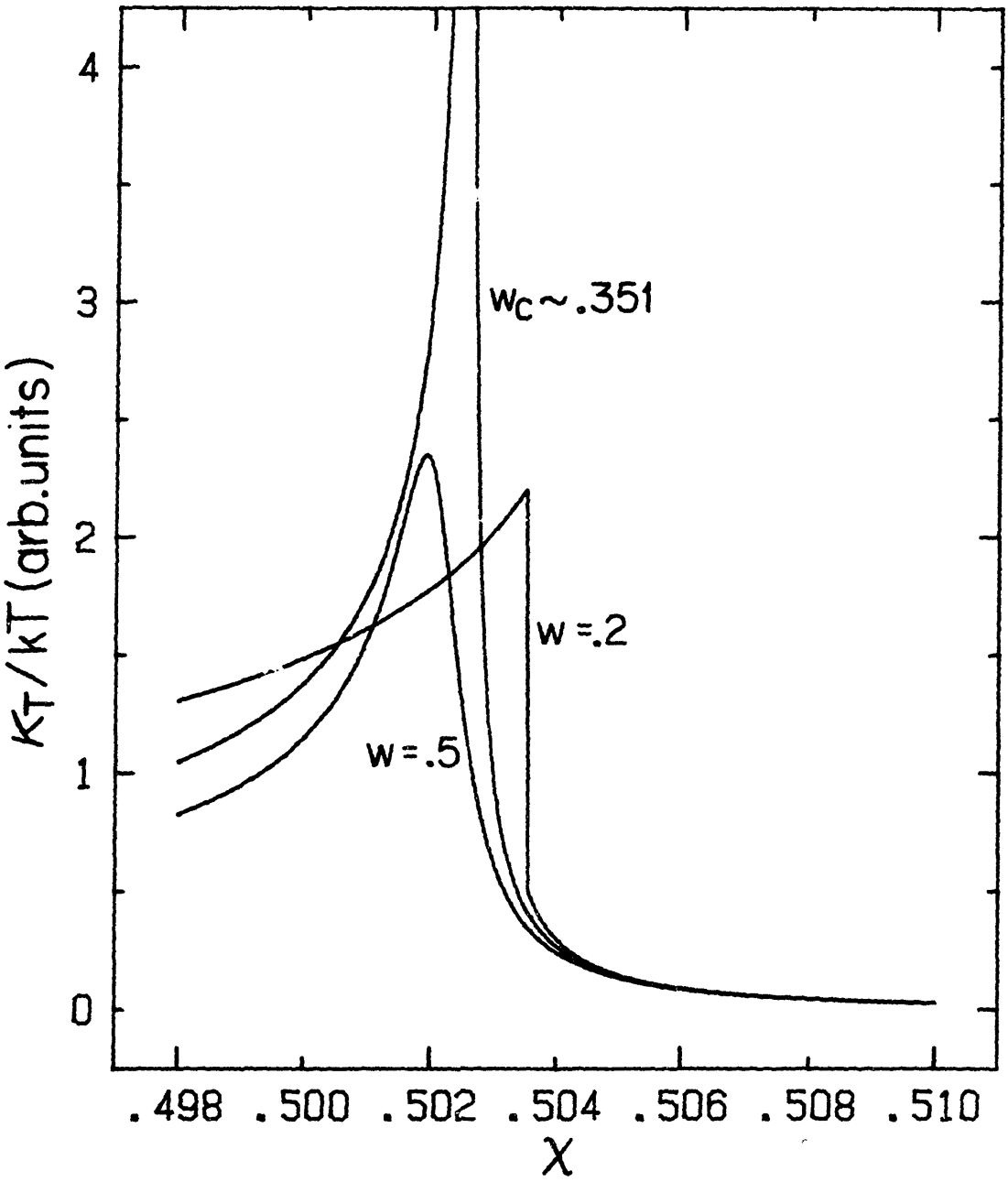

Figure 2.4 Compressibility of a Single Polymer. The three curves correspond to the same values of the flexibility as in Figures 2.1 and 2.3. The compressibility diverges at χ_c for $w = w_c$.

In the theory presented above, ternary interactions appear only in the entropy terms. Post and Zimm [5], appended this theory for the Gaussian coil with consideration of ternary interactions in the heat of mixing term. The resulting corrections slightly increase the expansion factor in the globule state. The added terms, however, retain the lattice coordination number as a parameter.

References

1. P.J. Flory, Principles of Polymer Chemistry, Cornell University Press, Ithaca (1953).

2. T. Tanaka, S. Ishiwata, and C. Ishimoto, "Critical behavior of density fluctuations in gels", Phys. Rev. Lett. 38(14) pp. 771-774 (1977).

3. O.B. Ptitsyn and Y.Y. Eizner, "Theory of globule to coil transitions in macromolecules", Biofizika 10(1) pp. 3-6 (1965).

4. Y.Y. Eizner, "Globule-coil transitions in homogeneous macromolecules", Vysokomol. Soyed. A11(2) pp. 364-371 (1969).

5. C.B. Post and B.H. Zimm, "Internal condensation of single DNA molecule", Biopolymers 18 pp. 1487-1501 (1979).

CHAPTER 3

LIGHT SCATTERING THEORY

3.1. Introduction

Expressions for the expansion factor and compressibility of a single polymer chain in dilute solution were derived in the previous chapter. This chapter is concerned with the physical basis for the measurement of these quantities. The technique of dynamic light-scattering provides the means to determine not only the average dimensions of the individual molecules, but also the internal dynamics of single molecules. The internal dynamics will be shown to be directly related to the compressibility.

3.2. Light Scattering

Like all scattering experiments, light scattering involves shooting a well-characterized probe (laser-generated photons) into the system under study and determining the response (or state) of the system by measuring the alterations in the probe. In general, the interaction can be an exchange of energy or momentum. In the type of light scattering experiments performed in this work, the interaction is the quasi-elastic scattering of the incident photons by density fluctuations in the polymer solution. The energy shift implied by the "quasi" is due solely to the doppler shift imposed on the light by the motion of the density fluctuations.

3.2.1. The Scattered Field

The coordinate system used in the following discussion, based on the geometry of the light scattering apparatus described in the next chapter, is shown in Figure 3.1. The incident electric field, $\vec{E}_o$, consists of plane waves polarized in the +z direction. The scattered field is detected in the direction θ at a point $\vec{R}$, distant compared to the dimensions of the scattering volume. We consider only scattering in the x-y plane. The familiar solution to Maxwell's equations for the scattered electric field at the point $\vec{R}$ is [1]

$$\vec{E}_s(\vec{R},t) = \frac{e^{ik_oR}}{4\pi R\epsilon_o}\vec{k}_s\times[\vec{k}_s\times\int_V \delta\epsilon(\vec{r},t)\vec{E}_o(\vec{r},t)e^{-i\vec{k}_s\cdot\vec{r}}d^3\vec{r}] \ . \qquad (3.1)$$

The scattering is from inhomogeneities in the scattering medium that has a dielectric constant

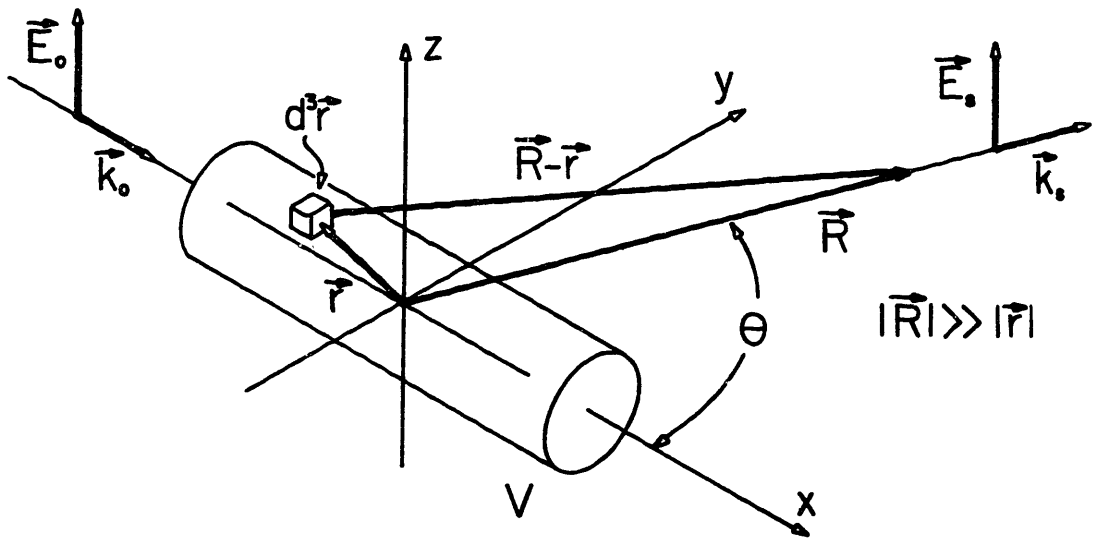

Figure 3.1 Scattered Field Geometry. The incident field consists of plane waves polarized in the $+\hat{z}$ direction. The scattered field is detected in the direction θ at a point $\vec{R}$ that is much farther from the origin than the dimensions of the scattering volume V.

$$\varepsilon(\vec{r},t) = \varepsilon_0 + \delta\varepsilon(\vec{r},t) \ . \qquad (3.2)$$

It is assumed the medium is isotropic, and the fluctuations $\delta\varepsilon(\vec{r},t)$ are small compared to ε_0. The laboratory scattering angle θ defines the direction of the scattered field wave vector, $\vec{k}_s$. The integration is over the scattering volume, V.

We write the explicit $\vec{r}$ and t dependence of the incident field, $\vec{E}_0 = E_0 e^{i(\vec{k}_0\cdot\vec{r} - \omega t)}\hat{z}$, and introduce the scattered wave vector $\vec{k}$, (see Figure 3.2), where $\vec{k} = \vec{k}_i - \vec{k}_s$. The scattered field amplitude is then given by

$$E_s(\vec{R},t) = \frac{E_0 k_s^2 e^{i(k_s R - \omega t)}}{4\pi R\varepsilon_0} \int_V \delta\varepsilon(\vec{r},t) e^{-i\vec{k}\cdot\vec{r}} d^3\vec{r} \ . \qquad (3.3)$$

The integral is the spatial Fourier transform of the dielectric fluc-

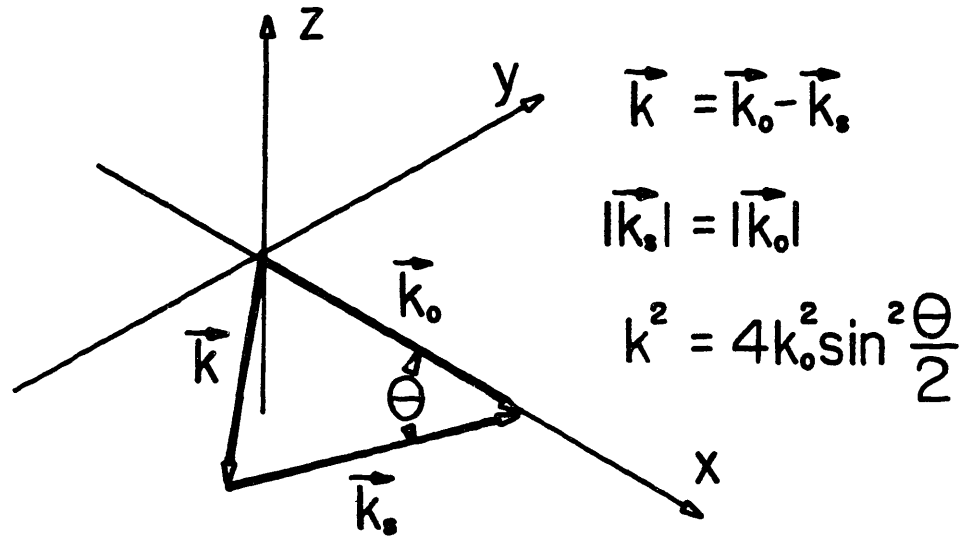

Figure 3.2 The Scattered Wave Vector. For elastic scattering, the magnitude of the scattered wave vector $\vec{k}_s$ is the same as the incident wave vector $\vec{k}_0$. The length of $\vec{k}$ is then determined by the law of cosines, where $k_0 = 2\pi n/\lambda$, with n the refractive index of the medium and λ the vacuum wavelength of the incident beam.

tuations,

$$\delta\varepsilon(\vec{k},t) = \int_V \delta\varepsilon(\vec{r},t)e^{-i\vec{k}\cdot\vec{r}}d^3\vec{r} \ , \tag{3.4}$$

meaning that only fluctuations with wave vector $\vec{k}$ contribute to the scattered field. Fluctuations of different length scales can be probed by changing $|\vec{k}|$, generally by varying the scattering angle θ.

3.2.2. Correlation Function

The dynamic properties of polymers in the solution are revealed through analysis of the temporal behavior of the scattered field. Although over a long time the amplitude of the scattered field is random, since it reflects the random thermal fluctuations of the scattering medium, at sufficiently short intervals there can be self-correlation. A suitable measure is the normalized first-order auto-correlation function of the scattered electric field,

$$g^{(1)}(t) = \frac{\langle E_s(0)E_s^*(t)\rangle}{\langle|E_s(0)|^2\rangle} \ . \tag{3.5}$$

where the brackets mean a time average. The process responsible for the fluctuations in dielectric is assumed to be a stationary, allowing the time origin to be chosen arbitrarily. By the ergodic hypothesis the time average, which can be measured, is identical to the ensemble average.

In the self-beating, or homodyne, light-scattering method employed in these experiments, the correlation function of the scattered light intensity is measured, since the photocathode of the photomultiplier is a square law detector. The second-order correlation

function of the scattered field is therefore required,

$$g^{(2)}(t) = \frac{\langle E_s(0)E_s^*(0)E_s(t)E_s^*(t)\rangle}{\langle|E_s(0)|^2\rangle^2} . \tag{3.6}$$

This expression can be simplified by assuming the process responsible for the temporal fluctuations in the scattered field is a Gaussian random process, and the scattered field obeys Gaussian statistics. The factorization property of a multi-dimensional Gaussian distribution of, say, four functions A, B, C, and D, each a function of the same set of Gaussian random variables, asserts that the correlation function $\langle ABCD\rangle$ can be expressed as

$$\langle ABCD\rangle = \langle AB\rangle\langle CD\rangle + \langle AC\rangle\langle BD\rangle + \langle AD\rangle\langle BC\rangle . \tag{3.7}$$

Applying this property to Equation 3.6 yields,

$$\begin{aligned} g^{(2)}(t) &= \frac{\langle E_s(0)E_s^*(0)\rangle\langle E_s(t)E_s^*(t)\rangle + \langle E_s(0)E_s^*(t)\rangle\langle E_s(t)E_s^*(0)\rangle}{\langle|E_s(0)|^2\rangle^2} \\ &= 1 + |g^{(1)}(t)|^2 . \end{aligned} \tag{3.8}$$

The form of the measured correlation function varies slightly because of optical geometry (or diffraction) effects and the digital nature of photoelectron generation within the detector. The result for the measured correlation function is,

$$C(t) = \langle n\rangle^2[1 + f(A)|g^{(1)}(t)|^2] , \tag{3.9}$$

where $\langle n\rangle = o(\Delta\tau)\langle|E_s(0)|^2\rangle$ is the average photo-count rate to the correlator, with o related to the quantum efficiency of the detector

and $\Delta\tau$ is the sampling interval of the correlator. The quantity, f(A), is the spatial coherence factor, directly related to the number of coherence areas illuminated at the detector surface. The coherence area is the size of the Airy disk in the diffraction pattern of the illuminated volume at the detector.

There are two terms neglected in Equation 3.9. One is the shot-noise term, originating in the very short time correlation within the electron bunches generated in the photomultiplier. This is nearly a δ-function at $t = 0$ and does not appear in the measured correlation function at the sampling intervals used in these experiments. Another term is related to the fluctuations in number density within the scattering volume. Although our solutions were dilute, the concentration was high enough to make this term negligible.

3.2.3. Diffusion Coefficient

What are the fluctuations in dielectric responsible for the fluctuations in the scattered electric field? On a length scale that encompasses the entire macromolecule, the fluctuations can be pictured to arise from the buffeting of the polymer molecules by the much smaller, thermally agitated solvent molecules. The local fluctuations in the dielectric constant are directly proportional to the fluctuating presence or absence of polymer. The Onsager regression hypothesis [2,3] justifies use of the diffusion equation to describe the decay of the local concentration fluctuations, $\delta c(\vec{r},t)$,

$$\frac{\partial \delta c(\vec{r},t)}{\partial t} = D\nabla^2 \delta c(\vec{r},t) \ , \qquad (3.10)$$

where D is the diffusion coefficient. Using the proportionality, $\delta\varepsilon(\vec{r},t) \propto \delta c(\vec{r},t)$, the diffusion equation can be written,

$$\frac{\partial \delta\varepsilon(\vec{r},t)}{\partial t} = D\nabla^2 \delta\varepsilon(\vec{r},t) \ . \tag{3.11}$$

Taking the spatial Fourier transform of this equation yields the solution,

$$\delta\varepsilon(\vec{k},t) = \delta\varepsilon(\vec{k},0)e^{-Dk^2t} \ . \tag{3.12}$$

The fluctuations with wave vector $\vec{k}$ decay with time constant $\tau = 1/Dk^2$.

The Einstein formula relates the diffusion coefficient of a particle in solution to the thermal energy k_BT, and a friction factor f appropriate to the particle in the solvent,

$$D = \frac{k_BT}{f} \ . \tag{3.13}$$

For a spherical particle, Stoke's law states,

$$f = 6\pi\eta R_H \ , \tag{3.14}$$

where η is the solvent viscosity, and R_H is the radius of the particle. For an expanded polymer coil in solution, R_H is identified as a generalized hydrodynamic radius with a complicated and not well-understood relation to the actual polymer configuration.

Finally, combining Equation 3.3 for the scattered field, Equation 3.9 for the measured correlation function, and Equation 3.12, the solution to the diffusion equation, results in

$$C(t) = \langle n \rangle^2 [1 + f(A)e^{-2Dk^2 t}] . \qquad (3.15)$$

The quantity $\langle n \rangle^2$ is the "baseline" of the correlation function (the average intensity) and is measured directly by the correlator instrument, while f(A) and the quantity $2Dk^2$ are determined by fitting the data to an exponential function. Normally, $g^{(1)}(t)$ is composed of a sum or distribution of exponentials, reflecting the non-monodispersity of the scattering particles or fluctuations. Thus there are several fitting procedures used for C(t), each appropriate to the a priori assumed distribution. Some fitting techniques are described in Appendix A.

3.2.4. Static Properties

To determine static properties, only the time-averaged value of the intensity of the scattered field and its dependence on $\vec{k}$ is measured. Such a measurement gives information on the mass distribution of the scattering particles, and hence, the radius of gyration. The difference between the polarizability of each mass element of the scatterer (monomeric segment) and the surrounding medium causes the scattering. When the path difference for light scattered from different parts of the molecule to the detector becomes a significant fraction (~1/20) of λ, destructive interference results in decreased intensity. Thus the angular distribution of the scattered light for larger particles is more asymmetric than for smaller particles. Simple shapes such as spheres, rods, or coils can be distinguished experimentally from the precise angular dependence of he scattered light.

The average scattered intensity, as a function of $\vec{k}$, is, from Equation 3.3,

$$I(\vec{k}) = \langle E_s(\vec{k},t)E_s^*(\vec{k},t)\rangle$$
$$= \frac{E_o^2 k_s^4}{(4\pi R\varepsilon_o)^2} \left\langle \int_V \int_V \delta\varepsilon(\vec{r}_1)\delta\varepsilon(\vec{r}_2) e^{i\vec{k}\cdot(\vec{r}_1 - \vec{r}_2)} d^3\vec{r}_1 d^3\vec{r}_2 \right\rangle \tag{3.16}$$

The dielectric constant ε is a macroscopic quantity expressing the response of the medium to the electric field. To evaluate the double integral we use a microscopic model for the scattering particles. The appropriate microscopic quantity is the excess polarizability α of each monomeric segment of the polymer over that of the surrounding solvent. Macroscopic electrodynamics shows ε and α are related as,

$$\varepsilon = 1 + 4\pi\alpha \ . \tag{3.17}$$

Thus

$$\delta\varepsilon(\vec{r}) = 4\pi\alpha \sum_{l=1}^{n} \sum_{i=1}^{N} \delta(\vec{r} - \vec{r}_i^{\,l}) \ , \tag{3.18}$$

where the δ-function locates the i^{th} segment of the 1^{th} molecule in the scattering volume and the sums are over the N segments of the n molecules, each segment having identical polarizability, α. The integrals in Equation 3.16 can then be transformed into sums,

$$I(\vec{k}) = \frac{E_o^2 k_s^4}{R^2 \varepsilon_o^2} \alpha^2 \left\langle \sum_{l=1}^{n} \sum_{k=1}^{n} \sum_{i=1}^{N} \sum_{j=1}^{N} e^{-i\vec{k}\cdot(\vec{r}_i^{\,l} - \vec{r}_j^{\,k})} \right\rangle \ . \tag{3.19}$$

The polymer solution is considered sufficiently dilute so that there is no spatial correlation among different molecules. Thus the terms $e^{i\vec{k}\cdot(\vec{r}^{\,l} - \vec{t}^{\,k})}$ average to zero for $l \neq k$. Then,

$$I(\vec{k}) = \frac{E_o^2 k_s^4}{R^2 \varepsilon_o^2} \langle n \rangle \alpha^2 \langle \sum_{i=1}^{N} \sum_{j=1}^{N} e^{-i\vec{k}\cdot(\vec{r}_i - \vec{r}_j)} \rangle , \tag{3.20}$$

where $\langle n \rangle$ is simply the average number of molecules in the scattering volume.

Let us first consider scattering at low angles with $|\vec{k}\cdot\vec{r}| \ll 1$. Then the exponential can be expanded,

$$I(\vec{k}) = \frac{E_o^2 k_s^4}{R^2 \varepsilon_o^2} \langle n \rangle \alpha^2 \langle \sum_{i=1}^{N} \sum_{j=1}^{N} [1 - k^2 |\vec{r}_i - \vec{r}_j|^2 \cos^2\theta_{ij}] \rangle . \tag{3.21}$$

Averaging over all orientations of $\vec{r}_i - \vec{r}_j$ about $\vec{k}$, the terms in brackets become,

$$\begin{aligned} I(\vec{k}) &= \frac{E_o^2 k_s^4}{R^2 \varepsilon_o^2} \langle n \rangle \alpha^2 [N^2 - k^2 \langle \sum_{i=1}^{N} \sum_{j=1}^{N} |\vec{r}_i - \vec{r}_j|^2 \frac{1}{4\pi} \int_0^{2\pi} d\phi \int_{-1}^{1} \cos^2\theta_{ij} \, d\cos\theta \rangle] \\ &= \frac{E_o^2 k_s^4}{R^2 \varepsilon_o^2} \langle n \rangle \alpha^2 [N^2 - \frac{k^2}{3} \langle \sum_{i=1}^{N} \sum_{j=1}^{N} |\vec{r}_i - \vec{r}_j|^2 \rangle] . \end{aligned} \tag{3.22}$$

The double summation is over a single molecule. Considering the origin at the center of gravity of that molecule and expanding the product,

$$\begin{aligned} \langle \sum_{i=1}^{N} \sum_{j=1}^{N} |\vec{r}_i - \vec{r}_j|^2 \rangle &= \langle \sum_{i=1}^{N} \sum_{j=1}^{N} [|\vec{r}_i|^2 + |\vec{r}_j|^2 - 2\vec{r}_i \cdot \vec{r}_j] \rangle \\ &= 2N \sum_{i=1}^{N} |\vec{r}_i|^2 \end{aligned} \tag{3.23}$$

as the cross terms average to zero.

The radius of gyration, R_G, of a polymer is the root-mean-square distance of the mass elements from molecular center of gravity, expressed as,

$$R_G^2 = \frac{\sum_{i=1}^{N} m_i |\vec{r}_i|^2}{\sum_{i=1}^{N} m_i} = \frac{\sum_{i=1}^{N} |\vec{r}_i|^2}{N} , \tag{3.24}$$

where we consider the mass, m_i, of each segment to be identical. Substituting Equations 3.24 and 3.24 into 3.23 yields

$$I(\vec{k}) = \frac{E_o^2 k_s^2}{R^2 \varepsilon_o^2} \langle n \rangle \alpha^2 N^2 \left[1 - \frac{(kR_G)^2}{3}\right] . \tag{3.25}$$

The factor in square brackets is the molecular structure factor, $S(\vec{k})$, and here is correct for any shape molecule provided $kR_G \ll 1$. Figure 3.3 shows $S(\vec{k})$ in this limiting case. Also plotted are the calculated structure factors [4] for Gaussian coils,

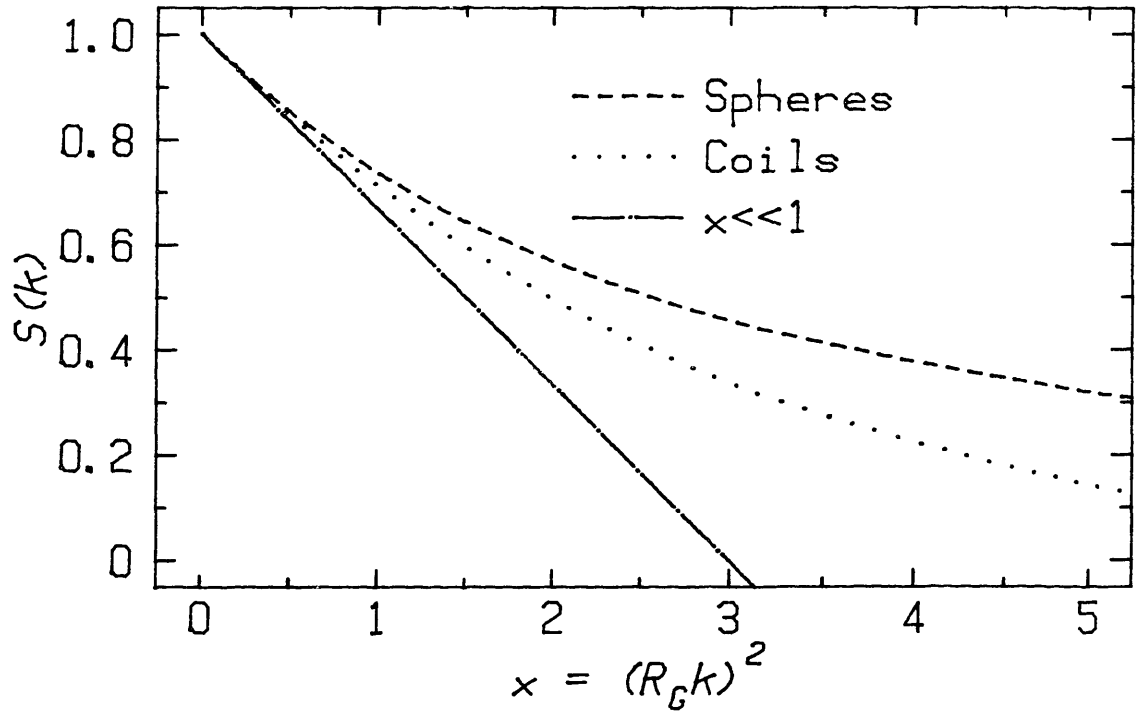

Figure 3.3 Molecular Structure Factors. The molecular structure factor is shown for coils (dashed line), for spheres (dotted line), and in the limit $kR_G \ll 1$ (dashed-dotted line).

$$S(\vec{k}) = \frac{2}{(kR_G)^4}\left[e^{-(kR_G)^2} - 1 + (kR_G)^2\right] , \tag{3.26}$$

and spheres (R is the sphere radius, $R_G^2 = \frac{3}{5}R^2$),

$$S(\vec{k}) = \left[\frac{3}{(kR)^3}\left[\sin(kR) - kR\cdot\cos(kR)\right]\right]^2 . \tag{3.27}$$

By comparing the measured angular dependence of the scattered light intensity to the structure factor, at minimum, the radius of gyration can be determined, and possibly the molecular shape.

3.2.5. Measurement of $S(\vec{k})$

The previous sections show that the angular dependence of the scattered intensity is determined by the size and shape of the dilute polymers in solution. Of course, the measured scattered intensity includes the isotropic background scattering from density fluctuations of the solvent. The classical method for obtaining the excess scattering due solely to the polymer is to subtract the measured intensity of pure solvent from that of solvent plus polymer. For the dilute solutions needed to observe the globule state, the method requiring two separate measurements of the intensity fails. The experimental uncertainty in the value for the net scattered intensity obtained from the difference in the two measurements overwhelms the signal. However, during this work we developed a new method that yields the excess scattering of the solute in dilute solutions from a single measurement.

For a two-component system consisting of solvent and polymer, the first-order correlation function is a sum of two exponentials,

$$g^{(1)}(t) = a_1 e^{-t/\tau_1} + a_2 e^{-t/\tau_2} , \tag{3.28}$$

where component 1 is the solvent and component 2 is the polymer. From Equation 3.9, the measured homodyne correlation function for this system is

$$C(t) = \langle n \rangle^2 \left[1 + f(A) \frac{|a_1 e^{-t/\tau_1} + a_2 e^{-t/\tau_2}|^2}{|a_1 + a_2|^2}\right] . \tag{3.29}$$

Since the solvent molecules are much smaller than the wavelength of the incident light, and the measurements are performed far from the critical point of the solution, a_1 is constant over angle. The structure factor $S(\vec{k})$ is therefore contained in the angular dependence of a_2. Normally $a_1 \ll a_2$, but for solutions as dilute as those required in our experiments $a_1 = a_2$. The relaxation time for diffusion of the solvent molecules is $\sim 10^3$ times shorter than that for the polymers. Since the digital correlator forms the product $I(t)I(t+\Delta\tau)$, where $\Delta\tau$ is the clock time for sampling, and since the clock time is also much greater than τ_1, the first exponential in Equation 3.29 is completely decayed before the first interval begins. In Figure 3.4 Equation 3.29 is plotted for the cases where $a_1 = 0$ and $a_2 = 1$, where $a_1 = 1$ and $a_2 = 0$, and where $a_1 = a_2 = 1$. The open circles represent the observed correlation function.

Extrapolating Equation 3.29 to t = 0 yields,

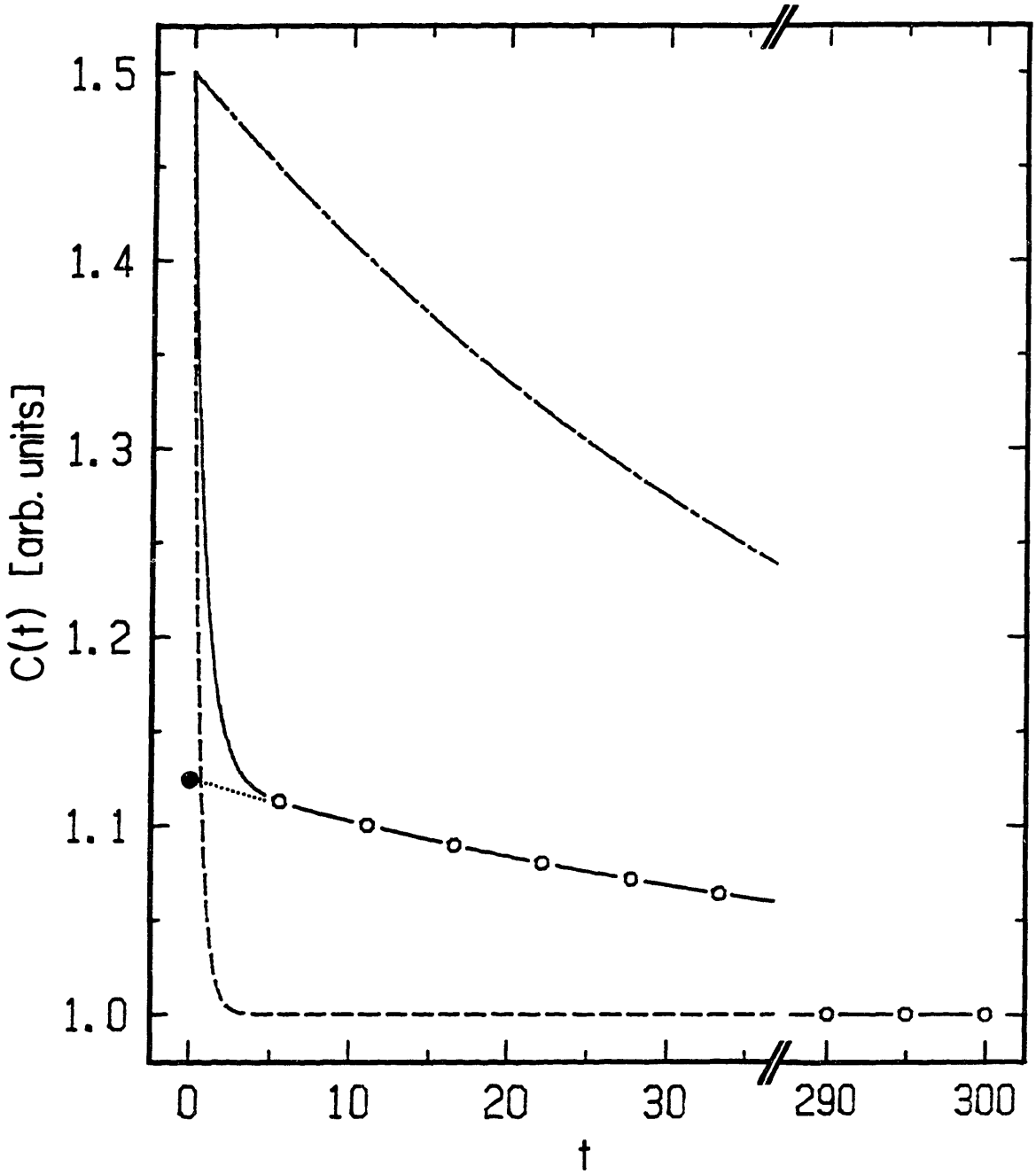

Figure 3.4 Contributions to the Correlation Function. The upper curve is the contribution to the homodyne correlation function from the solute from Equation 3.29 with $f(A) = 0.5$ and $\langle n \rangle^2 = 1$. The lower curve is the contribution from the solvent. The solid line is the combined correlation function when $a_1 = a_2$ and $\tau_1 = \tau_2/100$. The open circles represent the observed data points. The filled circle is the value at $t = 0$ extrapolated from the observed points.

$$C_{OBS}(t\to 0) = \langle n\rangle^2\left[1 + f(A)\frac{a_2^2}{(a_1 + a_2)^2}\right] . \qquad (3.30)$$

This value is represented by the filled circle in the figure. In the limit $t\to\infty$,

$$C_{OBS}(t\to\infty) = \langle n\rangle^2 , \qquad (3.31)$$

which is the measured baseline. Combining the previous two equations algebraically,

$$\frac{C_{OBS}(t\to 0) - C_{OBS}(t\to\infty)}{C_{OBS}(t\to\infty)} = f(A)\frac{a_2^2}{(a_1 + a_2)^2} . \qquad (3.32)$$

Or, in a more useful form,

$$\frac{a_2}{a_1} = \left[\left[\frac{f(A)C_{OBS}(t\to\infty)}{C_{OBS}(t\to 0) - C_{OBS}(t\to\infty)}\right]^{1/2} - 1\right]^{-1} . \qquad (3.33)$$

This equation gives the angular dependence of light scattered from the polymer molecules. The spatial coherence factor, f(A), depends only on the optical geometry of the light scattering apparatus, and can be determined by direct measurement. For a concentrated solution (of latex spheres, for example) with $a_1 \ll a_2$, the ratio formed in Equation 3.30 is just f(A).

This method of determining the static scattering properties only works for dilute solutions. If the net scattering from the solute is much greater than that from solvent, all that will be measured is the spatial coherence factor.

3.3. Internal Motion

The motions of the segments within the polymer molecules result in density fluctuations within the solution just as the translational diffusion of the entire molecule does. The length scale of these fluctuations is, of course, much shorter. At small laboratory scattering angles (small $|\vec{K}|$, large length scale), only the translational diffusion of the macromolecules contributes to the scattering. As the length scale probed is made smaller by going to larger scattering angles, intramolecular fluctuations begin to contribute to the observed correlation function. We now recalculate the temporal correlation function of the dielectric (or density) fluctuations, taking into account the contribution from the internal motion.

For this calculation, we model the polymer molecules as elastic spheres. The elasticity will be characterized by the bulk modulus, K, derived for the Gaussian coil in the previous chapter. We consider the lowest order collective motion of the polymer segments to be adequately modeled by isotropic fluctuations in the radius of the sphere.

Let the equilibrium radius of the sphere be a_0, and the fluctuations in size be given by $a(t) = a_0 + \Delta a(t)$, where $\Delta a(t) \ll a_0$. If $\vec{R}_i(t)$ locates the center of mass of the ith sphere in the scattering volume, then the density distribution is given by

$$\rho(\vec{r},t) = \rho_0 \sum_i H(a_i(t) - |\vec{r} - \vec{R}_i(t)|) \ , \tag{3.34}$$

where H(x) is the unit-step function with $H(x) = 1$ for $x \geq 0$ and is

zero otherwise. The sum is over the particles in the scattering volume. The spatial Fourier transform is

$$\rho(\vec{k},t) = \rho_o \sum_i \int_V H(a_i(t) - |\vec{r} - \vec{R}_i(t)|) e^{i\vec{k}\cdot\vec{r}} d^3\vec{r} \ , \tag{3.35}$$

where the integral is over the scattering volume. We let $\vec{r}_i'(t) = \vec{r} - \vec{R}_i(t)$ and can then write

$$\begin{aligned} \rho(\vec{k},t) &= \rho_o \sum_i e^{-i\vec{k}\cdot\vec{R}_i(t)} \int_V H(r_i'(t) - a_i(t)) e^{i\vec{k}\cdot\vec{r}_i'(t)} d^3\vec{r}_i'(t) \\ &= \rho_o \frac{4\pi a_o^3}{3} \sum_i e^{-i\vec{k}\cdot\vec{R}_i} P(ka_i(t)) \ , \end{aligned} \tag{3.36}$$

where

$$\begin{aligned} P(ka(t)) &= \frac{3}{4\pi a_o^3} \int_V H(r - a(t)) e^{i\vec{k}\cdot\vec{r}} d^3\vec{r} \\ &= \frac{3}{(ka_o)^3} [\sin ka(t) - ka(t) \cos ka(t)] \end{aligned} \tag{3.37}$$

is the dissymmetry factor associated with spherical particles. The temporal density-density correlation function then becomes,

$$\langle \rho(\vec{k},t) \rho^*(\vec{k},0) \rangle = \rho_o^2 \sum_i \sum_j \langle P(ka_i(t)) P(ka_j(0)) e^{i\vec{k}\cdot(\vec{R}_i(t) - \vec{R}_j(0))} \rangle \tag{3.38}$$

The exponential factor is associated with the translational diffusion of the particles. We note there is no correlation among the particles, and none between translational and internal motion. The normalized density-density correlation function is then,

$$\begin{aligned} \frac{\langle \rho(\vec{k},t) \rho^*(\vec{k},0) \rangle}{\langle |\rho(\vec{k},0)|^2 \rangle} &= \frac{\langle P(ka(t)) P(ka(0)) \rangle \langle e^{i\vec{k}\cdot(\vec{R}(t) - \vec{R}(0))} \rangle}{\langle |P(ka_o)|^2 \rangle} \\ &= \frac{\langle P(ka(t)) P(ka(0)) \rangle}{\langle |P(ka_o)|^2 \rangle} e^{-D_o k^2 t} \ , \end{aligned} \tag{3.39}$$

where D_o is the translation diffusion coefficient. Since the

fluctuations in a(t) are small, we can expand P(ka(t)) about ka_0,

$$P(ka(t)) = P(ka_0) + k\Delta a(t)\frac{\partial P(x)}{\partial x}\Big|_{x=ka_0} + \cdots . \tag{3.40}$$

Thus

$$\langle P(ka(t))\,P(ka(0))\rangle = P^2(ka_0) + k^2\langle \Delta a(t)\Delta a(0)\rangle\left[\frac{\partial P(x)}{\partial x}\Big|_{x=ka_0}\right]^2 . \tag{3.41}$$

The final task is to evaluate $\langle \Delta a(t)\Delta a(0)\rangle$. We write it as

$$\langle \Delta a(t)\Delta a(0)\rangle = \langle \Delta a^2(0)\rangle \frac{\langle \Delta a(t)\Delta a(0)\rangle}{\langle \Delta a^2(0)\rangle} \tag{3.42}$$

to evaluate separately the amplitude of the fluctuations and their time dependence. The elastic energy per unit volume, E, for deformation of the sphere is [5]

$$E = \frac{3K}{2}\left(\frac{\Delta a}{a_0}\right)^2 \tag{3.43}$$

where K is the bulk modulus of the material. By the equipartition theorem, the thermal energy per unit volume associated with the fluctuations, Δa, is

$$E = \frac{k_B T/2}{4\pi a_0^3/3} . \tag{3.44}$$

Thus

$$\langle \Delta a^2(0)\rangle = \frac{k_B T}{4\pi a_0 K} \tag{3.45}$$

To evaluate the time dependence of the fluctuations, we write the equation of motion for the elastic sphere in a viscous medium. Let $\vec{u}(\vec{r},t)$ represent the displacement of a point $\vec{r}$ in the particle from its average location at time t. The equation of motion is

$$\rho \frac{\partial^2 u}{\partial t^2} = \vec{\nabla} \cdot \overleftrightarrow{\sigma} - f \frac{\partial u}{\partial t} , \tag{3.46}$$

where ρ is the average density of the sphere, and the last term characterizes the friction force per unit volume within the sphere. We can neglect shear and so define $\overleftrightarrow{\sigma}$, the stress tensor, as $\sigma_{ik} = K u_{ik} \delta_{ik}$ where

$$u_{ik} \equiv \frac{1}{2}\left[\frac{\partial u_k}{\partial x_i} + \frac{\partial u_i}{\partial x_k}\right] . \tag{3.47}$$

The boundary condition requires $\vec{\nabla} \cdot \overleftrightarrow{\sigma} = 0$ at $r = a_o$. We simplify by considering only the lowest order radial mode and write $\vec{u}(\vec{r},t) = u(r)e^{-\Gamma t}\hat{r}$. With such a simplification Equation 3.46 reduces to

$$r^2 \frac{\partial^2 u(r)}{\partial r^2} + 2r \frac{\partial u(r)}{\partial r} + r^2 q^2 u(r) = 0 , \tag{3.48}$$

where

$$q^2 = \frac{f\Gamma - \rho\Gamma^2}{K} . \tag{3.49}$$

Equation 3.48 is the zeroth order spherical Bessel equation. The solution is

$$u(r) = j_o(qr) = \frac{\sin(qr)}{qr} . \tag{3.50}$$

The boundary conditions require $q = n\pi/a_o$, with n an integer. For the lowest mode, n = 1. Solving Equation 3.49 for Γ yields,

$$\Gamma = \frac{f}{2\rho}\left[1 \pm \left(1 - \frac{4Ks^2\rho}{f^2}\right)^{1/2}\right] . \tag{3.51}$$

As with gels [6], the fluctuations within the single polymer are overdamped. The square root can be expanded with the result $\Gamma = K/f$.

Thus,

$$u(t) \sim e^{-\frac{K}{f}\left(\frac{\pi}{a_o}\right)^2 t} \quad . \tag{3.52}$$

Since $\Delta a(t) = u(a_o,t)$,

$$\frac{\langle \Delta a(t)\Delta a(0)\rangle}{\langle \Delta a^2(0)\rangle} = e^{-D_{int}\left(\frac{\pi}{a_o}\right)^2 t} \quad , \tag{3.53}$$

where

$$D_{int} \equiv \frac{K}{f} \quad . \tag{3.54}$$

The final result for the first order correlation function, including internal motion, is then,

$$g^{(1)}(t) = \left[1 + \frac{k_B T}{4\pi a_o^3 K} F(ka_o) e^{-D_{int}\left(\frac{\pi}{a_o}\right)^2 t}\right] e^{-D_o k^2 t} \quad . \tag{3.55}$$

where

$$\begin{aligned} F(x) &= \left[\frac{x}{P(x)} \frac{\partial P(x')}{\partial x'}\bigg|_{x'=x}\right]^2 \\ &= \left(\frac{x^3}{1 - x\cot x} - 3x\right)^2 \end{aligned} \tag{3.56}$$

In the two-exponential form (used in the fits to the experimental correlation functions),

$$g^{(1)}(t) = A_1 e^{-t/\tau_1} + A_2 e^{-t/\tau_2} \quad , \tag{3.57}$$

we have

$$\tau_1^{-1} = D_1 k^2 \quad , \tag{3.58}$$

$$\tau_2^{-1} - \tau_1^{-1} = D_{int}\left(\frac{\pi}{a_o}\right)^2 \quad , \tag{3.59}$$

and

$$\frac{A_2}{A_1} = \frac{k_B T}{4\pi a_o^3 K} F(ka_o) \quad . \tag{3.60}$$

In principle, then, the temperature dependence of the internal segment diffusivity and the bulk modulus (or compressibility) of the individual polymer molecules can be determined from dynamic light scattering.

The friction coefficient, f, is not well understood, so we can not yet predict the temperature dependence of D_{int}. However, that dependence can be given by considering the spatial correlation length ξ of the fluctuations. As Kawasaki [7] originally proved for binary fluid mixtures and Tanaka [8] has shown for gels, the internal diffusivity should be related to ξ in the single polymer as,

$$D_{int} = \frac{k_B T}{6\pi\eta\xi} \quad . \tag{3.61}$$

Except near the critical point, where ξ diverges, the correlation length should be proportional to the amplitude of the fluctuations Δa, determined in Equation 3.45. Therefore

$$D_{int} \sim \frac{(a_o k_B T K)^{1/2}}{\eta} \quad . \tag{3.62}$$

Since the temperature dependence of K has been given using mean-field theory in Chapter 2, the light-scattering determinations of D_{int} can now be compared with predictions. The result of such a comparison is shown in the next chapter.

References

1. L.D. Landau and E.M. Lifshitz, The Classical Theory of Fields, Pergamon Press, Oxford (1975).

2. L. Onsager, "Reciprocal relations in irreversible processes. I.", Phys. Rev. 37 pp. 405-426 (1931).

3. L. Onsager, "Reciprocal relations in irreversible processes. II.", Phys. Rev. 38 pp. 2265-2279 (1931).

4. B.J. Berne and R. Pecora, Dynamic Light Scattering, John Wiley & Sons, New York (1976).

5. L.D. Landau and E.M. Lifshitz, Theory of Elasticity, Pergamon Press, Oxford (1975).

6. T. Tanaka, L.O. Hocker, and G.B. Benedek, "Spectrum of light scattered from a viscoelastic gel", J. Chem. Phys. 59(9) pp. 5151-5159 (1973).

7. K. Kawasaki, "Kinetic equations and time correlation functions of critical fluctuations", Ann. Phys. 61(1) pp. 1-56 (1970).

8. T. Tanaka, "Dynamics of critical concentration fluctuations in gels", Phys. Rev. A 17(2) pp. 763-766 (1978).

CHAPTER 4

EXPERIMENTS AND RESULTS

4.1. Introduction

The investigations of the coil-globule transition that comprise this dissertation consisted of four experiments. The motivation for the initial experiment was provided by Tanaka's [1] observation of a collapse phase transition in macroscopic polyacrylamide gels immersed in a mixed solvent of acetone and water. The phase transition could be induced in these gels by varying either the temperature or the solvent composition. In the first attempt to observe the single polymer collapse [2] we used the same chemical system as the gel, and varied solvent composition, as in most of the gel experiments. After successful observation of the collapse in that system, we pursued the investigation in a simpler system of polymer and single solvent.

The solution used in the other three experiments was polystyrene in cyclohexane. The polystyrene and cyclohexane combination has long been a favorite of polymer chemists, and there is much literature on the properties of the solutions [3]. All that work, though, was for solutions at temperatures in the vicinity of, or greater than the θ-temperature, where the polymer is in the coil state.

In our second experiment (the first with polystyrene) we determined the coexistence curve of the solution in the dilute regime and observed the coil-globule transition in measurements of the

hydrodynamic radius [4]. The third experiment was a determination of the radius of gyration [5] using the method introduced in Chapter 3, while the fourth experiment was a characterization of the intramolecular motion of the single molecules through the transition [6].

4.2. Polyacrylamide in Acetone-Water

In experiments by Tanaka [1], macroscopic gels made of covalently crosslinked polyacrylamide networks immersed in an acetone-water mixtures were observed to undergo a discrete and reversible collapse. The collapse occurred with a change in either the temperature or acetone concentration of the solvent, and the phenomenon was interpreted as a first-order phase transition. Water is a good solvent for polyacrylamide, while acetone is a poor solvent. Variation of the solvent composition is equivalent to changing the interaction parameter χ, introduced in Equation 2.11. At the collapse, the volume of the gel changed by a factor of several hundred. These observations suggested to us a similar transition might be observed in single linear polyacrylamide molecules using light scattering techniques.

The polyacrylamide used in our experiments was of molecular weight $5\text{-}6\times10^6$ (Polysciences -- polydispersity index unknown). A single chain of the polymer contains about 80,000 acrylamide monomers and has a backbone length of about 24μm. In the solutions we used, the concentration of polymer was generally less than 10μg ml^{-1}. At this concentration, the mean distance between adjacent polymers is nearly 1μm, much larger than the average polymer size, thus

preventing interpolymer entanglement and aggregation.

Contamination of the sample solution by dust is always a problem in light scattering, more so for dilute solutions, and especially so for dilute solutions where water is the solvent. Dust scatters light strongly and distorts the correlation function of the light scattered by the polymer molecules. For the measurements, we constructed a device to vary the solvent mixture without adding dust to the sample. The cell holder cap was fitted with two hollow needles. One needle was connected through a 0.4μm filter to a syringe. The other allowed displaced air to escape. The cell was partially filled with an acetone-water mixture or an acetone-water mixture containing the polymer. To vary the solvent composition, a sample solution, pure water or pure acetone, was added through the syringe. The new solvent composition could be determined from the number of drops added. A small magnetic stirring bar which remained in the cell was used to mix the solution.

The correlation function of light scattered from the sample at a 90° angle was measured using a 64-channel clipped correlator (Nicoli Instruments). All measurements were made at 25°C.

The hydrodynamic radius, R_H, was obtained by fitting the correlation function, with methods described in Appendix A, using a second order cumulants expansion with the baseline fixed by the average count rate. The values obtained for R_H are plotted in Figure 4.1. At low acetone concentrations, R_H is large, about 500Å. Near an acetone concentration of 39%, the polymer shows a sharp decrease in

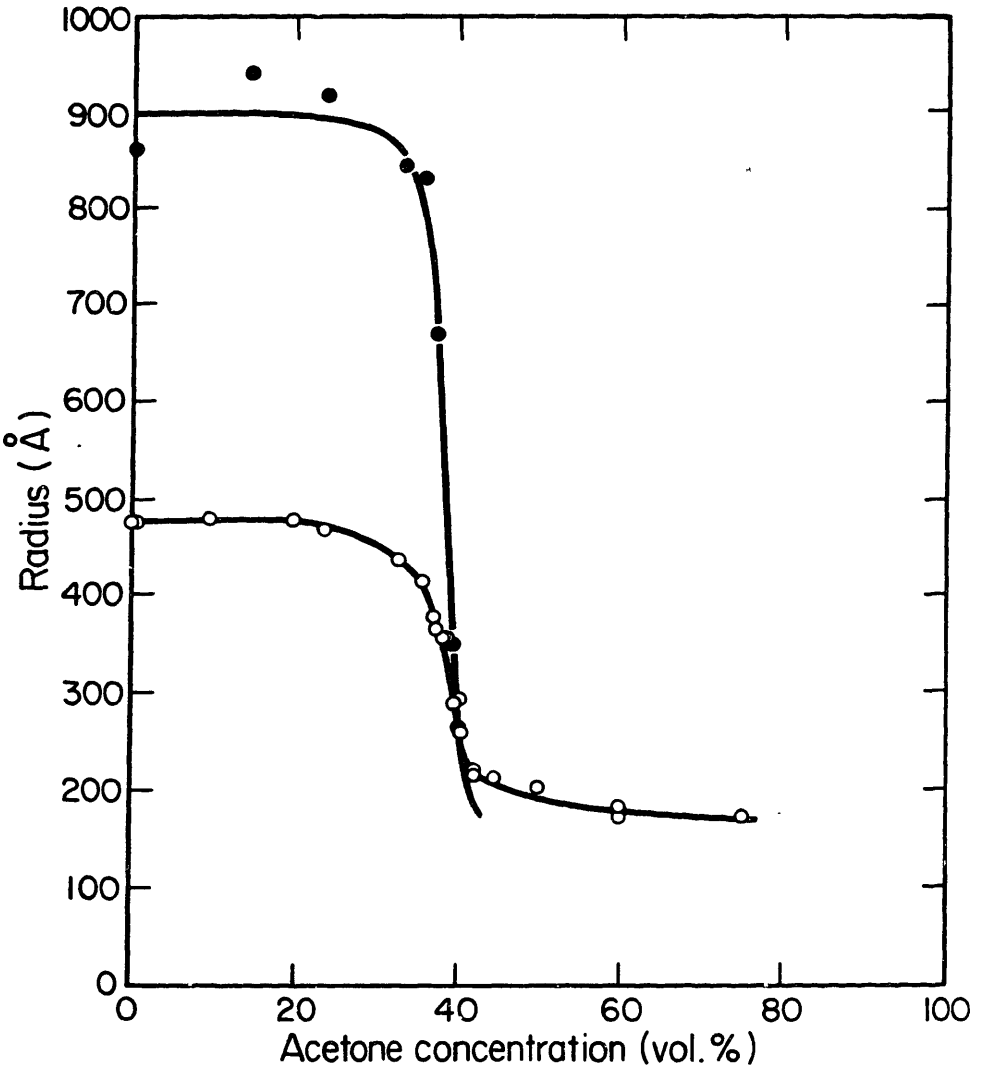

Figure 4.1 R_H and R_G for a Single Polyacrylamide Chain. The molecular weight of the polyacrylamide is $5\text{-}6\times10^6$. The solvent is acetone-water mixtures at 25°C. The open circles are for the hydrodynamic radius, determined by dynamic light-scattering. The filled circles are for the radius of gyration, determined by the classical dissymmetry method.

hydrodynamic radius to about 200A. With a further increase in acetone concentration, the polymer radius remains constant. The transition was reversible.

We also determined the radius of gyration, R_G, of the chain from the angular dissymmetry of the scattered light intensity, using the classical method. These results are also shown in Figure 4.1. The transition is seen to occur at the same acetone concentration as that seen in the curve of the hydrodynamic radius. It was impossible to continue these measurements of R_G to higher acetone concentrations since the the classical method is inadequate at the low level of scattering from the dilute solutions.

In the coil state, the values for R_H are a poor representation of the polymer size. At a 90° scattering angle, the intramolecular fluctuations contribute significantly to the correlation function. Without taking this contribution into account, the value obtained for R_H is too low.

More recent experiments and theoretical considerations [7] on the phase transition in polyacrylamide gels have shown that ions within the gel and charged groups attached to the network are important in the free energy equation. To simplify the theoretical description of the phase transition in single polymers, we continued the studies in a single solvent solution.

4.3. Polystyrene in Cyclohexane

4.3.1. Coexistence Curve and Hydrodynamic Radius

Samples were prepared using $M_W = 27 \times 10^6$ polystyrene (Polysciences lot 3-1761, $M_W/M_N = 1.3$), and high-quality cyclohexane (Fisher 99-Mol% pure). Both were used as supplied with no additional purification. We did not characterize the molecular weight distribution of the polymer samples and were refused any additional information from the manufacturer on their characterization of the sample.

All glassware and sample cells were carefully cleaned and handled to prevent contamination by dust or other impurities. A stock solution of about 10mg of polystyrene dissolved in 10ml of warm (~55°C) cyclohexane was prepared in a tube. For initial dissolution of the polymer, the tube was mechanically rotated end-over-end in a warm oven for several hours. The stock solution remained in the oven for several days to allow complete dispersion of the polymer and to allow any introduced dust to settle. Unlike the acetone-water solvent, cyclohexane tends to exclude large dust particles. Next, ~20-200μl of the stock solution were added to a rectangular cuvette containing ~2-3ml of warm cyclohexane. For the most dilute samples, a two-step dilution was required.

The cuvettes were capped within teflon stoppers. A teflon encapsulated thermistor (YSI model 702) was inserted through the stopper to monitor the solution temperature. In these experiments, the temperature of the solution was controlled to better than

±0.05°C. The Argon-ion laser source was operated at powers between 200 and 1200mW, depending on the solution concentration. All measurements were made at an effective forward scattering angle of 23°.

The first task in characterization of the dilute solution behavior of polystyrene in cyclohexane was determination of the coexistence (or phase separation) curve in the dilute regime. The coexistence curve is a plot of the temperatures and concentrations that separate phases of mostly polymer (bulk phase) and phases of mostly solvent (dilute solution) from unstable states. In dilute solution at a fixed concentration, as the solution temperature is lowered, a state is reached where the distinct solution phase separates into two phases by inter-molecular aggregation of the polymer.

The phase separation temperature can be readily detected by simple light scattering measurements. The scattering intensity of the solution is monitored as the temperature of the solution is decreased in steps. The intensity is constant at each temperature while the solution is of one phase. The intensity first rises at the coexistence or phase separation temperature because of the formation of interpolymer aggregates that scatter more light than the smaller isolated molecules. Eventually, the aggregates settle out of solution and the intensity drops. The initial rise in intensity, however, marks the phase separation temperature.

Our data for the phase separation temperature is plotted in Figure 4.2a. Scaling arguments [8] predict that the data for different molecular weights should fall on the same curve if the concentration

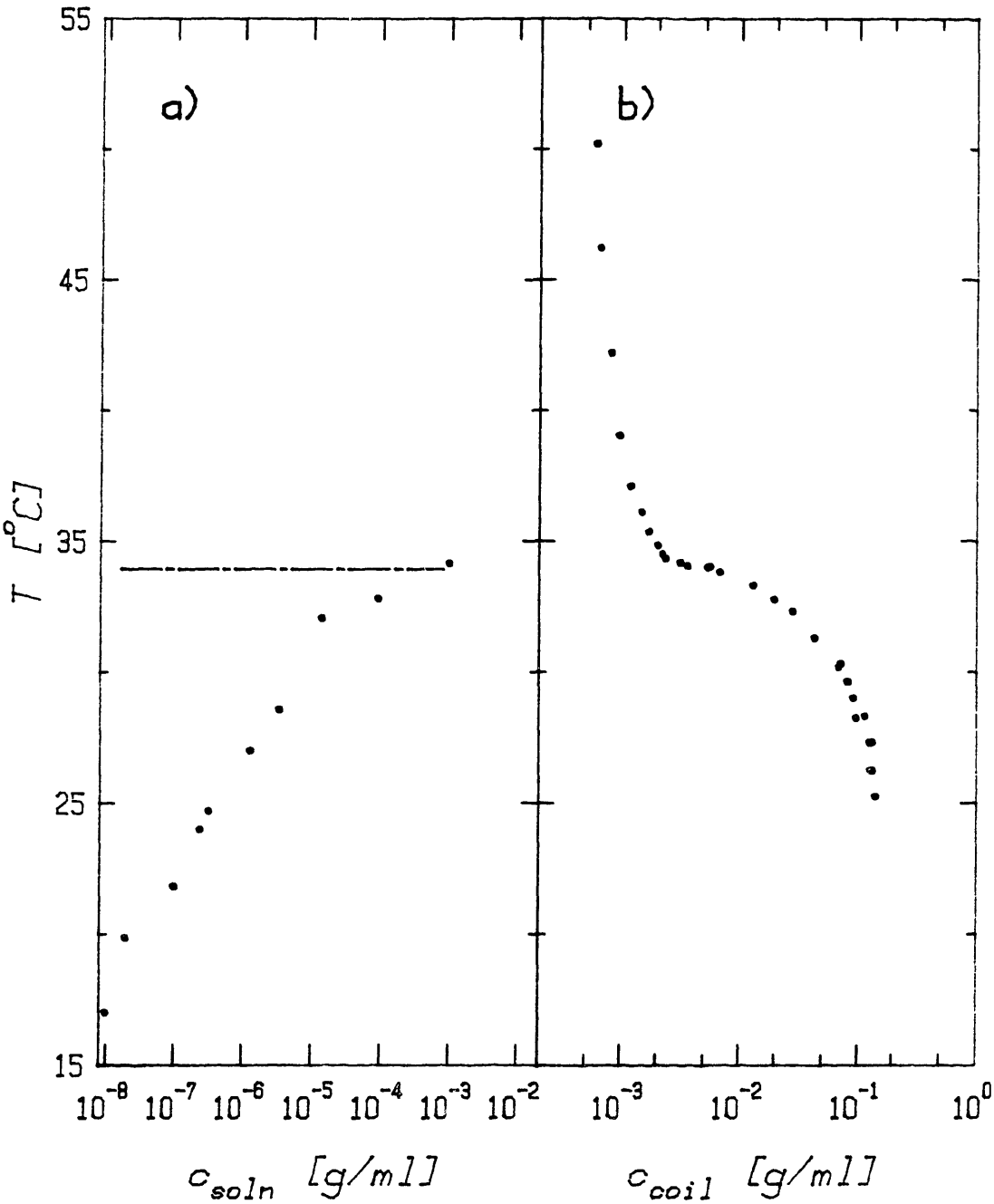

Figure 4.2 Coexistence Curve for Polystyrene in Cyclohexane. a) the phase separation temperature of the polymer solution determined by light scattering for $M_W = 2.7 \times 10^6$. The horizontal line indicates the coil-globule transition temperature. b) the values of R_G plotted in Figure 4.6 are used to estimate the polymer concentration within the single chains, where $c_{coil} = M_W/(N_A \frac{4}{3}\pi R_G^3)$, N_A being Avagadro's number.

and reduced temperature $\tau = (T - \theta)/\theta$ are both scaled by $M_W^{1/2}$. The data are plotted in such a manner. in Figure 4.3 along with data for polystyrene of several lower molecular weights in more concentrated solutions.

As in the previous experiment with polyacrylamide, the measured correlation function was fitted using a second order cumulants expansion to obtain the hydrodynamic radius. The results for several concentrations of polymer are shown in Figure 4.4. For each sample R_H follows nearly the same curve. The radius in the coil state is ~1250Å. Near 32°C, the polymer collapses to a globule with a radius of ~500Å. Although most measurements were made while lowering the temperature, the transition could be reversed by raising the temperature. As in the polyacrylamide measurements, the hydrodynamic radius is too low owing to the inclusion of scattering from intramolecular motion in the correlation function.

4.3.2. Radius of Gyration

Most of the theories of the coil-globule transition deal with the radius of gyration rather than the hydrodynamic radius. Thus, we wanted to measure R_G directly. Such a measurement required a new technique, as explained in Chapter 3. Determination of R_G requires measurement of the angular dependence of the intensity of light scattered from the polymer. Instead of measuring the difference in intensities between pure solvent and solution, as in the classical method, we obtained the angular dependence from the correlation function.

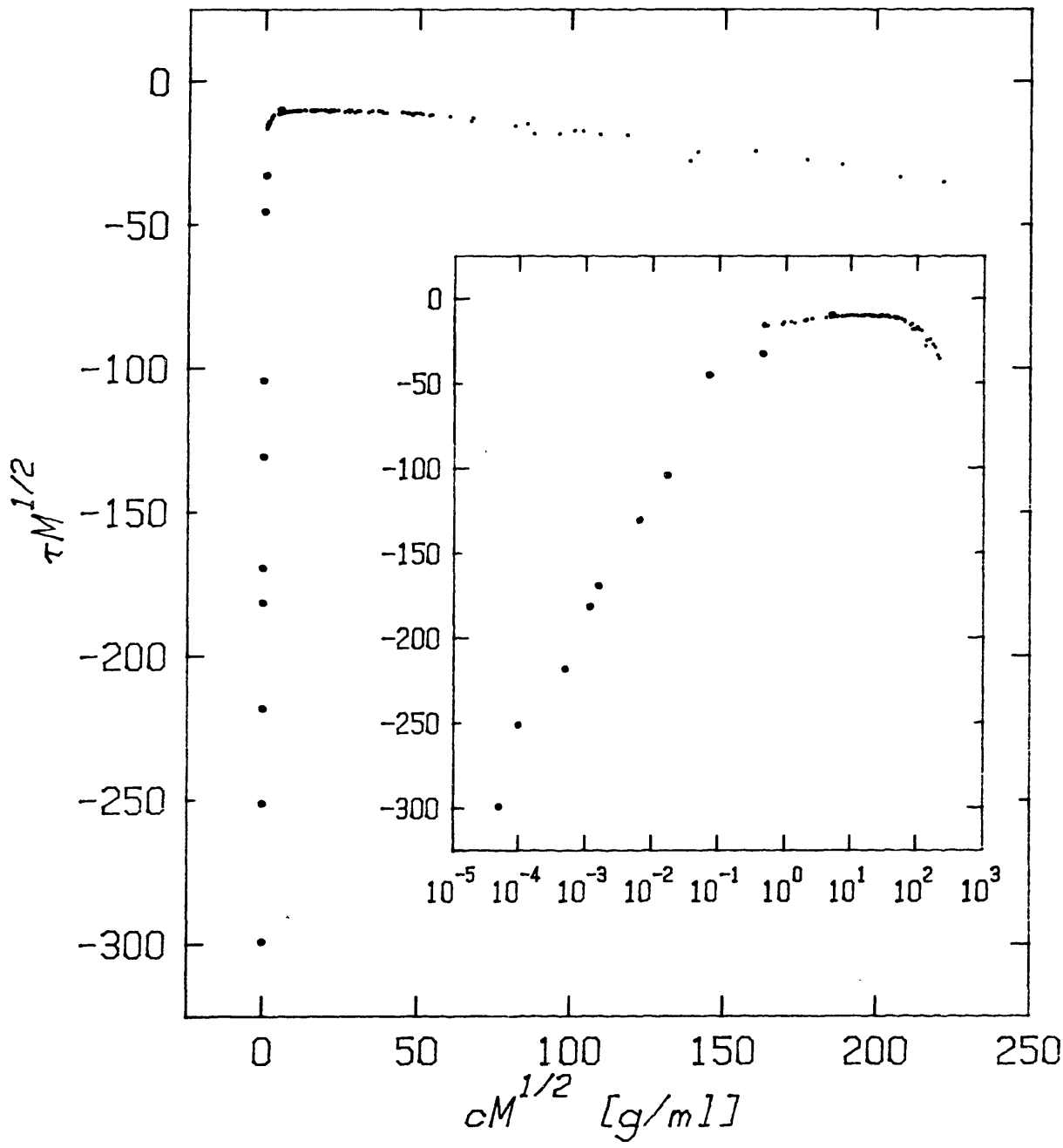

Figure 4.3 Scaled Coexistence Curve. The densely placed points correspond to data from Shultz and Flory [9] for molecular weights 4.36×10^4, 8.9×10^4, 2.50×10^5, and 1.27×10^6 with θ = 34.05°C. The remaining points represent this work, where the molecular weight was 2.7×10^7 and θ = 34.75°C. The inset is of the same data, but with a logarithmic concentration axis.

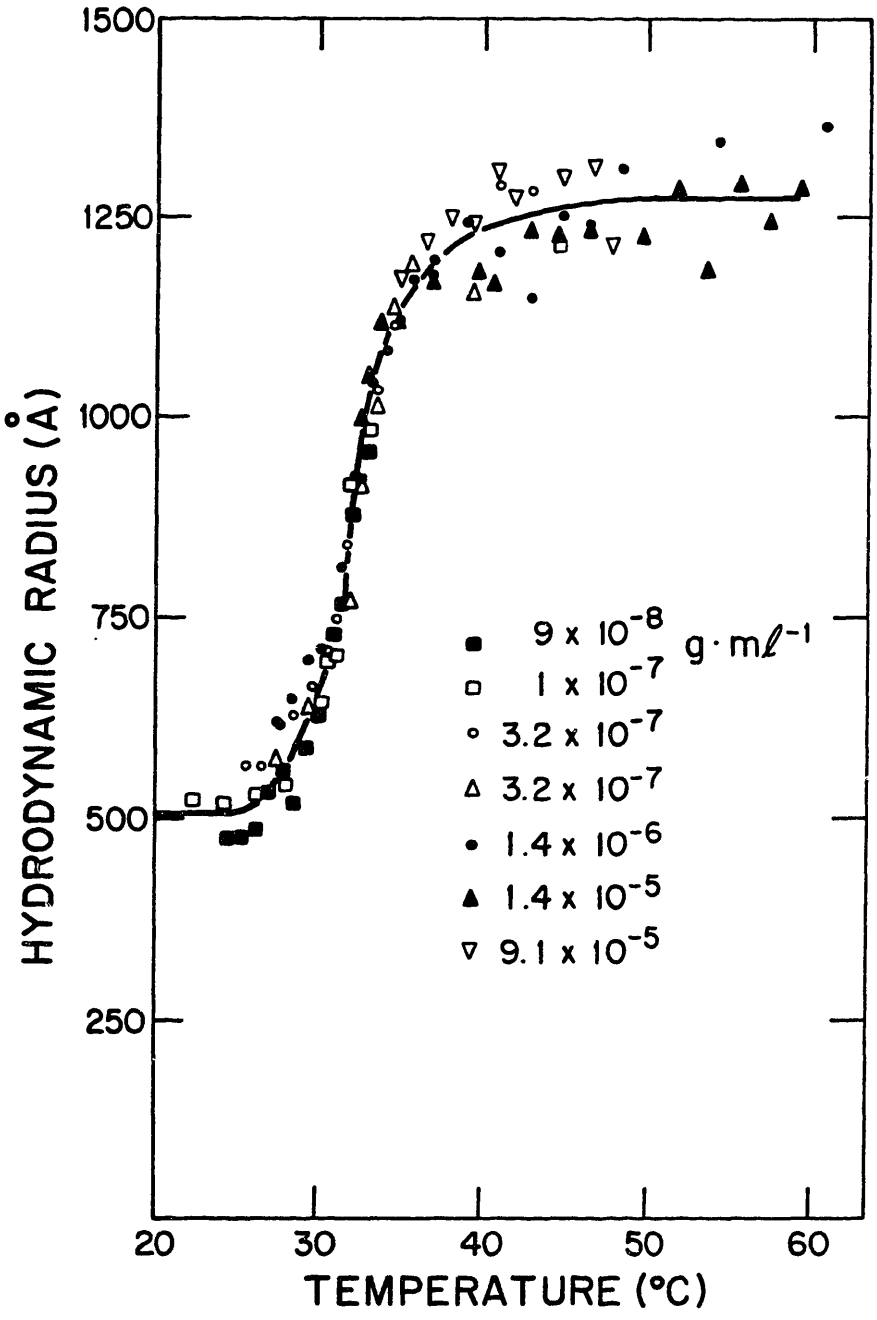

Figure 4.4 Hydrodynamic Radius for a Single Polystyrene chain. The temperature dependence of the hydrodynamic radius of polystyrene ($M_w = 2.7 \times 10^7$) in cyclohexane is plotted for several concentrations of polymer.

Material, sample preparation, and apparatus were identical with the previous experiment except for the correlator, which was a full 4-bit-by-4-bit machine (Nicomp Instruments). With a full correlator, fluctuations in the average scattering intensity cause no distortion of the correlation function. Since the solute scattering intensity was the target of the measurements, it is unlikely a clipped correlator would have worked.

Equation 3.33 gives the ratio of the amplitude of scattering from the solute, a_2, to that from the solvent, a_1, in terms of the extrapolated values of the correlation function at $t = 0$ and $t = \infty$,

$$\frac{a_2}{a_1} = \left[\left[\frac{f(A) C_{OBS}(t \to \infty)}{C_{OBS}(t \to 0) - C_{OBS}(t \to \infty)} \right]^{1/2} - 1 \right]^{-1} . \qquad (4.1)$$

where $f(A)$ depends only on the optical geometry. The factor $f(A)$ was measured at each angle using a concentrated solution of latex spheres (Dow Diagnostics). Since a_1 is constant over angle, the angular dependence of a_2/a_1 reflects the angular dependence of the scattering from the solute. Figure 4.5 is a plot of a_1/a_2 vs. $\sin^2(\frac{\theta}{2})$ (proportional to k^2) at several temperatures. The radius of gyration was determined by fitting these curves using the small-angle approximation for the static structure factor, as explained in the previous chapter.

The values obtained for R_G are shown in Figure 4.6. New measurements of R_H, determined with the full correlator, are also plotted. These agree with the previous results except for slightly larger values for the coil state. Below 29.6°C, the ratio of R_G to

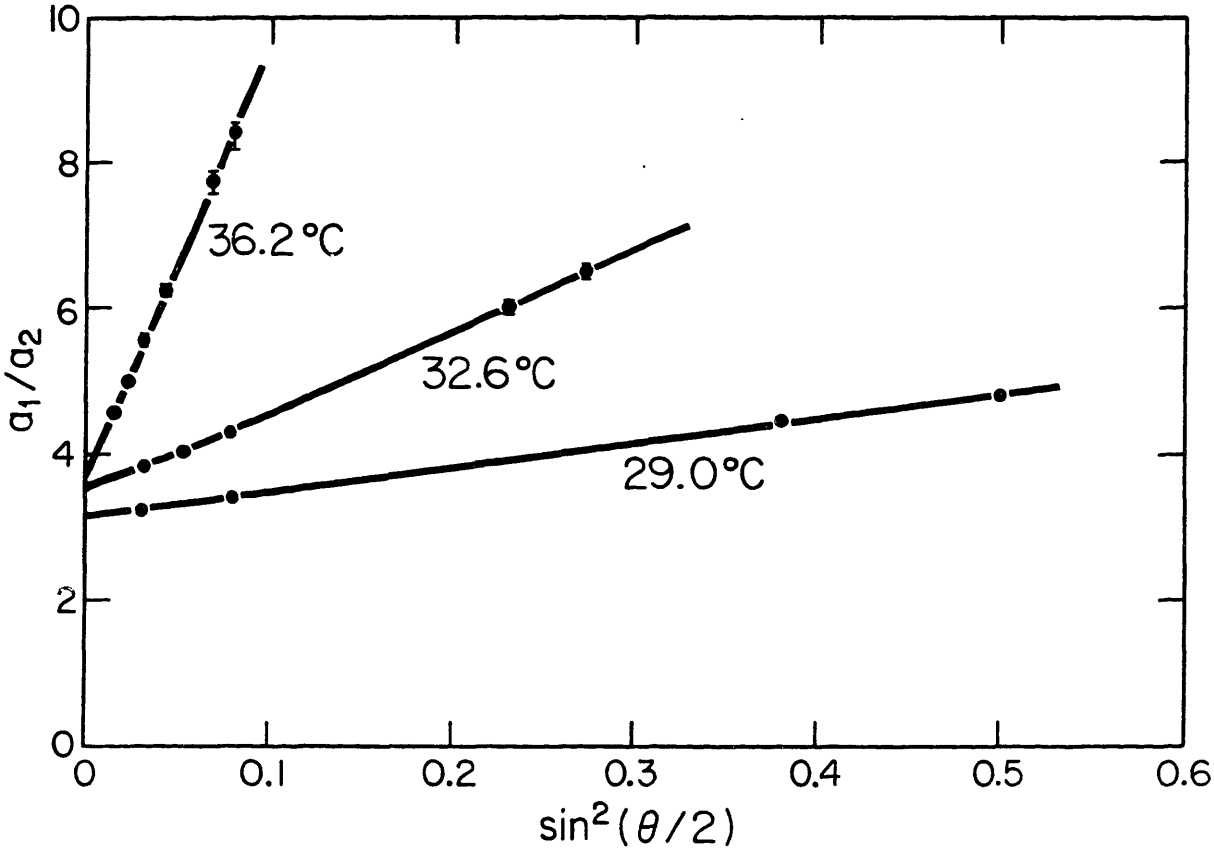

Figure 4.5 Angular Dependence of Scattering. This is a plot of the inverse relative scattering intensity as a function of angle at several temperatures. The size of the polystyrene molecule at a particular temperature determines the slope of each line. A larger slope corresponds to a bigger particle. The intercept is systematically lowered with decreasing temperature owing to the decrease in background scattering from the solvent.

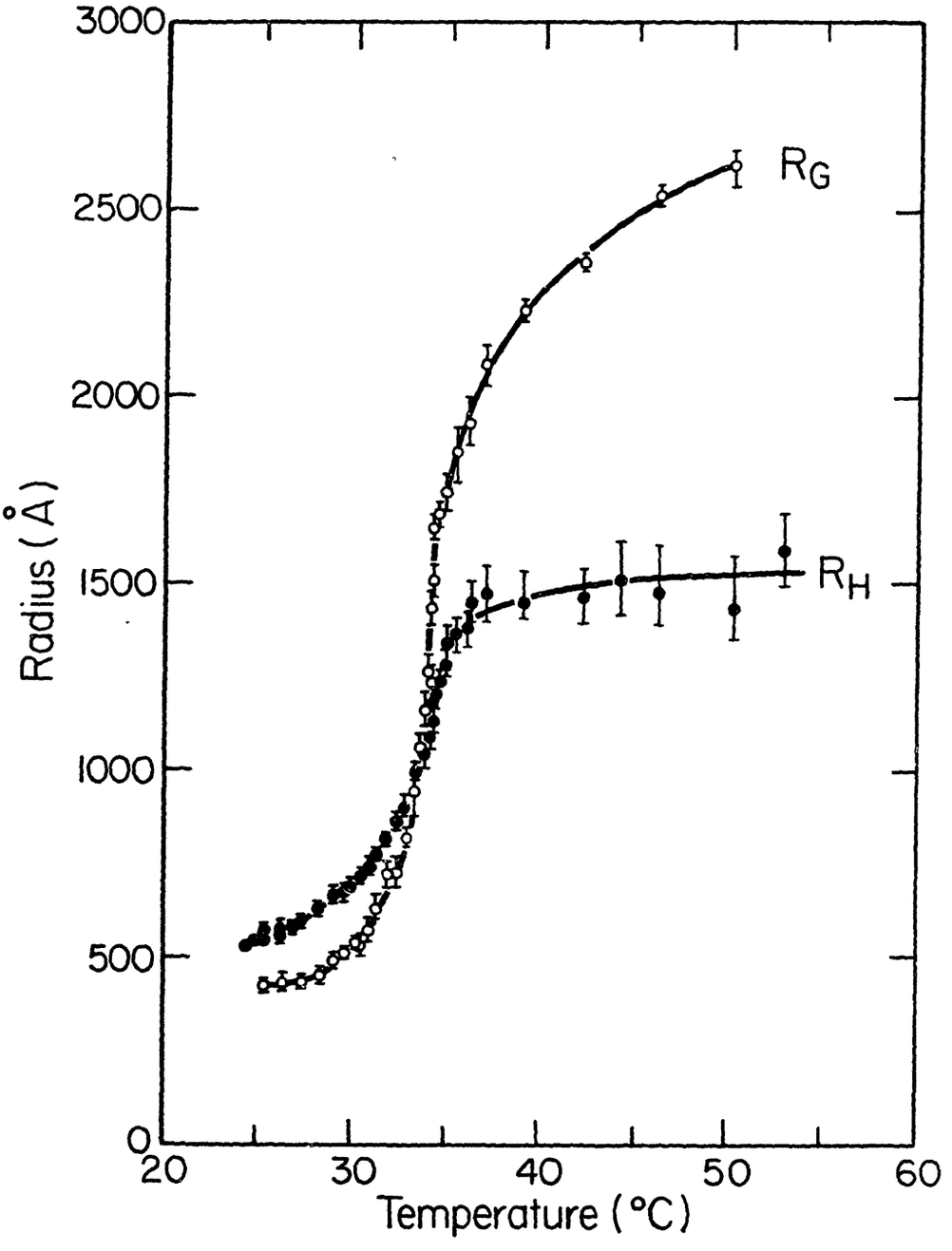

Figure 4.6 R_H and R_G for a Single Polystyene Chain. The solid lines are to guide the eye in this plot of the results for polystyrene ($M_W = 27 \times 10^6$) in cyclohexane.

R_H is 0.74±0.04, close to $(3/5)^{1/2} \approx 0.77$, the value of the ratio for a solid isotropic sphere. This is convincing evidence the polymer has collapsed to a state where the solvent is completely excluded from the molecule. Above 36°C the polymer is in the expanded coil state. In Figure 4.2b, the values of R_G are used to estimate the polymer concentration within the single coil. The temperature dependence of the coil concentration is plotted alongside the solution coexistence curve. It is provocative to see that at the transition to the globule state, the coil concentration is very near the concentration of the solution at phase separation.

Figure 4.7 is a log-log plot of R_G and R_H below the θ temperature as a function of the reduced temperature. In the compact globule state, the slopes are -0.34±0.04 and -0.36±0.04 for R_G and R_H respectively. The slope for the radius of gyration agrees with the mean field theory prediction of -1/3 of Equation 2.32. The hydrodynamic radius should be directly proportional to the radius of gyration in the globule state, and the data bear this out.

4.3.3. Intramolecular motion

The measurement of the internal motion was made on a new apparatus, described in Chapter 5, that had improved temperature control and provisions for computerized scans of temperature and scattering angle. A 4-bit-by-4-bit, 136-channel correlator (Brookhaven Instruments) was used. The added channels were desirable because the correlation function was to be analyzed for two exponentials; 4 or 5 parameters would be fitted. The same polystyrene, but

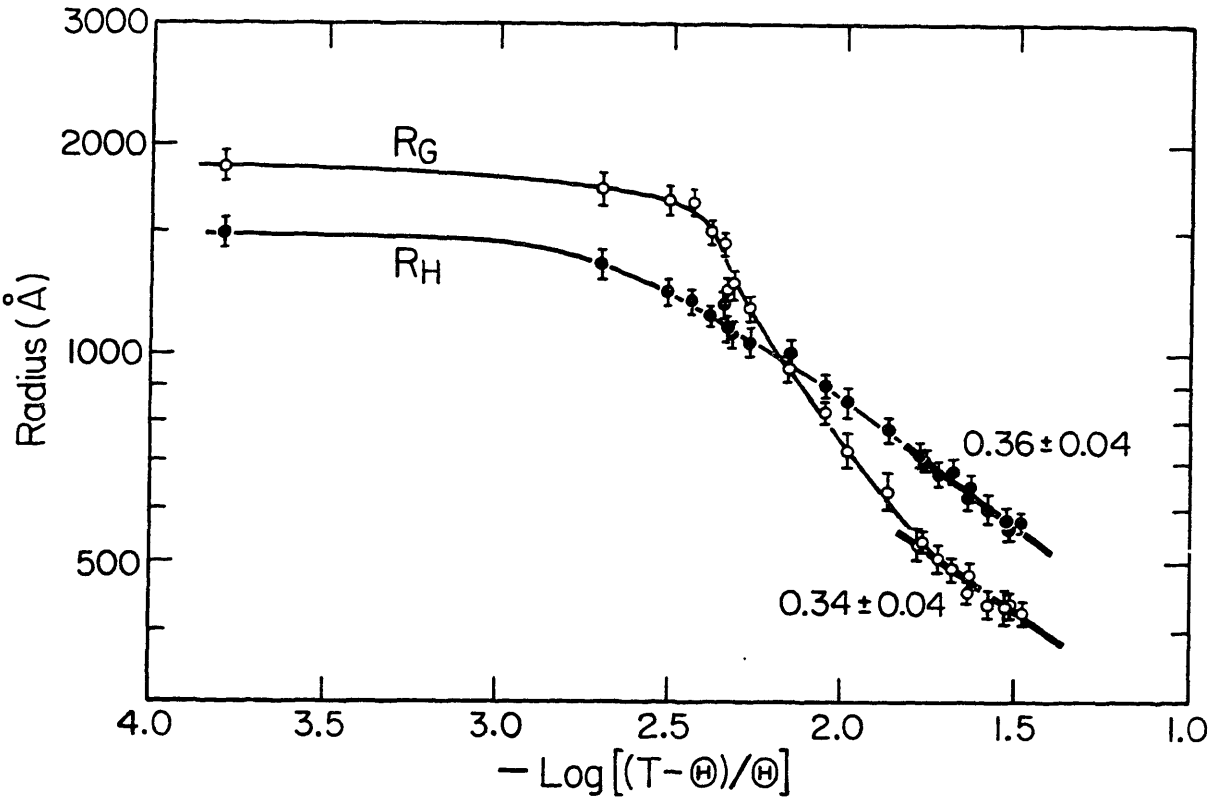

Figure 4.7 Asymptotic Behavior of the Radius for $T < \Theta$. Both R_G and R_H are plotted in this log-log plot as a function of the reduced temperature $\tau = |T - \Theta|/\Theta$. The limiting slopes for the globule state agree with the mean-field and scaling predictions of -1/3.

higher quality cyclohexane (Fisher HPLC grade), was used in this experiment.

An established procedure was used to characterize the internal motion [10,11]. At each temperature, correlation functions were measured at forward scattering angles ($x = k^2R_G^2 < 1$) to determine D. The correlation function was then measured at higher scattering angles and fit to

$$C(t) = [A_1 e^{t/T_1} + A_2 e^{t/T_2}]^2 + B \ , \qquad (4.2)$$

where T_1 is fixed by D, so only A_1, A_2, T_1, and B need to be varied.

Figure 4.8a shows the behavior of the normalized amplitude of internal motion, $A_2/(A_1 + A_2)$, as a function of x at 33.9°C. Figure 4.8b shows the inverse relaxation time, T_2^{-1}, also as a function of x at the same temperature. The translation relaxation rate, T_1^{-1}, is plotted as a straight line through the origin. The difference between T_1^{-1} and T_2^{-1} in the region where they are parallel is proportional to the segment diffusivity, D_{int} (see Equation 3.59). For higher values of x, the effect of the higher-order modes corresponding to shorter length-scale density fluctuations is apparent -- the two exponential form is no longer appropriate to describe the measured correlation function.

Figure 4.9a reproduces the results showing the collapse in the radius of gyration as the temperature is lowered. Figure 4.9b is a plot of the diffusivity of the internal motion, defined as $D_{int} = R_G^2/(T_2^{-1} - T_1^{-1})$. Equation 3.59 puts $D_{int} = (\frac{a_o}{\pi})^2/(T_2^{-1} - T_1^{-1})$,

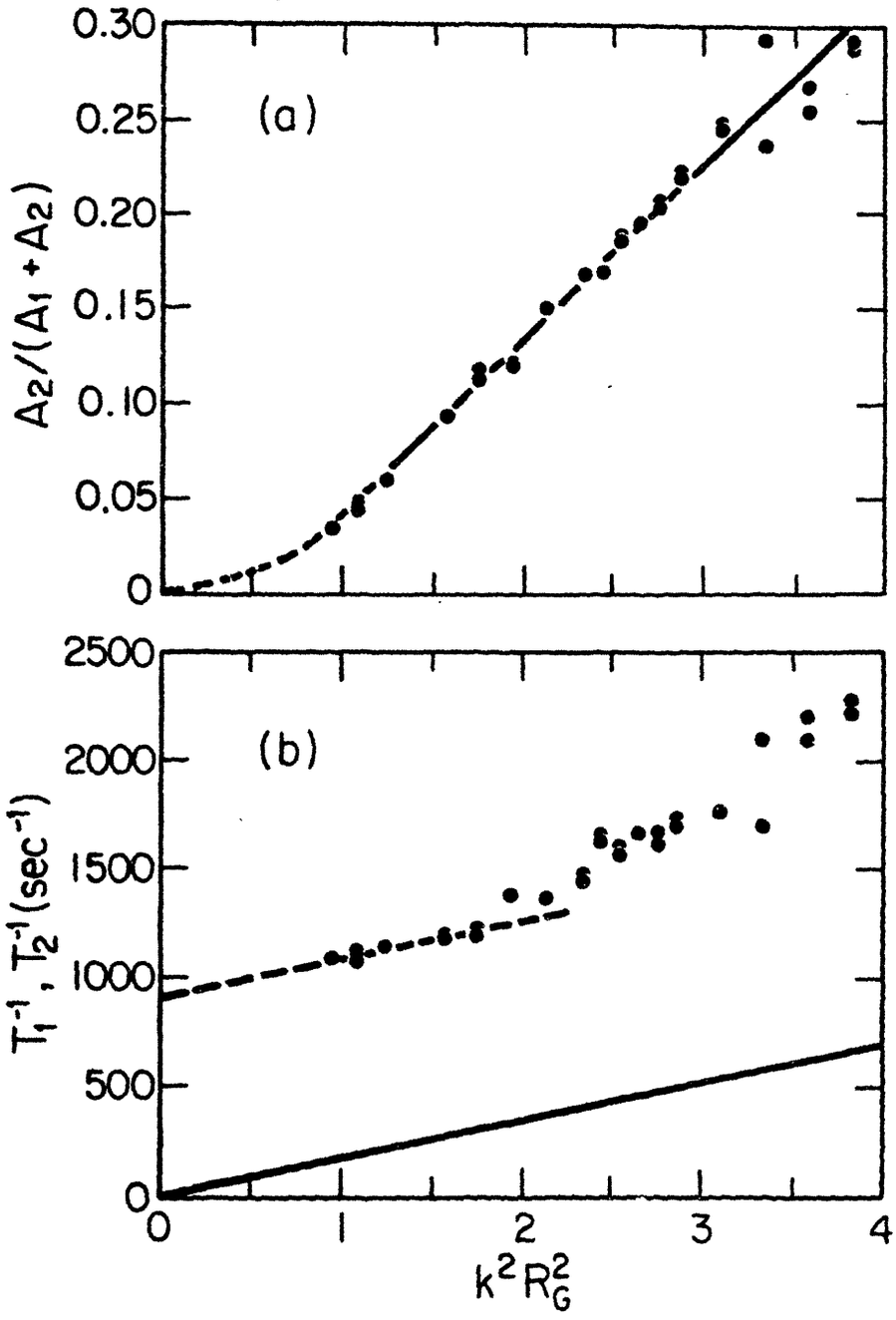

Figure 4.8 Angular Dependence of Intramolecular Quantities. The characteristics of the intramolecular fluctuations at 33.9°C are plotted as a function of the parameter $x = k^2R_G^2$. a, the normalized amplitude. b, the frequency of internal motion. The solid line is the frequency associated with translational diffusion. Points representing the frequency of the lowest order mode of internal motion fall parallel to the solid line at small values of x.

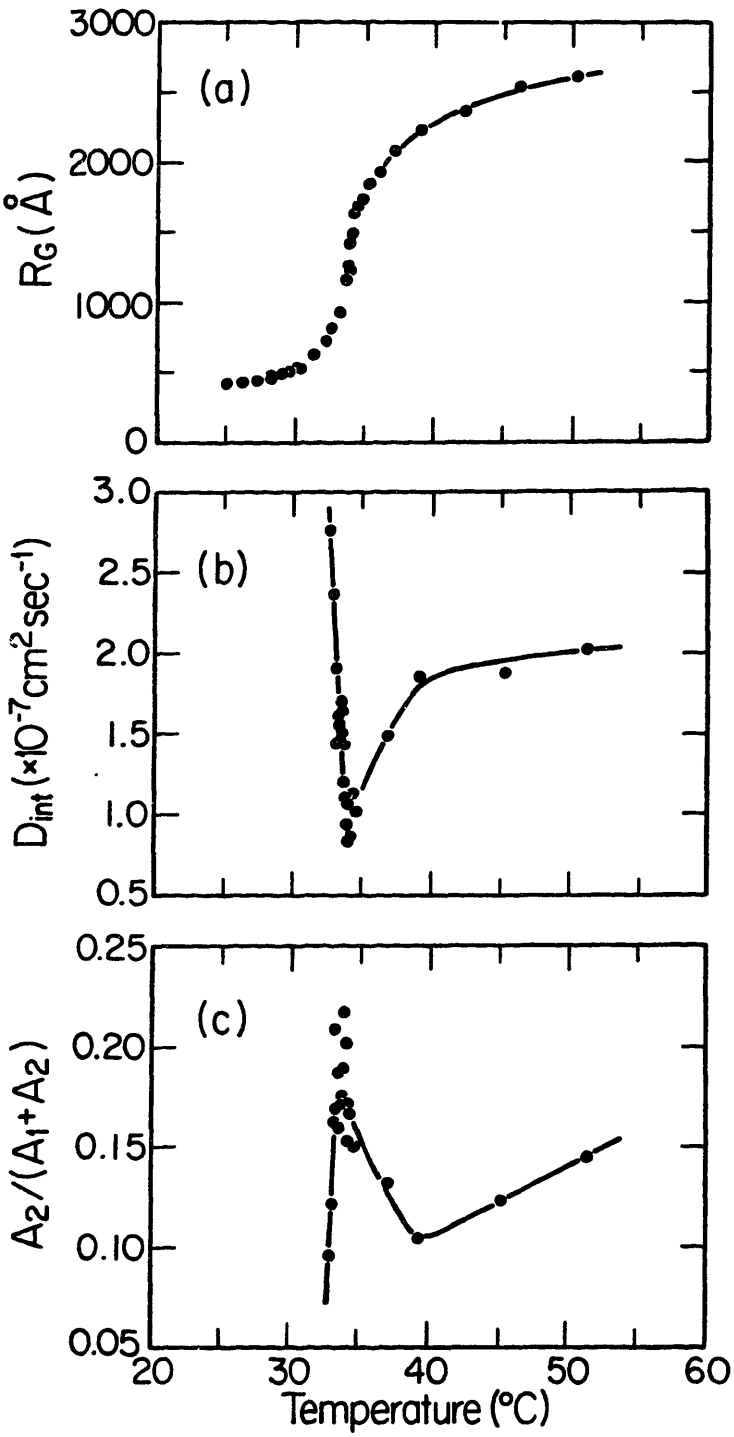

Figure 4.9 Temperature Dependence of Intramolecular Quantities. The behavior of the intramolecular fluctuations as a function of temperature (lines to guide the eye). a, the collapse seen in the radius of gyration (from Figure 4.6). b, the internal diffusivity of the segments, $D_{int} = R_G^2(T_2^{-1} - T_1^{-1})$. c, the amplitude of the fluctuations at x = 2.5.

where a_0 is the radius of the model elastic sphere. We simply assume $a_0 \propto R_G$. The slowing-down of the intramolecular motion at the transition is apparent in the plot. Figure 4.9c is a plot of the normalized amplitude $A_2/(A_1 + A_2)$ versus temperature at $x = 2.5$. This plot shows the sharp increase in the amplitude of the fluctuations at the transition temperature.

4.3.4. Comparison with Theory

A theory for the expansion factor of the radius of gyration was derived in Chapter 2. The result was

$$\alpha^5 - \alpha^3 - \frac{y}{\alpha^3} = z \ , \tag{4.3}$$

where

$$y = \frac{3^{7/2}}{\pi^3} w^4 \ , \tag{4.4}$$

$$\alpha = \frac{R_G}{r_0} \ , \tag{4.5}$$

and

$$z = \left(\frac{9}{2\pi}\right)^{3/2} \left(1 - \frac{\theta}{T}\right) \psi N^{1/2} w^2 \ . \tag{4.6}$$

Here, w characterizes the flexibility of the polymer chain, r_0 is the radius of gyration under conditions where R_G scales as $N^{1/2}$, θ is the temperature at which the effect of binary interactions vanishes dues to the compensating entropy terms in the free energy, ψ characterizes the energy of interaction between the components of the solution, and N is the number of statistical elements in the chain.

There are effectively four parameters in this equation. They are w, r_o, Θ, and $\psi N^{1/2}$. There is no way to separate the last two factors. Fitting the equation simultaneously for these parameters to the data of Figure 4.6 results in w = 0.472, r_o = 1660Å, Θ = 34.75°C, and $\psi N^{1/2}$ = 350. The goodness of fit can be judged from Figure 4.10. The fitted value of the flexibility is well above the critical flexibility (cf. Figure 2.2), and in the region of the second order transition. Other estimates of the flexibility of the polystyrene chain are higher than that obtained here [13,14]. Values for Θ quoted in the literature [15] range from 34.5°C to 35.4°C, which agree with the result obtained in the fit.

An empirical formula that summarizes data from many sources [16] for polystyrene in Θ solvents relates R_G to molecular weight as,

$$\langle R_G^2(T=\Theta)\rangle^{1/2} = 0.29 M_W^{1/2} \qquad (\pm 2.5\%) \qquad \text{Å} . \tag{4.7}$$

At T = Θ the fit to Equation 4.3 gives R_G = 1711Å which corresponds to $M_W = 34.8\times10^6$. For $R_G = r_o$ = 1660Å, the empirical formula predicts $M_W = 32.8\times10^6$. In either case, it seems likely that the value quoted by the manufacturer ($M_W = 27\times10^6$) may be slightly low.

The predictions at the end of Chapter 3 for the temperature dependence of the intramolecular quantities are shown in Figure 4.11. Figure 4.11a is of the internal (or segment) diffusivity (cf. Equation 3.62),

$$D_{int} \sim \frac{(a_o kTK)^{1/2}}{\eta} , \tag{4.8}$$

while Figure 4.11b is of the relative amplitude of the lowest order

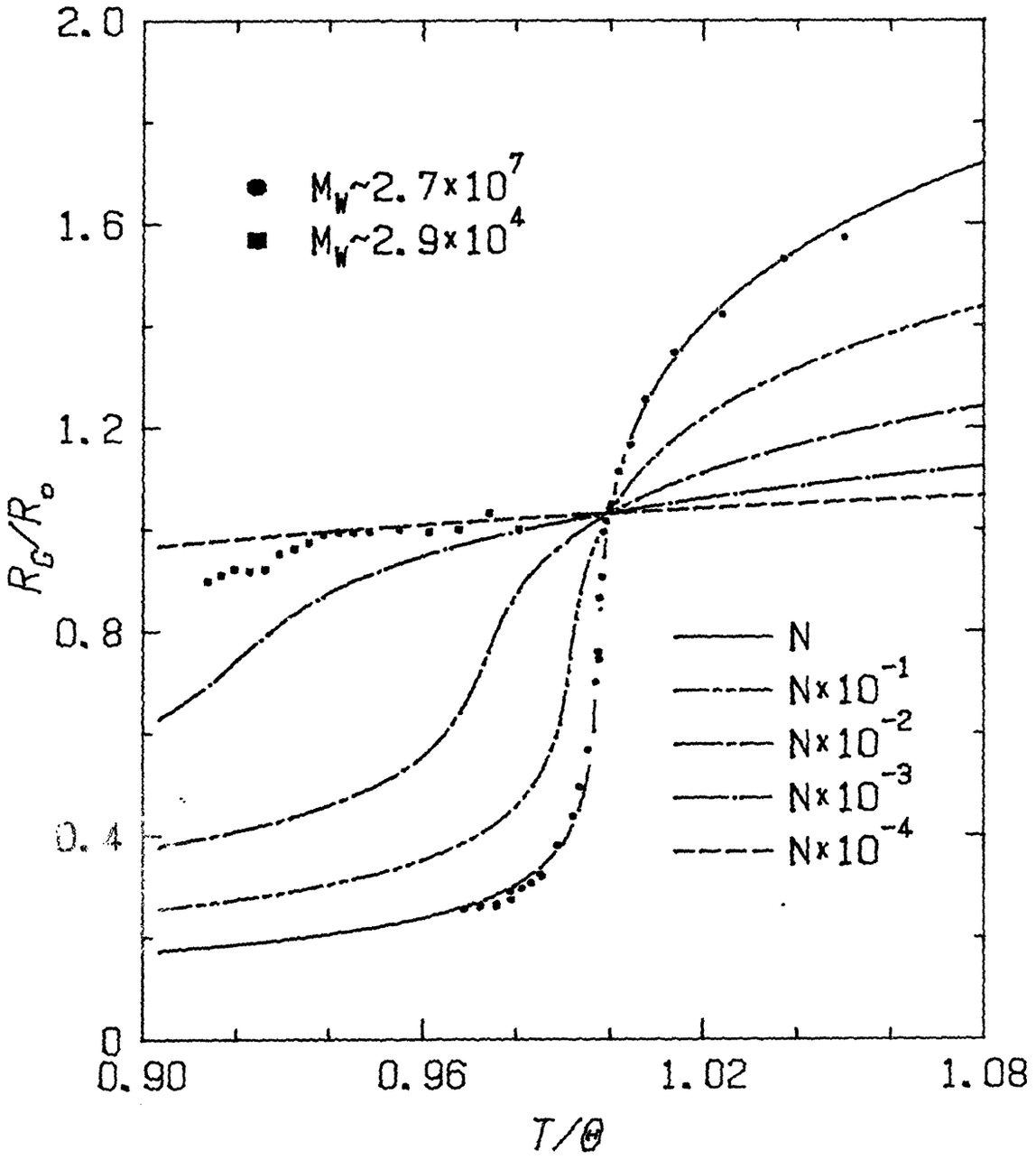

Figure 4.10 Fit of Expansion Factor to Mean-Field Theory. The data points include the results from Figure 4.6 and neutron scattering data from a low molecular weight specimen [12]. The solid curve is the best fit to Equation 2.28. The fitted parameters are $\psi N^{1/2} = 350$, $w = 0.472$, $\theta = 34.75$, and $\langle r_o^2 \rangle^{1/2} = 1660$A. The remaining curves use the same parameters except N is reduced by successive powers of 10, corresponding to lower molecular weights. (Accomplished by scaling $\psi N^{1/2}$ by successive powers of $10^{1/2}$.)

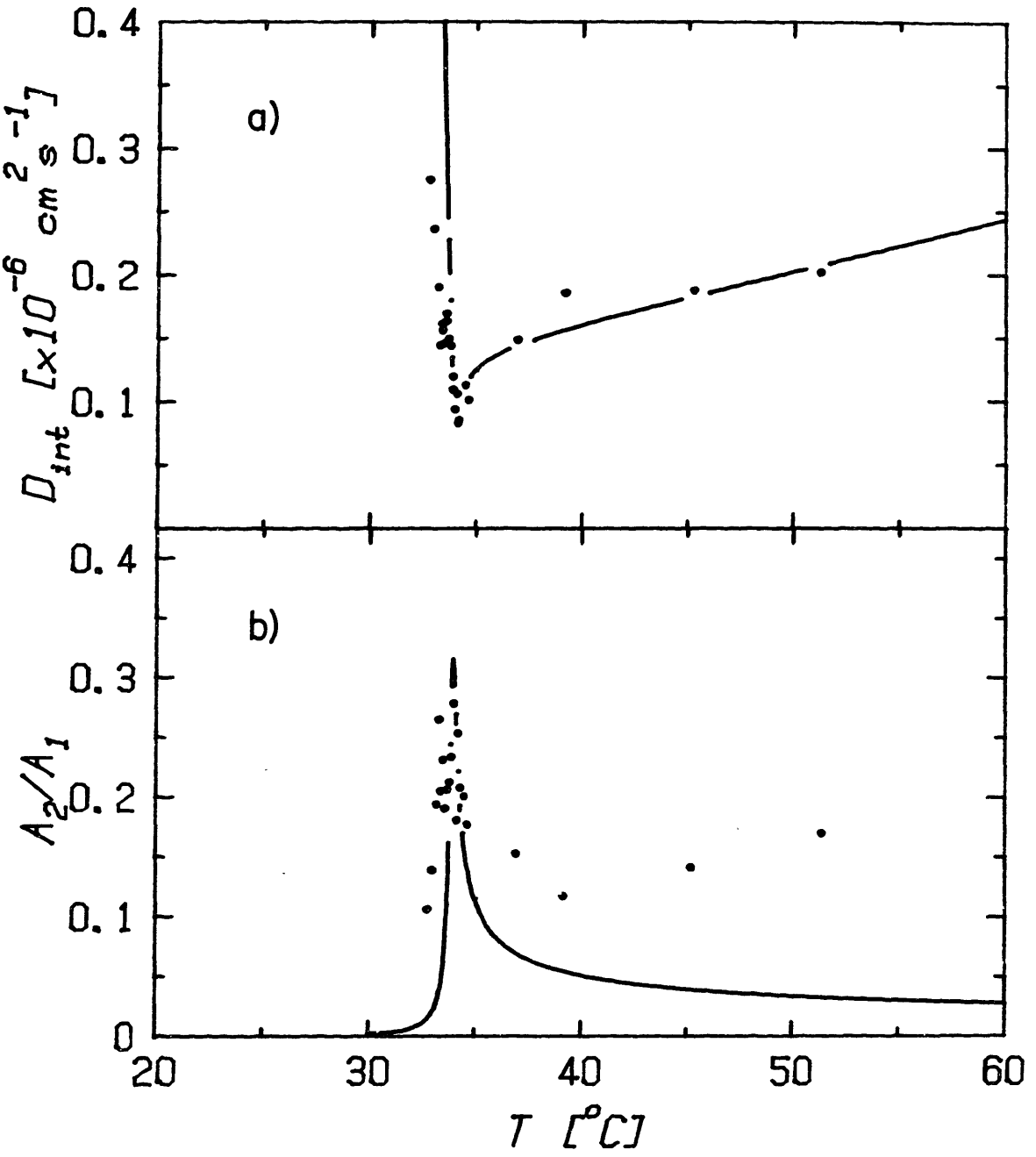

Figure 4.11 Comparison of Intramolecular Data with Theory. The data points are from Figure 4.9. The solid lines are theoretical curves from Equation 3.62 for D_{int} and Equation 3.60 for A_2/A_1. In these equations, the bulk modulus K is given by Equation 2.42. All parameters except the proportionality constants are obtained from the fit displayed in Figure 4.10.

mode of the intramolecular fluctuations (cf. Equation 3.60),

$$\frac{A_2}{A_1} \sim \frac{kT}{4\pi a_o^3 K} F(ka_o) \ . \qquad (4.9)$$

The radius of the elastic sphere, a_o, used in the model is replaced by R_G. R_G and the bulk modulus, K, are calculated using the same parameters as for Figure 4.10. The proportionality constants used in the plots are estimates -- the data do not conform to the theoretical curves well enough for a fit to work.

4.4. Other Work

Although the preponderance of the literature relating to the coil-globule transition is the work of theoreticians and includes mean-field theories, scaling and renormalization arguments, and numerical simulations, there are a handful of experimental studies that relate to the phenomenon. None of these experiments, however, revealed the dimensions of a single polymer in the globule state. Both classical [17-19] and dynamic light-scattering [19-21] techniques have also been applied by other groups in their attempts to observe the coil-globule transition. In addition neutron scattering [12], sedimentation [22], and viscometry [17,21,23] measurements have been reported.

The neutron-scattering results are shown in Figure 4.10. The authors claimed the exponent for the temperature dependence of the expansion factor was -1/3 for the globule state, in agreement with the predictions of the theory. They argued that by choosing polymers of low molecular weight, a larger range in temperature between the Θ

temperature and the solution coexistence curve could be obtained. However, the authors overlooked the fact that the coil-globule transition temperature is also a function of molecular weight, as can be seen in Figure 4.10. The transition is broadened as the value of N decreases. Thus, the polymer collapse occurs at lower temperatures for lower molecular weight molecules. Comparing their data and ours with the theory, it appears the temperature range involved in the neutron experiment was near the onset of the transition, and the slope of -1/3 they obtained was only coincidental.

All the light scattering experiments cited were unable to continue measurements to the globule state owing to the onset of phase separation in the insufficiently dilute solutions used. Some authors did not believe observation of the globule state was even possible, stating it was "unlikely that the single collapsed coil can exist before phase separation begins." [18]

The sedimentation and viscosity experiments are difficult, if not impossible, with very dilute solutions, and so were also hindered by phase separation at the solution concentrations used in the experiments. Also, these techniques are not very sensitive to dimerization, trimerization, etc, of the molecules, compared to light scattering.

References

1. T. Tanaka, "Collapse of gels and the critical endpoint", Phys. Rev. Lett. **40**(12) pp. 820-823 (1978).

2. I. Nishio, S.T. Sun, G. Swislow, and T. Tanaka, "First observation of the coil-globule transition in a single polymer chain", Nature **281**(5728) pp. 208-209 (1979).

3. Polymer Handbook, ed. J. Brandrup and E.H. Immergut, Wiley, New York (1975).

4. G. Swislow, S.T. Sun, I. Nishio, and T. Tanaka, "Coil-globule phase transition in a single polystyrene chain in cyclohexane", Phys. Rev. Lett. **44**(12) pp. 796-798 (1980).

5. S.T. Sun, I. Nishio, G. Swislow, and T. Tanaka, "The coil-globule transition: Radius of gyration of polystyrene in cyclohexane", J. Chem. Phys. **73**(12) pp. 5971-5975 (1980).

6. I. Nishio, G. Swislow, S.-T. Sun, and T. Tanaka, "Critical density fluctuations within a single polymer chain", Nature **300**(5889) pp. 243-244 (1982).

7. T. Tanaka, D. Fillmore, S.T. Sun, I. Nishio, G. Swislow, and A. Shah, "Phase transitions in ionic gels", Phys. Rev. Lett. **45**(20) pp. 1636-1639 (1980).

8. J.P. Cotton, M. Nierlich, F. Boue, M. Daoud, B. Farnoux, G. Jannink, R. Duplessix, and C. Picot, "Experimental determination of the temperature-concentration diagram of flexible polymer solutions by neutron scattering", J. Chem. Phys. **65**(3) pp. 1101-

1108 (1976).

9. A.R. Shultz and P.J. Flory, "Phase equilibria in polymer-solvent systems", Am. Chem. Soc. J. **74** pp. 4760-4767 (1953).

10. Wu-Nan Huang and J.E. Frederick, "Determination of intramolecular motion in a random-coil polymer by means of quasielastic light scattering", Macromolecules **7**(1) pp. 34-39 (1974).

11. T.A. King, A. Knox, and J.D.G. McAdam, "Internal motion in chain polymers", Chem. Phys. Lett. **19**(3) pp. 351-354 (1973).

12. M. Nierlich, J.P. Cotton, and B. Farnoux, "Observation of the collapse of a polymer chain in poor solvent by small angle neutron scattering", J. Chem. Phys. **69**(4) pp. 1379-1383 (1978).

13. Y.Y. Eizner, "Globule-coil transitions in homogeneous macromolecules", Vysokomol. Soyed. **A11**(2) pp. 364-371 (1969).

14. C.B. Post and B.H. Zimm, "Internal condensation of single DNA molecule", Biopolymers **18** pp. 1487-1501 (1979).

15. H.-G. Elias and H.G. Buhrer, "Theta solvents", in Polymer Handbook, ed. J. Brandrup and E.H. Immergut, Wiley, New York (1975).

16. M. Schmidt and W. Burchard, "Translational diffusion and hydrodynamic radius of unperturbed flexible chains", Macromolecules **14** pp. 210-211 (1981).

17. C. Cuniberti and U. Bianchi, "Dilute solution behavior of polymers near the phase separation temperature", Polymer **15** pp.

346-350 (1974).

18. E. Slagowski, B. Tsai, and D. McIntyre, "The dimensions of polystyrene near and below the theta temperature", Macromolecules 9 pp. 687-688 (1976).

19. P. Stepanek, C. Konak, and B. Sedlacek, "Coil-globule transition of a single polystyrene chain in dioctyl phthalate", Macromolecules 15(4) pp. 1214-1216 (1982).

20. D.R. Bauer and R. Ullman, "Contraction of polystyrene molecules in dilute solution below the Θ temperature", Macromolecules 13(2) pp. 392-396 (1980).

21. R. Perzynski, M. Adam, and M. Delsanti, "Dynamic measurements on polymer chain dimensions below the Θ-temperature", J. Physique 43(1) pp. 129-135 (1982).

22. P. Vidakovic and F. Rondelez, "Temperature dependence of the hydrodynamic radius of flexible coils in solutions. 2. Transition from the Θ to the collapsed state", Macromolecules 17(3) pp. 418-425 (1984).

23. Z. Priel and A. Silberberg, "Conformation of poly(methacrylic acid) in alcohol-water mixtures", J. Polymer Sci. A-2 8 pp. 689-726 (1970).

CHAPTER 5

THE LIGHT SCATTERING APPARATUS

5.1. Introduction

Since the design of the light scattering apparatus was important to the success of our measurements of the coil-globule transition, that apparatus is described in some detail in this chapter. Although three instruments were used during the experiments, with two of them built especially for these measurements, only the final and most elaborate one will be considered in depth.

The optical requirements of the basic light scattering instrument are simple. An incident beam of monochromatic, collimated, and polarized light is needed. A laser is the most convenient source for such a beam. This incident beam is brought to a focus within the sample by a lens. In collecting the scattered light, two apertures define the scattering angle and limit the size of the scattering volume. Detection is provided for with a photomultiplier tube that converts the scattered light to an electrical signal. Other elements of the apparatus include a sample holder and electronics for analyzing the detected signal. In addition to these components, the apparatus includes devices for precise regulation and measurement of sample temperature, and connections to a laboratory computer for experiment control, data acquisition, and data reduction.

5.2. Stray Light and Convection

When dynamic light scattering is used for the study of dilute solutions, particular attention must be paid to the problem of stray light reaching the detector and to the problem of convective flow within the scattering volume. Stray light is light scattered or reflected from portions of the apparatus that has the same frequency spectrum as the incident light. Stray light is a problem if it reaches the photomultiplier surface, where it mixes with the frequency-shifted scattered light resulting in a heterodyned signal. Such a signal produces a correlation function proportional to the function $g^{(1)}(t)$ defined in Equation 3.5. The characteristic decay times of exponentials in $g^{(1)}(t)$ are twice those of the homodyne correlation function. All else being equal, the weaker the signal from the scattering volume, the more the correlation function will be distorted as a result of heterodyning.

Convection can result either from uneven heating of the sample by the temperature control system or from local heating of the solution by the incident beam. In the presence of convection, which can be characterized by a time-independent velocity field $\vec{v}(\vec{r})$, the diffusion equation (3.10) contains additional terms,

$$\frac{\partial \delta c(\vec{r},t)}{\partial t} = D\nabla^2 \delta c(\vec{r},t) + \vec{v}(\vec{r})\cdot\vec{\nabla}\delta c(\vec{r},t) + \delta c(\vec{r},t)\vec{\nabla}\cdot\vec{v}(\vec{r}) \ ,$$

where $\delta c(\vec{r},t)$ is the local concentration fluctuation and D the diffusion coefficient. For $\vec{v}$ constant (uniform convective flow), the solution to the above equation for the Fourier component of the concentration fluctuation with wave vector $\vec{k}$ is

$$\delta c(\vec{k}, t) \propto e^{-Dk^2 t - i\vec{k}\cdot\vec{v}} .$$

The homodyne correlation function, $g^{(2)}(t)$, is proportional to $|\delta c(\vec{k},t)^{*}\delta c(\vec{k},t)|$, and uniform flow has no effect. However, in the presence of stray light and the associated heterodyning, the uniform flow will add an obvious sinusoidal component to the correlation function. Non-uniform flow, perhaps more likely in a small sample cell, can distort the correlation function even in the absence of heterodyning. In any case, it is not possible to obtain worthwhile data when the correlation function suffers from significant distortion.

5.3. The Sample Cell

In general, either a cylindrical or rectangular cell may be used to contain the sample solution. As summarized in Table 5.1, considerations in the choice of cell type include the the cell surface quality, and the ease of low angle work, temperature control, and automated scanning of angles. The quality of the cell surface is important since scattering from surface imperfections is one source

Table 5.1 Comparison of Rectangular and Cylindrical Cells

	Quality surfaces	Low angle work	Temperature control	Automated angle scan
Cylindrical	Rare	Difficult	Simple	Easy
Rectangular	Common	Possible	Difficult	Complicated

of stray light. Good cylindrical glass is difficult to find, and even at its best, does not match the optically flat and parallel surfaces of readily available rectangular cells. Cylindrical cells also pose problems at forward scattering angles, especially when the cells are of small diameter, since the unscattered beam will diverge as it passes from the glass into the air. Finally, accurate alignment at low angles is more difficult with cylindrical cells. Because the central axis of the cylinder cannot be easily determined, problems arise in centering the incident beam and in positioning the collection optics. Cylindrical cells do offer certain advantages, however. First, precise temperature control is generally simpler. It is difficult to design holders for rectangular cells without exposing a portion of the cell to air. Such exposure leads to temperature control problems. A cylindrical cell holder, however, can be designed to immerse the cell entirely in a thermostating and index-matching fluid. Second, automated control of the scattering angle is readily carried out when a cylindrical cell is used. The cell position and detection optics do not need to be readjusted as the scattering angle is changed (which is necessary with a rectangular cell), since the light path from the sample to the detector is symmetric at all angles.

The first system we built employed a rectangular cell. The cell fit into an aluminum block with heating and cooling provided by a Peltier-effect module attached to one side of the block. We found it difficult to eliminate temperature gradients across the cell. The

best results were obtained when an auxiliary heating element was placed in a hole drilled in the block on the side of the sample opposite the module. Heat to the sample cell was carefully adjusted to maintain constant temperature on both sides of the cell, as determined by two sensors and by observation of the correlation function. Although we obtained adequate results in the polyacrylamide experiment (performed at constant temperature) and in the measurements of the radius of gyration of polystyrene, temperature control was tedious and unreliable. Because our plans to measure the intramolecular motion required correlation functions at many combinations of temperature and scattering angle, we designed a new system emphasizing improved temperature control and computerized experiment management. The cylindrical cell is best suited to these requirements and was chosen for the new apparatus.

5.4. Overall Design

Figure 5.1 is a block diagram of the cylindrical-cell, light-scattering apparatus. Apparent are the many connections between the elements of the apparatus and the computer. Scattering angle and temperature of the sample are under computer control, and scattering intensity and temperature are monitored by the computer. In addition, the computer has complete remote control of the correlator operating parameters.

Figure 5.2 is a scale drawing of the primary mechanical and optical components. The laser and rotary table are mounted on a rigid aluminum slab. A post fits through the center of the rotary table

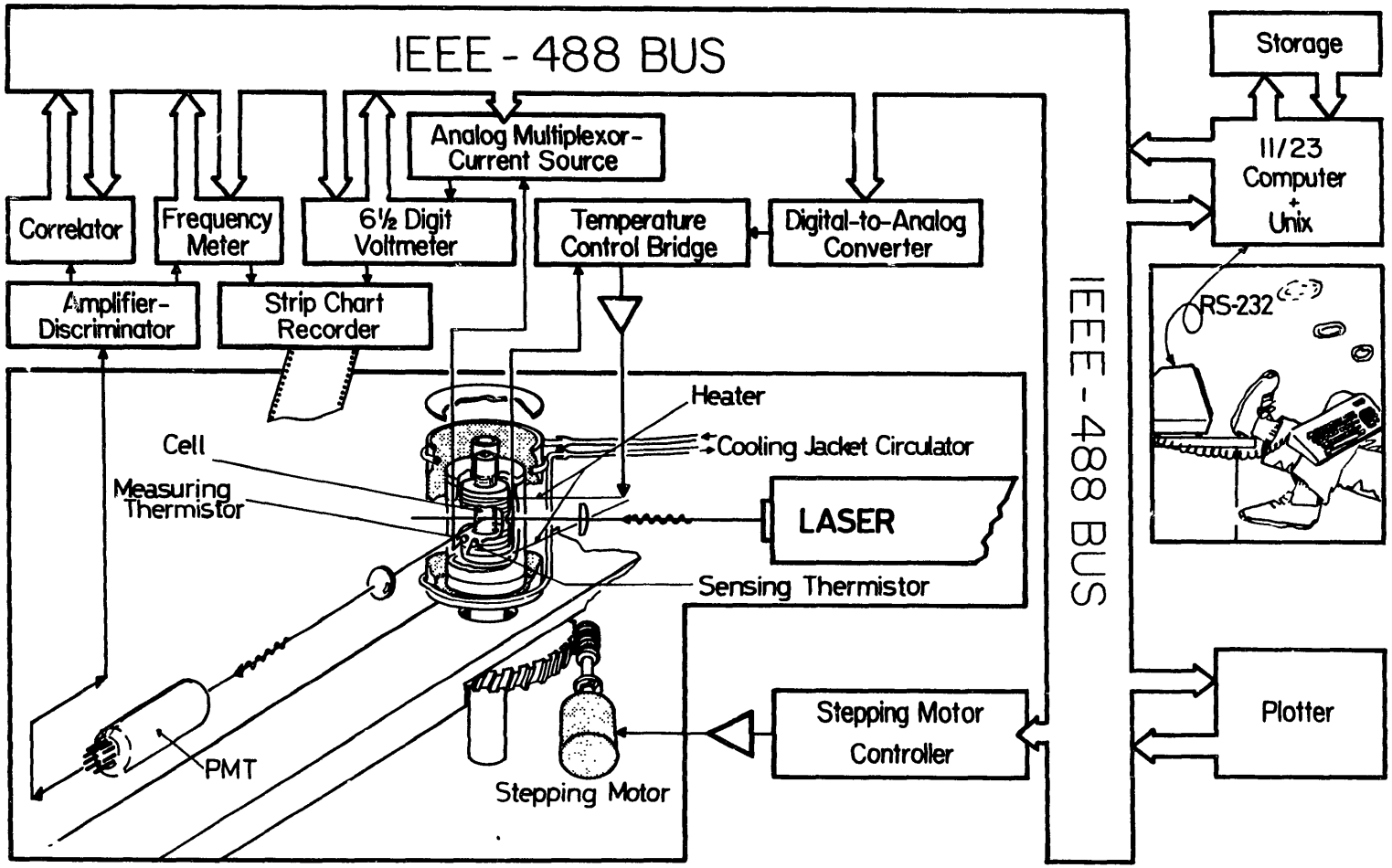

Figure 5.1 Components of the Light-Scattering System.

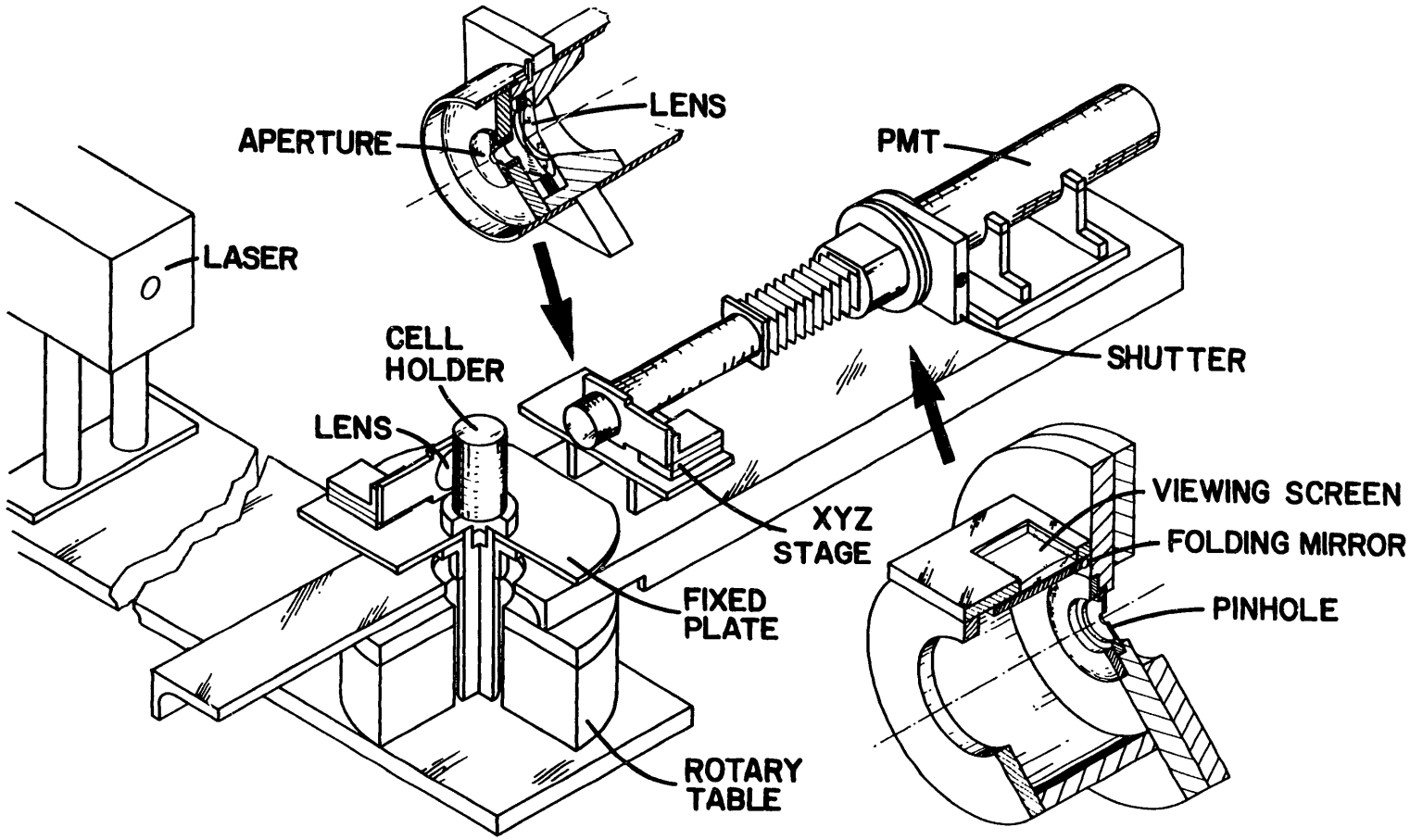

Figure 5.2 Rotating Arm and Collection Optics.

and is also fastened to the slab. A platform to hold the focusing lens and the cell holder is attached to the post. An aluminum channel is bolted to the top of the rotary table to support the detection optics. The entire assembly rests on a fairly massive (~500lbs) wooden table. The table legs sit on inflated inner tubes to damp out building vibrations.

A stepping motor attached to the worm drive of the rotary table and controlled by computer varies the scattering angle with an angular resolution of 0.01° per step. There was no measurable error in the reproducibility of the angular position.

A lens is inserted behind the first aperture on the rotating arm to form a twice-magnified image of the illuminated volume at the plane of the second aperture. A folding mirror, ground-glass screen assembly, salvaged from a single-lens reflex camera, is mounted in front of the second aperture. When the mirror is down, the image can be viewed on the screen. This arrangement allows visual inspection of the scattering volume for proper focusing of the laser beam, dust in the sample, and the presence of stray light. The space between the first aperture and the photomultiplier is completely shielded from ambient light.

Figure 5.3 shows the dimensions of the collection optics. These dimensions will now be used to estimate the size of the scattering volume and the number of coherence areas illuminated at the detector. The magnification, M, of the illuminated volume at the pinhole P2 is given by the ratio of the object distance, s_o, and the image

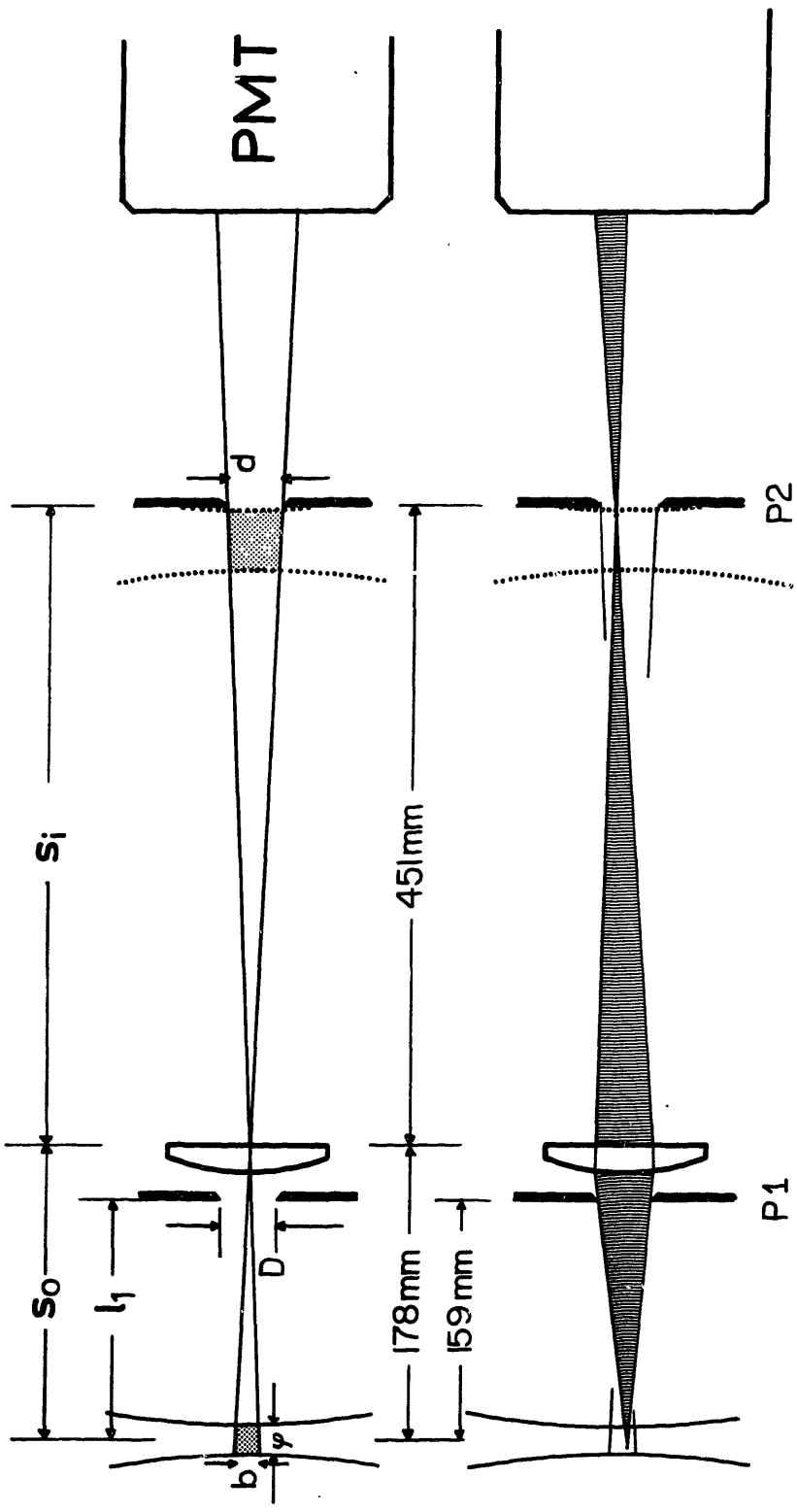

Figure 5.3 Dimensions of the Collection Optics. The diameter d of the pinhole P2 is 0.2mm, the diameter D of aperture P1 varies from 0.83mm to 1.5mm, and the diameter ϕ of the beam is ~0.1mm. The lens forms an image of the illuminated volume at P2. The length b of the scattering volume is determined by the magnification of the lens and d.

distance, s_i: $M = s_i/s_o \approx 2.53$. The diameter d of P2 is 0.2mm, and it limits the length b of the scattering volume, where $b = d/M \approx 0.08$mm. The diameter ϕ of the focused laser is about 0.1mm. Since $b < \phi$, the shape of the scattering volume at $\theta = 90°$ is a cylinder with its axis along the line of the collection optics. Its volume is $\phi\pi(b/2)^2 \approx 0.0005\text{mm}^3$. At other scattering angles b, and hence, the scattering volume, are increased by the factor $1/\sin\theta$.

The meaning of the coherence area is illustrated in Figure 5.4,

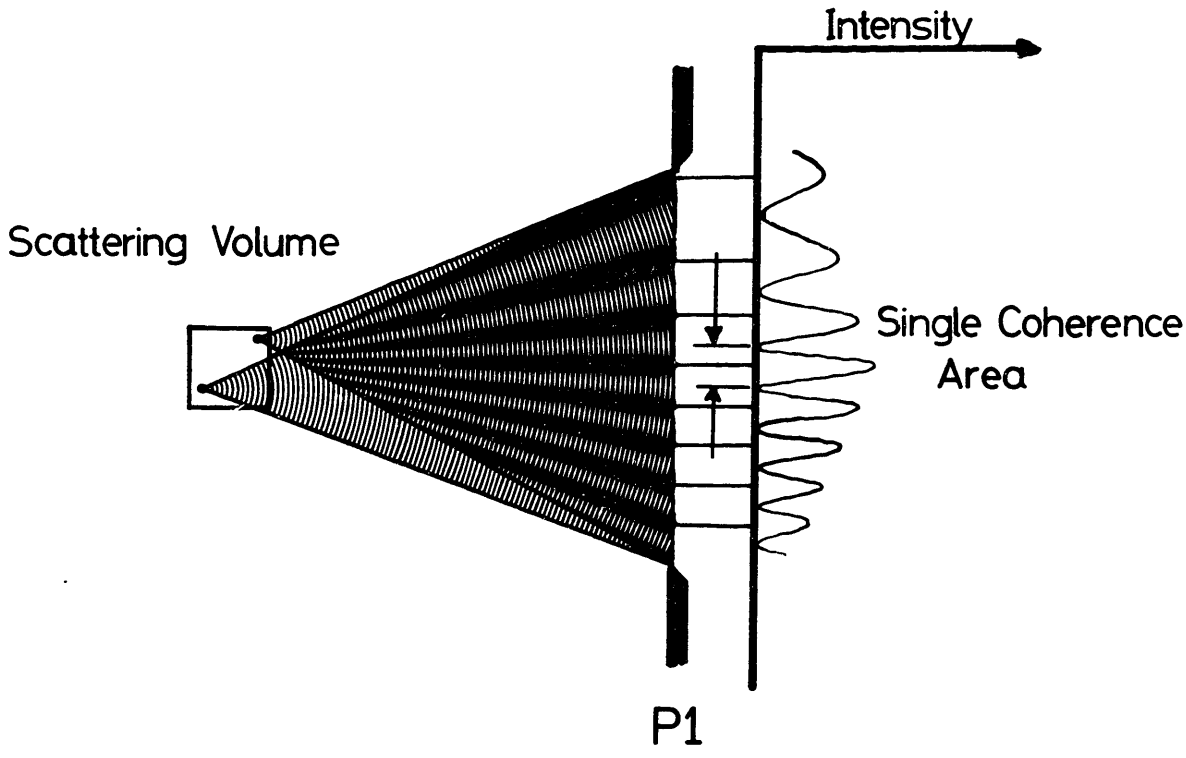

Figure 5.4 The Coherence Area. The wavefronts from two uncorrelated scatterers in the scattering volume combine constructively forming an interference pattern at the aperture P1. The coherence area is proportional to the square of the distance between successive minima. A rigorous calculation requires summing the wavefronts from all points in the scattering volume.

which shows the resultant intensity from two scattered beams originating from opposite corners of the scattering volume. A rigorous determination of the coherence area requires integrating the phase differences of the scattered beam at the reference plane from each point in the scattering volume. This calculation is identical to a determination of the Fraunhofer or far-field diffraction pattern of the scattering volume. If we consider the scattering volume to be a disk, and the coherence area at P1 to be the area of the central maximum of the diffraction pattern of a disk, the coherence area is $A_C \sim (\lambda l_1/b)^2$. The diameter D of aperture P1 determines the number of coherence areas N_C illuminated at the detector, where $N_C \sim (D/2)^2/A_C \approx 0.24$, for D = 1mm and $\theta = 90°$. At other scattering angles N_C increases by the factor $1/\sin^2\theta$. For example, at $\theta = 20°$ with D = 1mm, $N_C \approx 2$. In the experiments, several different apertures were used for P2 with diameters from .38mm to 1.5mm.

5.5. Laser Source

A Spectra-Physics model 164 Argon-ion laser generates the incident beam. The green line at 5145A was chosen for the experiments. Table 5.2 is a list of the magnitude of the inverse scattering vector for a series of scattering angles at this wavelength. This magnitude corresponds to the length scale of the concentration fluctuations in the samples that are probed at each scattering angle (see Equation 3.4).

The laser head contains an integral beam splitter which directs a fraction of the beam onto a photo-diode. The photo-diode is

Table 5.2 Length scale (in A) vs. scattering angle for cyclohexane at 34.5°C

θ	k^{-1}	θ	k^{-1}	θ	k^{-1}
5	6600	35	956	80	448
10	3300	40	842	90	407
15	2210	45	753	100	376
20	1660	50	682	120	333
25	1330	60	576	140	307
30	1110	70	502	160	292

connected to circuitry that monitors and regulates the beam intensity. We relied on this built-in power monitor to gauge the intensity of the incident beam. Incident power was typically 100-200mW. High laser power, while shortening accumulation time, caused local heating in the sample solution, generating convective flow. Usually a neutral density filter was inserted into the beam path so the laser could be operated at higher powers where the beam was apparently less susceptible to ripple from the power supply.

5.6. Detection

The scattered light is converted to electric pulses by a photomultiplier tube (EMI model 9368A, photocathode diameter 0.1in, selected for low dark current). The photomultiplier is biased at -1800V (with a Fluke model 415B supply). The photomultiplier housing (EMI model RFI1/B-263F) contains an integral pre-amplifier and discriminator (EMI model APED-1). The discriminator output is buffered (by a 74-128 integrated circuit) to provide replicas of the

signal for the digital correlator and a count-rate meter (Hewlett-Packard model 5300B/5308A/5312A/5311B). The meter can be read by the computer (typically at 10-30 second intervals) and can also be connected to a strip-chart recorder to provide a record of the scattered intensity. An increase in the scattering intensity as the temperature of the solution is lowered, or as the solvent mixture becomes poor, is one indication of the onset of interpolymer aggregation.

5.7. The Correlator

The state of the art of commercial digital correlators improved over the 5 years of these experiments. The first correlator from Nicomp Instruments had 64 channels to accumulate the correlation function. Limitations in the speed of digital circuits at that time required use of a clipping scheme to restrict the correlation product to one bit. The next-generation correlator from Nicomp provided true multiplication up to 4 bits, meaning the input count rate could vary by a factor of 16 with no distortion of the correlation function. We next obtained a 136-channel 4-bit correlator (Brookhaven Instruments model BI2020). Additional channels improve the quality of the fits to the correlation function when studying the internal motion of single polymers, where the correlation function consists of at least two exponentials of different decay times.

The Nicomp correlators, after modification, could be started, stopped, and cleared under computer control, and the accumulated correlation function could be read directly into the computer. The Brookhaven correlator has these features, but also allows remote

control of the clock (sample) time and input prescale factor. With this correlator, the computer can be programmed to optimize these parameters for the intensity of the scattered light and the characteristic time of the correlation function, which change drasticly while scanning the scattering angle. In practice, the computer was programmed to fit a short-duration correlation function at each new scattering angle. The clock time required to produce a constant number of decays over the 136 channels was calculated and sent to the correlator, and a new sample correlation function was obtained. The procedure generally required two or three iterations and took about 1 minute.

5.8. The Cell Holder

The sample solutions are contained in quartz cuvettes of 12mm outer diameter. Figure 5.5 shows the finned teflon stoppers designed to cap the cells. The fins are thin enough to flex and form a tight seal. A hole through the center of the cap allows air to escape when the cells are closed. A screw covered with teflon tape seals the hole.

Figure 5.6 is a cutaway drawing of the cell holder. The cell fits into the brass inner cylinder and is centered by the tapered walls on the bottom and by a delrin compression ring at the top. Concentricity between the inner cell holder and the steel center post attached to the baseplate is achieved by accurate machining of the 4 intermediate pieces. Steel pins pressed into the connecting pieces secures the alignment. All brass pieces were treated using the

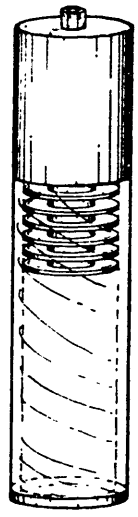

Figure 5.5 Cell with Stopper. The finned teflon stopper seals the cell to prevent evaporation of the volatile cylcohexane solutions. A teflon-covered screw seals the pressure-release hole that is drilled through the stopper.

ebanol-C process, to blacken the surfaces and reduce reflections.

Index-matching paraffin oil fills the cell holder to the level of the inlet hole. A small peristaltic pump circulates the oil from the cell holder through a filter to remove the dust introduced when the cell is changed.

Figure 5.7 is cross section of the cell holder at the level of the beam. At this level the walls of the inner cylinder are shaped to minimize reflections. There is a small pinhole suspended within the oil between the entrance window and the cell to limit reflections. A piece of neutral density filter is suspended between the cell and the exit window to absorb the unscattered beam. The entrance window is a quartz disk with an anti-reflection coating. Scattered light is collected through the cylindrical window, which

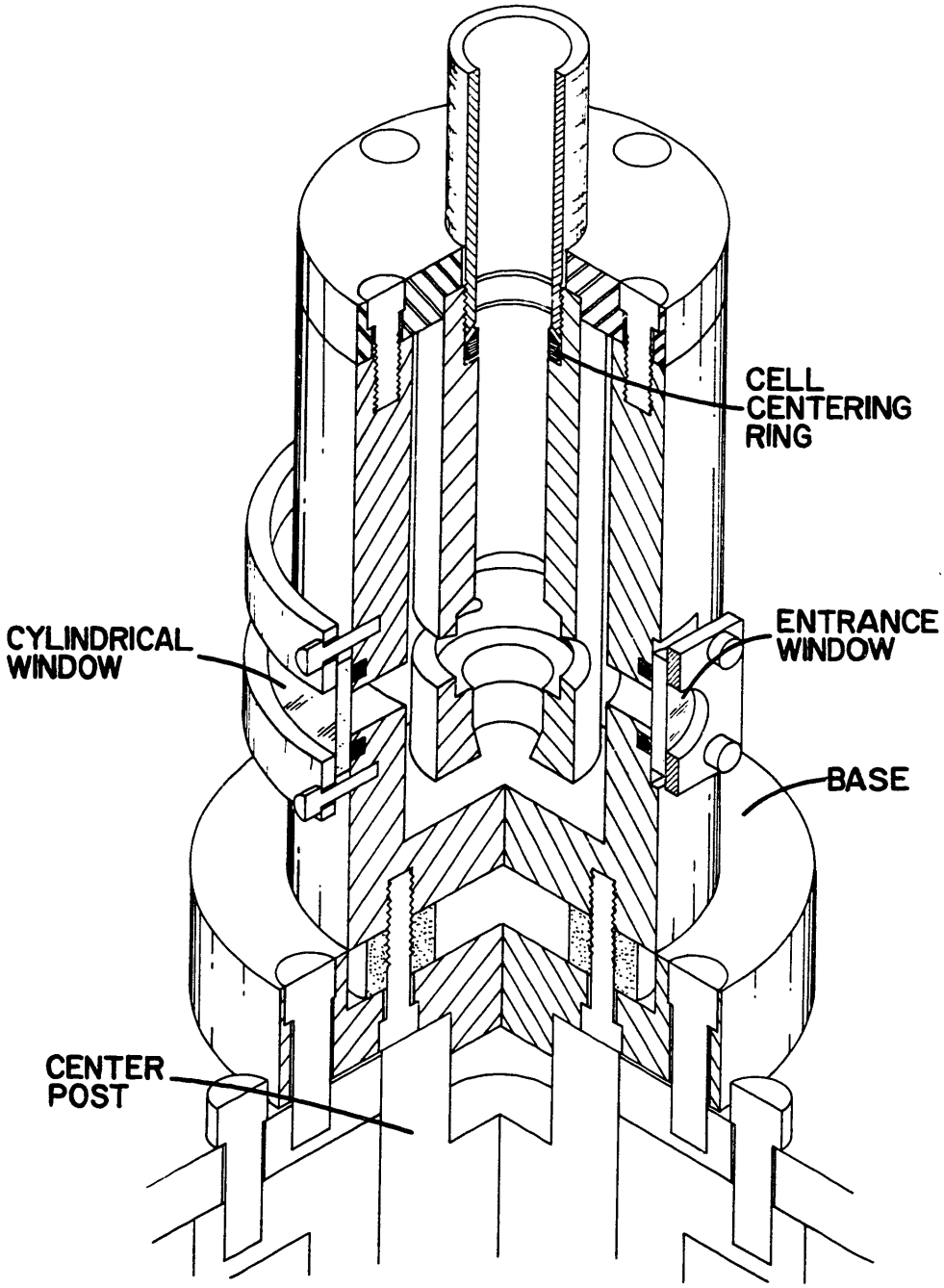

Figure 5.6 The Cylindrical Cell Holder. The cylindrical projection on the bottom of the base fits into the hole on the top of the center post to align the cell holder with the center of rotation of the rotary table.

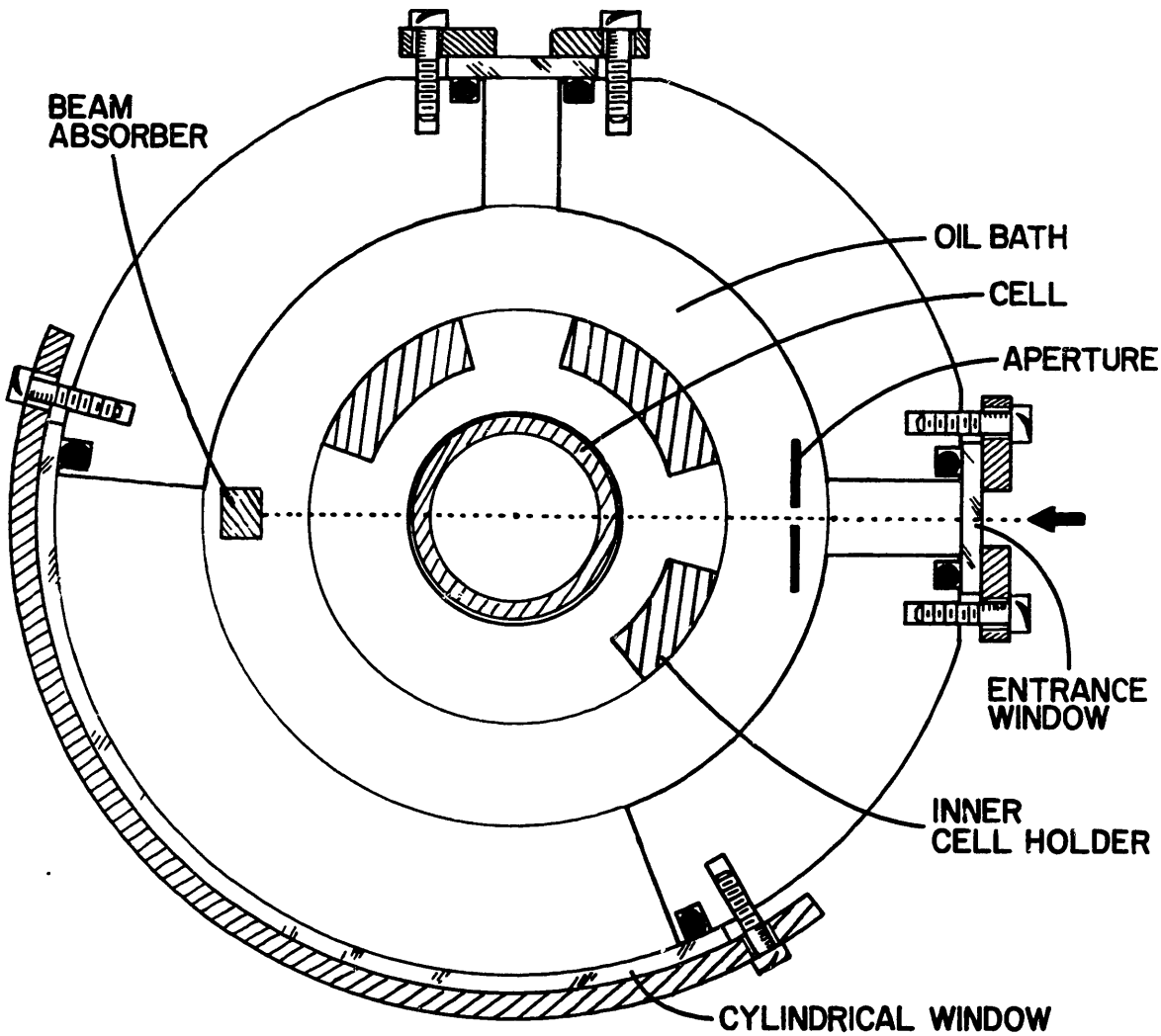

Figure 5.7 Cell Holder Cross-Section. The section is taken at the level of the windows. The aperture, the beam absorber, and the cutaway portions of the inner cell holder are included in the design to prevent stray light from reaching the detector.

was fabricated from Suprasil II grade quartz. The window subtends an arc of 150°. Sixteen screws are used to hold the window in place. Great care was required in tightening these screws to avoid introducing stresses that would crack the window. The third window shown in the figure is used only to aid visual inspection of the cell holder interior. All the windows are mounted with o-ring seals to prevent leakage of the index-matching fluid.

5.9. Optical Alignment Procedure

The mechanical construction of the system is stable. Realignment is generally only necessary when components are changed. The general procedure for alignment follows.

(1) The position of the rotary table is adjusted to put its axis of rotation in line with the axis of the fixed post. A dial-indicator is fastened to the top of the rotary table with the indicating point in contact with the fixed post. The rotary table is turned, its position on the base slab adjusted, and the mounting bolts secured.

(2) A centering point is placed in a hole drilled for this purpose in the center of the fixed post, and the position of the laser adjusted so that the beam passes through the center of rotation at the proper height.

(3) The cell holder is temporarily put into position on the fixed post, and the reflection from the beam-entrance window back to the laser is used to set the inclination of the laser beam per-

pendicular to the surface of the window.

(4) The cell holder is removed, the height and centering of the beam is rechecked, and the previous step repeated, until the laser is satisfactorily aligned.

(5) The rotating arm is placed at 0°, and the mounting of the photomultiplier/pinhole assembly set for the beam to hit the pinhole on center. The rotary table angle indicator is set to read 0° at this time.

(6) The collecting lens on the rotating arm is put into place and positioned using the reflections back to the laser to set the lens perpendicular to the beam while maintaining the centering of the beam on the rear pinhole.

(7) The cell holder is put into place and bolted into position guided by the reflection of the laser beam off the beam-entrance window back to to laser.

(8) The laser focusing lens is positioned again using reflections.

(9) The rotating arm is moved off 0°, and the collection lens is adjusted again in the vertical direction to maximize the scattering intensity. The focusing lens is adjusted to put the point of maximum beam convergence in the center of the cell. The collection lens is then adjusted to bring the image of the beam into focus on the viewing screen.

5.10. Temperature Control

Measurements were made at temperatures in the range 25-50°C. Temperature stability of the cell was better than 1mK over 10 hours. The thermal isolation of the cell holder and the elements related to temperature control are illustrated in Figure 5.8. The inner cell holder and the outer can are brass to provide thermal mass. The cover and base are stainless steel, a material with relatively low thermal conductivity. In addition, the outer can is separated from the base by ceramic spacers to limit heat flow through the base to the fixed plate. The index-matching paraffin oil that fills the cell holder also serves as a thermostating fluid for the cell. Heat is supplied through 3.5m of teflon-encased nichrome resistance wire wrapped around the inner cell holder (resistance = 20.4Ω).

A second stage of regulation is provided by a brass cylinder with brazed-on copper tubing that fits over the outer can. A temperature controlled circulator (Lauda model K-2/R) pumps fluid, generally a few degrees below the temperature of the cell, through the tubing. Foam insulation covers the entire assembly. To further limit heat flow, the base of the cell holder below the ceramic spacers is heated by resistance elements. The electric power sent through these elements and the temperature of the circulator are adjusted manually to keep the voltage across the cell-heater resistance wire as low as possible. The temperature of the sample can be scanned over several degrees before these auxiliary heaters need to be readjusted. The ceramic spacers and base plate heaters were not

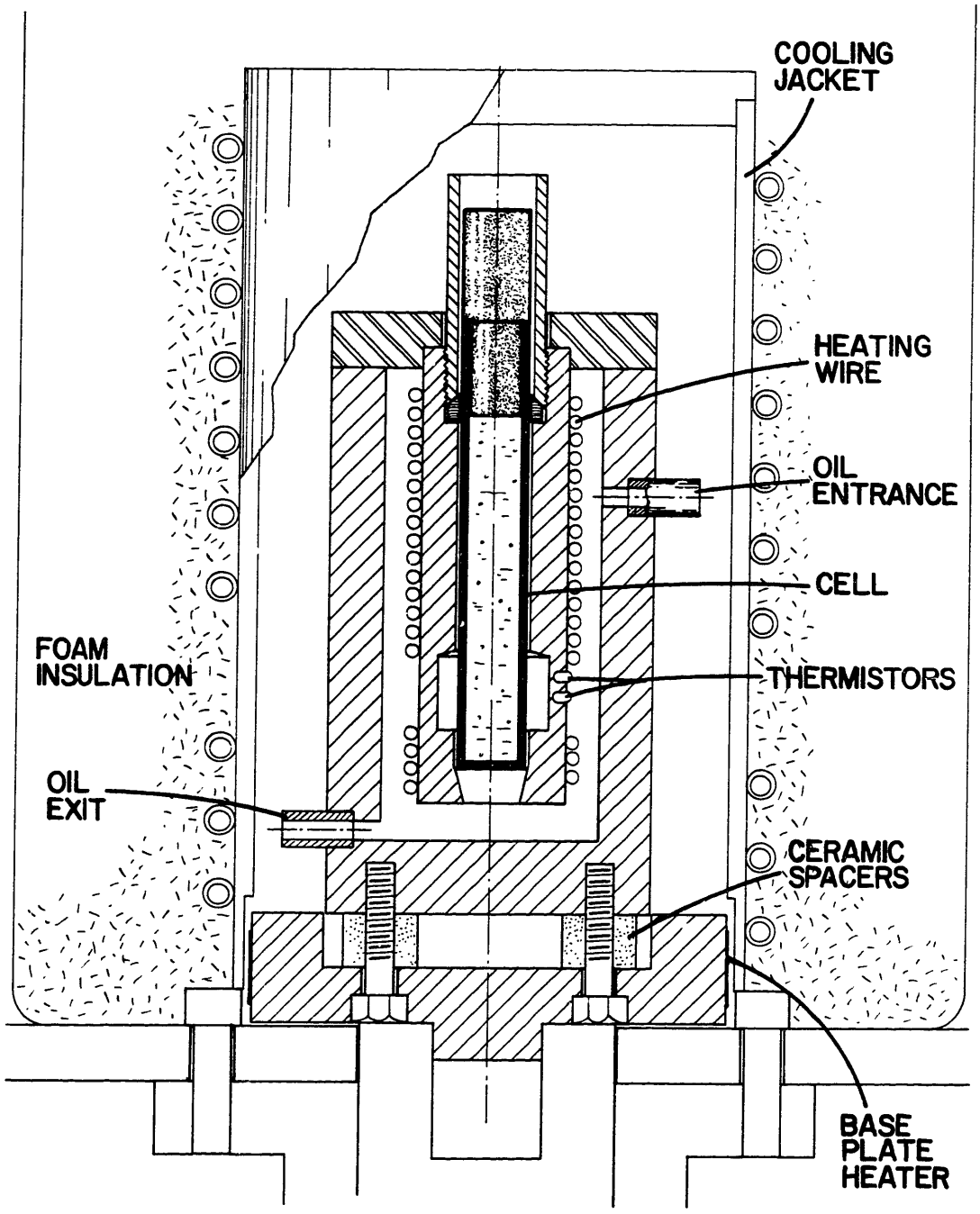

Figure 5.8 Temperature Control of the Cell Holder. The wires leading to the thermistors and the heating wire are not shown. They are fed through holes in the cover of the real cell holder.

part of the original design, but were added in an attempt to eliminate temperature gradients.

The main element of the controlling electronics is a precision, low-noise resistance bridge. An epoxy-coated thermistor (YSI model 44032) embedded in the inner cell holder is one arm of the bridge. Complimentary to that arm is a variable resistance set to balance the thermistor at a particular temperature. The amplified difference voltage of the bridge drives a programmable power supply (Kepco model OPS 55-2M) that provides up to 20 Watts through the resistance wire. A computer generated offset voltage can be added to the bridge offset voltage to scan the temperature about the set point.

5.11. Temperature Measurement

The temperature sensor is another thermistor identical to the one in the bridge, also embedded in the inner cell holder. A current source, powered by a 1.35V Mercury cell battery and consisting of a low-drift, low-noise operational amplifier (Analog Devices OP-07) and resistors, supplied ~10μA. A computer-controlled relay alternately switched the current source between a 100MΩ precision resistor and the thermistor. The voltage V across either element was then determined using a $6\frac{1}{2}$-digit voltmeter which was periodically read over the computer interface. The source current i_s was calculated from the reading when the precision resistor was in line using Ohm's law, with $i_s = V/100M\Omega$. The resistance R of the thermistor was then calculated from i_s and the voltage across the thermistor.

The temperature-resistance relationship of the thermistor is described well by the empirical Steinhart equation [1],

$$\frac{1}{T} = A + B\ln(R) + C[\ln(R)]^3 .$$

The coefficients $A = 9.322\times10^{-4}$, $B = 2.221\times10^{-4}$, and $C = 1.262\times10^{-7}$ were determined by fitting the equation with simultaneous measurements of the resistance of the thermistor and direct measurements of the temperature using a quartz thermometer (HP model 2804A). At 25°C, for a 1°C temperature change, R changes by 1240Ω. Resolution in the temperature measurements was ~0.5mK.

References

1. J.S. Steinhart and S.R. Hart, Deep Sea Res. **15** p. 497 (1968).

CHAPTER 6

SUGGESTIONS FOR FUTURE EXPERIMENTS

Future studies of the coil-globule transition should be done with well-characterized polymers to remove doubt about whether the results are affected by polydispersity of the sample, branched chains, etc. The Toyo-Soda company of Japan can supply such samples of polystyrene. Further improvements in the light scattering instrument, particularly for uniform temperature control of the sample and elimination of stray light at forward scattering angles, are required to improve the quality of the data, especially in determination of the intramolecular dynamics.

To test the predictions of the molecular weight dependence of the phenomenon, measurements must be carried out for a homologous series of polymers. Many of the theories are presumed valid only in the thermodynamic limit of infinite molecular weight. This limit may be effectively satisfied with the 20-50 million molecular weight polymers commercially available. Measurements using successively smaller polymers will test the range of applicability of the theories. To test the predictions regarding the influence of the flexibility of the polymer on the type of phase transition from coil to globule, new polymer-solvent systems must be investigated. Recent observations by Tanaka [1] of a first-order phase transition in gels made of polyisopropylacrylamide in water suggest single chains of this polymer may also undergo a first-order phase transition. If a

polymer-solvent system is found that undergoes a discrete collapse, the effect of the finite size of the three-dimensional statistical system should be apparent in a progressive rounding of the transition at lower molecular weights [2]. Such data would provide a test of statistical mechanical theories for finite systems.

References

1. Y. Hirokawa and T. Tanaka, "Volume phase transition in a non-ionic gel", pp. 203-208 in Physics and Chemistry of Porous Media (Schlumberger-Doll Research, 1983), ed. D.L. Johnson and P.N. Sen, American Institude of Physics, New York (1984).

2. C. Domb, "Phase transition in a polymer chain in dilute solution", Polymer **15** pp. 259-262 (1974).

APPENDIX A

FITTING THE CORRELATION FUNCTION

Fitting the correlation function involves choosing an appropriate functional form for the correlation function and then adjusting the parameters of the function to minimize the differences between it and the observed correlation function. If $C_{FIT}(t_i)$ is the fitting function and $C_{OBS}(t_i)$ is the observed correlation function, where t_i is the delay time at the ith channel, the differences between them are accumulated in the chi-squared sum,

$$\chi^2 = \sum_i^N \frac{(C_{FIT}(t_i) - C_{OBS}(t_i))^2}{N - N_{PAR}} , \qquad (A.1)$$

where N is the number of points and N_{PAR} is the number of fitted parameters. The lower the value of chi-squared, the better the fit.

The simplest homodyne correlation function is expected for a monodisperse solution of particles and has the form,

$$C_{FIT}(t_i) = [A_0 e^{A_1 t_i}]^2 + A_3 , \qquad (A.2)$$

where the A's are the adjustable parameters, and

$$A_1 = -\frac{1}{Dk^2} , \qquad (A.3)$$

with D the diffusion coefficient and k the magnitude of the scattering wave vector.

If the particle distribution is not monodisperse, but distributed about a mean size, the next simplest form for the fitting

function is expressed in the cumulants (or moments) expansion [1]. The fitting function takes the form

$$C_{FIT}(t_i) = [e^{A_0 + A_1 t_i + A_2 t_i^2 + A_3 t_i^3 + \cdots}]^2 + A_n \ . \qquad (A.4)$$

The parameters are combined to describe the distribution as follows. Equation A.3 holds for A_1. The percentage variance (or width) of the distribution is

$$\text{variance} = -\frac{4A_2^{1/2}}{A_1} \times 100 \ . \qquad (A.5)$$

Only the mean and the variance are required to characterize a Gaussian distribution. The skewness (or asymmetry) of the distribution about the Gaussian is

$$\text{skewness} = -\frac{6A_3}{A_2^{3/2}} \times 100 \ . \qquad (A.6)$$

Higher order moments are defined, but fitting the correlation function for the required added parameters is unlikely to produce significant results.

Another fitting function is also used in this work. If the scattering solution is expected to have two widely separated decay times, for instance, one associated with translational diffusion and one with internal motion, a two-exponential fitting function is appropriate,

$$C_{FIT}(t_i) = [A_0 e^{A_1 t_i} + A_2 e^{A_3 t_i}]^2 + A_3 \ , \qquad (A.7)$$

The computer fitting program implements two techniques to minimize chi-squared. If the baseline can be eliminated as a free

parameter in forms A.2 or A.4, the fitting function can be rewritten as (for A.4),

$$\frac{1}{2}\ln\left[C_{FIT}(t_i) - \text{baseline}\right] = A_0 + A_1 t_i + A_2 t_i^2 + A_3 t_i^3 + \cdots .$$

The resulting polynomial function can be fit by strictly analytical methods [2]. After the logarithm is taken, however, the fit would give a disproportionate weight to the points on the tail of the correlation function. To compensate, each point in C_{OBS} is customarily weighted by the factor $\left(C_{OBS}(t_i) - \text{base}\right)^2$.

There are two ways to fix the value of the baseline. Both are handled by the correlator electronics. The correlator maintains a count of the total input pulses and the elapsed time of the measurement. Their quotient is the average count (or calculated) baseline. For the second method, the correlator inserts many (~1000) clock periods after the last normal channel. The correlation function is expected to be completely decayed at this point, and its value is the so-called delayed baseline. These methods of fixing the baseline do not always produce the best fit to the data. For instance, if a large particle passes through the scattering volume, the correlation function at the delayed baseline channels may be raised.

When the fitting function cannot be converted to a polynomial, as for the cumulants expansion with the baseline a free parameter or for a double exponential, a non-analytic, iterative technique is necessary. The procedure requires choosing initial guesses for the parameters. In the fitting computer-program, the initial guesses are chosen automatically, using a heuristic method. First, $C_{OBS}(t)$ is

fit to a first order polynomial function using a fixed baseline. The values of A_0 and A_1 thus obtained and the fixed baseline are used as initial guesses to fit to a single exponential with the baseline as a free parameter. The fit to the polynomial function is then repeated, this time using the baseline obtained from the fit to the single exponential. The order of the polynomial is the same order as the target cumulants fit, or first order if the target fit is the double exponential form. The parameters obtained from this polynomial fit, along with the baseline from the single exponential fit, are the initial guesses for the cumulants fit. If the target fit is the double exponential, the amplitudes of the exponentials are taken as 80% and 20% of the zeroth order polynomial term. The initial guess for the decay rate of the larger amplitude exponential is set to four times A_1 from the polynomial fit. The second decay rate is set to A_1. Once the initial guesses are chosen, the procedure for searching parameter space for the minimum value of chi-squared uses the Marquardt algorithm as presented by Bevington [2].

References

1. D.E. Koppel, "Analysis of macromolecular polydispersity in intensity correlation spectroscopy: The method of cumulants", J. Chem. Phys. 57(11) pp. 4814-4820 (1972).

2. P.R. Bevington, Data Reduction and Error Analysis for the Physical Sciences, McGraw-Hill, New York (1969).

BIOGRAPHICAL NOTE

Gerry was born in 1952 in Grand Rapids, Michigan. He moved shortly thereafter, with his family, to the south suburbs of Chicago, where he grew up. He attended the University of Michigan in Ann Arbor sporadically from 1970 to 1978, eventually earning a B.S. in Physics, and graduating with High Honors. From 1978 to 1984, he worked towards his Physics Ph.D. under Professor Tanaka at MIT.

LIST OF PUBLICATIONS

1. I. Nishio, G. Swislow, S.-T. Sun, and T. Tanaka, "Critical density fluctuations within a single polymer chain", Nature **300**(5889) pp. 243-244 (1982).

2. T. Tanaka, D. Fillmore, S.T. Sun, I. Nishio, G. Swislow, and A. Shah, "Phase transitions in ionic gels", Phys. Rev. Lett. **45**(20) pp. 1636-1639 (1980).

3. S.T. Sun, I. Nishio, G. Swislow, and T. Tanaka, "The coil-globule transition: Radius of gyration of polystyrene in cyclohexane", J. Chem. Phys. **73**(12) pp. 5971-5975 (1980).

4. G. Swislow, S.T. Sun, I. Nishio, and T. Tanaka, "Coil-globule phase transition in a single polystyrene chain in cyclohexane", Phys. Rev. Lett. **44**(12) pp. 796-798 (1980).

5. T. Tanaka, A. Hochberg, I. Nishio, S.-T. Sun, and G. Swislow, "Light scattering from gels and a single polymer chain near phase transitions", pp. 29-38 in Light Scattering in Solids, ed. J.L. Birman, H.Z. Cummins, and K.K. Rebane, Plenum (1979).

6. I. Nishio, S.T. Sun, G. Swislow, and T. Tanaka, "First observation of the coil-globule transition in a single polymer chain", Nature **281**(5728) pp. 208-209 (1979).

7. T. Tanaka, G. Swislow, and I. Ohmine, "Phase separation and gelation in gelatin gels", Phys. Rev. Lett. **42**(23) pp. 1556-1559 (1979).

ACKNOWLEDGEMENTS

At the end of the long effort to complete the work of this dissertation, I want to recognize the people who helped me along the way. The two post-docs, Shao-Tang Sun and Izumi Nishio, who were with me from the beginning, were not only indispensable for the scientific progress we made, but were good companions as well. Their humor, encouragement, and patience with me will not be forgotten. Shao-Tang moved on before the real work of writing this dissertation began. Izumi, however, could find no escape, and I thank him for his help with the writing and for Figure 5.1.

I thank Jaro Ricka and Joyce Peetermans for their encouragement and companionship during these last few years. To my fellow students and assorted post-docs on the second floor of Building 13, past and present, your company and commiseration is gratefully acknowledged. Special thanks to Ben Ocko, a friend through it all.

I thank my parents for their unshakeable faith in me, and my brother and sisters for their encouragement. To my friend Norm Williams in Vermont, thanks for providing me retreat from the rigors of MIT.

Lastly, I thank my professor, Toyichi Tanaka, who liked my essay on "Why I Want to Go to MIT" well enough to offer me financial support. The enthusiasm he generated, the freedom he allowed, and the knowledge he shared helped me reach this goal.